*Supplement of*

# A Systematic Re-evaluation of Methods for Quantification of Bulk Particle-phase Organic Nitrates Using Real-time Aerosol Mass Spectrometry

Douglas A. Day,[1,2] Pedro Campuzano-Jost,[1,2] Benjamin A. Nault,[1,2,a] Brett B. Palm,[1,2,b] Weiwei Hu,[1,2,c] Hongyu Guo,[1,2] Paul J. Wooldridge,[3] Ronald C. Cohen,[3,4] Kenneth. S. Docherty,[5] J. Alex Huffman,[6] Suzane S. de Sá,[7] Scot T. Martin,[7,8] Jose L. Jimenez[1,2]

[1]Cooperative Institute for Research in Environmental Sciences, University of Colorado, Boulder, CO, USA
[2]Dept. of Chemistry, University of Colorado, Boulder, CO, USA
[3]Department of Chemistry, University of California Berkeley, Berkeley, CA, USA
[4]Department of Earth and Planetary Science, University of California Berkeley, Berkeley, CA, USA
[5]Jacobs Technology, Inc., Research Triangle Park, NC, USA
[6]Department of Chemistry and Biochemistry, University of Denver, Denver, CO USA
[7]School of Engineering and Applied Sciences, Harvard University, Cambridge, Massachusetts, USA
[8]Department of Earth and Planetary Sciences, Harvard University, Cambridge, Massachusetts, USA

[a]now at: Center for Aerosol and Cloud Chemistry, Aerodyne Research Inc., Billerica, MA, USA
[b]now at: Atmospheric Chemistry Observations and Modeling Laboratory, National Center for Atmospheric Research, Boulder, CO, USA
[c]now at: State Key Laboratory at Organic Geochemistry, Guangzhou Institute of Geochemistry, Chinese Academy of Sciences, Guangzhou, China

**Correspondence:** Douglas A. Day (douglas.day@colorado.edu) and Jose L. Jimenez (jose.jimenez@colorado.edu)

## S1 Field and laboratory dataset descriptions and data processing methods

### S1.1 Field datasets

Several AMS field datasets are used throughout this manuscript to refine and test the quantification methods, provide examples, and explore more advanced applications. The main datasets used here include and will be referred to as DC3, SEAC$^4$RS, KORUS-AQ, SOAR, MILAGRO, DAURE, BEACHON-RoMBAS, SOAS, and GoAmazon (IOP1/IOP2). All datasets were collected with a high-resolution time-of-flight AMS (HR-ToF-AMS) (DeCarlo et al., 2006). Table S3 provides a brief overview of the campaigns. Additional details are provided in this section.

Campaigns conducted onboard the NASA DC-8 research aircraft include: DC3 (Deep Convective Clouds & Chemistry (Barth et al., 2015; Nault et al., 2016)), SEAC$^4$RS (Studies of Emissions and Atmospheric Composition, Clouds and Climate Coupling by Regional Surveys (Fisher et al., 2016; Toon et al., 2016)), and KORUS-AQ (KORean-United States Air Quality mission; https://espo.nasa.gov/home/korus-aq; (Nault et al., 2018)). DC3 was conducted out of Salina, Kansas in spring 2012 and focused on investigating the effects of deep convective clouds on upper tropospheric composition and chemistry. SEAC$^4$RS was conducted out of Houston, Texas during late summer 2013, with a focus on effects of deep convection on pollution redistribution and chemistry and feedbacks, a regional survey of biogenic chemistry, and the evolution of anthropogenic and biomass burning emissions and effects on regional air quality. KORUS-AQ was conducted over South Korea and Seoul during spring 2016 to study the local and transport effects on air quality throughout the Korean Peninsula. Mass concentrations shown for aircraft campaigns are always reported in units of standard pressure and

temperature (1013 mbar, 273K; often denoted as ng $sm^{-3}$ or µg $sm^{-3}$, however usually omitting the "s" here as it is implied), while ground campaigns are reported under ambient conditions.

Ground-based campaigns include SOAR (Study of Organic Aerosols at Riverside (Docherty et al., 2011)), MILAGRO (Megacity Initiative: Local And Global Research Observations (Molina et al., 2010)), DAURE (Determination of the sources of atmospheric Aerosols in Urban and Rural Environments in the Western Mediterranean (Minguillon´ et al., 2011; Pandolfi et al., 2014), BEACHON-RoMBAS (Bio–hydro–atmosphere interactions of Energy, Aerosols, Carbon, $H_2O$, Organics and Nitrogen – Rocky Mountain Biogenic Aerosol Study (Ortega et al., 2014)), SOAS (Southern Oxidant and Aerosol Study (Carlton et al., 2018)), and GoAmazon (Martin et al., 2016, 2017). SOAR-1 (hereafter just SOAR) was conducted during summer 2005 in Riverside, California (eastern Los Angeles metropolitan region) to investigate chemical composition and sources of fine particles of inland Southern California. Details of the measurements used here can be found elsewhere (Docherty et al., 2011). MILAGRO was conducted during late winter / early spring 2006 in and around Mexico City and focused on understanding the emissions, transport, and transformation of pollution in a megacity. The measurements used here were collected at the "T0 urban supersite", 9 km NNE of the city center and are described in detail elsewhere (Aiken et al., 2009, 2010). DAURE was conducted during late winter / early spring and summer 2009 in the Western Mediterranean Basin to investigate urban and rural sources of aerosols in the region. Measurements used here were collected during the winter/spring intensive in Montseny, Spain, a rural location 50 km inland from Barcelona, and described elsewhere (Minguillon´ et al., 2011; Pandolfi et al., 2014). BEACHON-RoMBAS was conducted during summer 2011 at a mid-altitude pine forest in the Colorado Rocky Mountains with a focus on emissions of primary biological particles and SOA precursors, and their transformations and impacts in the atmosphere. Details of the measurements used here can be found elsewhere (Fry et al., 2013; Palm et al., 2017). SOAS was conducted during the summer of 2013 at a semi-polluted rural mixed forest in central Alabama with a focus on understanding effects of BVOC on oxidants and aerosols and how anthropogenic emissions influences control those processes in the Southeast US. Details of the measurements used here can be found elsewhere (Hu et al., 2016). In addition to standard ambient AMS data, we use AMS measurements collected after ambient gases and aerosol were processed in an oxidation flow reactor (OFR) with OH or $NO_3$ radicals (Hu et al., 2016; Palm et al., 2017). GoAmazon was conducted during the 2014 wet season (IOP1) and dry season (IOP2) of central Amazonia (sometimes) downwind of a large urban city (Manaus). Details of the measurements used here can be found elsewhere (de Sá et al., 2018, 2019; Palm et al., 2018).

### S1.2 Laboratory datasets

In addition to a range of field datasets used for this analysis, a smaller subset of laboratory measurements was included. AMS measurements were collected as part of a series of chamber studies investigating SOA (including $pRONO_2$) formed from reaction of terpenes (α-pinene and Δ-3-carene) with nitrate radicals under a range of seeds and oxidant-precursor ratios (Kang et al., 2016). Also, AMS measurements were made of HPLC-separated $pRONO_2$ products of SOA produced by reaction of 1-pentadecene + $NO_3$ radicals, according to the methods described in Farmer et al. (2010). Additionally, AMS measurements were made of SOA generated in a chamber from (high-NO) photooxidation of a series of n-alcohols (Liu et al., 2019). The terpene and alkanol SOA and HPLC-isolated products were

included to provide additional data to a survey of $R_{pRONO2}$ to that already reported in the literature (see Sect. 3). Specific details on the data used from those experiments are included in Table S1.

**S1.3 Data collection and processing**

Most details of the data collection and processing for each measurement dataset can be found in the references provided above. All HR-ToF-AMS data was analyzed with the latest standard ToF-AMS software packages available at the time (Squirrel, PIKA (DeCarlo et al., 2006; Sueper, 2021)). For ground-based and laboratory datasets the standard "MS" mode was used where the particle beam is alternately blocked ("closed") and transmitted ("open") with a chopper every ~5 s and data averaged and saved every 1–5 minutes. For aircraft measurements, data was collected in Fast MS mode (FMS (Kimmel et al., 2011)) where the chopper is open for most of a minute, collecting 1 Hz data and then backgrounds (closed) measured every minute for a few seconds - thus allowing for high-time resolution sampling required onboard fast-moving aircraft platforms. For some of the aircraft data presented here, data was analyzed as a 1-minute product, where the raw mass spectra are first averaged and then high-resolution peak fitting is done (which has improved signal-to-noise (S/N) over averaging 1-s peak-fitted data due to nonlinear effects associated with fitting less noisy spectra). The aircraft-based measurements were collected with a highly-customized aircraft version (Nault et al., 2018; Schroder et al., 2018). The only aspect of the aircraft sampling methods and configuration that may affect analysis of nitrates, other than possibly use of the FMS mode, is the presence of the cryopump-cooled shield surrounding the ionization region that substantially reduces backgrounds from some species, thus resulting in improved S/N of some species. For all datasets presented here, the lower spectral resolution (higher S/N) "V-mode" acquisition data (DeCarlo et al., 2006) was used except for SOAR and MILAGRO, where "W-mode" data was used.

Quantifying the $NO^+$ and $NO_2^+$ ion signals from ambient high-resolution AMS spectrum involves a few specific steps and assumptions, beyond the general HR peak-fitting methods described in DeCarlo et al. (2006). At *m/z* 30, where $NO^+$ is found, there are several other peaks that may be present in ambient aerosol such as $CH_2O^+$, $CH_4N^+$, $C_2H_6^+$, $H_2N_2^+$, $C^{18}O$, $^{13}CHO^+$, $^{13}C_2H_5^+$, $^{13}CHO_3N^+$, $^{30}Si^+$, $H^{29}Si^+$, $H^{15}NN^+$ (See Fig. S1 in Aiken et al. (2009); Farmer et al. (2010); Fig. S1 here). However, typically only $CH_2O^+$, $C^{18}O^+$, and $^{13}CHO^+$ would be expected to be close enough to the $NO^+$ peak or have appreciable signal to affect quantification of $NO^+$. The two isotope peaks are relatively small due to the ~1% and ~0.2% isotopic ratios, and thus are typically quantified by constraining to their isotopic parent ion peak. In contrast, $CH_2O^+$ can be of comparable signal to $NO^+$ and resides ~1.5 peak half-widths (in V-mode sampling) from $NO^+$; therefore, it can be precisely separated with HR peak fitting (Cubison and Jimenez, 2015).

At *m/z* 46, where $NO_2^+$ is found, there are several other peaks that may be present in ambient aerosol such as $CH_2O_2^+$, $CH_4NO^+$, $C_2H_6O^+$, $CH_2S^+$, $NS^+$, $C^{18}OO^+$, $^{13}CHO_2^+$, $^{13}CH_3NO^+$, $^{13}CCH_5O^+$, and $^{13}CHS$ (See Fig. S1 in Aiken et al. (2009); Farmer et al. (2010); Fig. S1 here). However, only $CH_2O_2^+$, $C^{18}OO^+$, $CH_2S^+$, $^{13}CHS$, and $^{13}CHO_2^+$ have substantial overlap with the $NO^+$ peak, and only $CH_2O_2^+$ and $C^{18}OO^+$ would be expected to contribute substantial signal compared to $NO_2^+$ for typical ambient aerosol. The sulfur-containing peaks would not be expected from organosulfates, which are known to form in the atmosphere; however, they might be produced by other compounds, such as sulfides, thiols, sulfoxides, or sulfones if they were present in substantial concentrations (which to our knowledge have not been

observed). Moreover, the isotopes peaks are often constrained to the parent peaks, minimizing any biases. $CH_2O_2^+$ is typically fit (and is ~1.2 peak half-widths separated from $NO_2^+$, in V-mode sampling) and $C^{18}OO^+$ is constrained to its isotopic parent ion ($CO_2^+$) which is precisely quantified. Uncertainties in quantification of the $NO_x^+$ peak ions will be systematically explored in a separate manuscript.

The standard process for constraining isotopic daughter peaks is to a) fit the parent peak at the lower *m/z*, b) fix the daughter peak according to the naturally occurring isotopic ratio (0.0108 for $^{13}C$, 0.0216 for $^{13}CC$, 0.00205 for $^{18}O$, 0.00411 for $^{18}OO$, etc.), and c) fit the remaining selected unconstrained peaks together with the constrained peaks. One exception related to $NO_x^+$ ion quantification is the $C^{18}O^+$, in the case that the $CO^+$ ion was not directly fit, which is typical for V-mode data and typical ambient concentrations. In that case, $CO^+$ is approximated as equal to the particle-phase $CO_2^+$ signal due to the difficulty of separating $CO^+$ from the large $N_2^+$ gas signal (Aiken et al., 2008). However, that step is part of the "fragmentation table" corrections and applied after the high-resolution peak fitting algorithm. Since the $C^{18}O^+$ almost exactly overlaps with the $NO^+$ peak (*m/z* 29.997990, 29.999161), the estimated $C^{18}O^+$ can simply be subtracted from the $NO^+$ signal without refitting the spectrum. Accounting for $C^{18}O^+$ interference in the $NO^+$ peak is typically not done in standard AMS processing. However, it was done for all datasets presented here except for the SOAR and MILAGRO datasets (where its effects are expected to be insignificant). Accounting for $C^{18}O^+$ interference has been standard practice in our $pRONO_2$ analyses since results presented in Fry et al. (2013), in order to most accurately account for organic ion interferences when nitrate concentrations are very low.

When nitrate concentrations are especially low (<10 ng $m^{-3}$, such as for the SOAS and BEACHON-RoMBAS datasets), it became clear that only "open-minus-closed" (OmC) peak fitting should be used (rather than "Diff"). In OmC fitting, the algorithm fits all peaks separately in the open and closed and then subtracts the integrated values ("sticks" in AMS parlance) to yield the aerosol signal. For "Diff", the background-subtracted high-resolution spectra are subtracted and then that "Diff" signal spectrum is peak fit. Using "Diff" at very low concentrations can result in the fits not converging which are assigned to zero. Including zeros or removing those points, when implementing further data averaging, would potentially bias the data. Use of OmC nearly always results in peak fitting convergence for open and closed spectral fitting, since even if aerosol concentrations are very low, some fitable signal is present in the background. Thus OmC results for near or below detection limit data will yield noisy signal above/below zero, which can be averaged to derive unbiased concentrations.

**S2 Further evaluation of calibration $R_{NH4NO3}$ and *RoR* using ambient data (supporting Sect. 4)**

Similar conclusions (to those presented in Sect. 4) can be inferred by inspection of the $R_{ambient}$ vs $pNO_3$ relationships for two campaigns that showed variable calibration $R_{NH4NO3}$ as shown in Fig. S9d (DAURE) and Fig. S9e (SEAC[4]RS). For the five-week DAURE campaign, nine $NH_4NO_3$ calibrations were performed, and $R_{NH4NO3}$ varied from 0.30 to 0.54 (Fig. S9d) for unknown reasons (no documented major instrumental changes). Calibration $R_{NH4NO3}$ were linearly interpolated to the sampling data (as shown by coloring in Fig. S9d), and $pNO_3$-binned averages were computed for three calibration $R_{NH4NO3}$ ranges. That treatment yields similar curves to those shown for studies with constant calibration $R_{NH4NO3}$ values. The averaged curves do not appear to reach the average calibration $R_{NH4NO3}$ at the highest concentrations sampled. It is not clear whether the highest observed fractions of $NH_4NO_3$ were not high enough to

observe that behavior, or if possibly the approximation of interpolation of variable calibrations did not fully capture the true reference $R_{NH4NO3}$ applicable to sampling periods. Nonetheless, the trends in $R_{ambient}$ are qualitatively consistent with average calibrations throughout the $pNO_3$ range.

Fig S9e presents a similar analysis for SEAC[4]RS; except $NH_4NO_3$ calibrations were performed more frequently, for every flight ($R_{NH4NO3}$ ranged from 0.4–1.49). However, calibrations during the same day as the flight were not possible, and thus the instrument was shut down and restarted between flights and calibrations. $pNO_3$-binned averages were computed for eight calibration ranges (each including 1–6 flights) and yielded curves similar to other studies with many leveling remarkably close to the calibration ratios at higher $pNO_3$. Those that did not, tended to have low upper ranges of concentrations. For SEAC[4]RS, $R_{ambient}$ tended to reach calibration $R_{NH4NO3}$ at much lower $pNO_3$ concentrations (in some cases as low as 1–3 μg $m^{-3}$), compared to other studies (~20 μg $m^{-3}$). See Sect. 7 for further discussion on these differences. Ratios at the lowest $pNO_3$ approximately grouped into two clusters, but mostly corresponded to their associated calibration $R_{NH4NO3}$. Estimating *RoR*s using each of the lowest $pNO_3$ bins yields an average value of 2.9 (±35%), while doubling the number of quantile averages (30 rather than 15 as shown in Fig. S9e) yields a *RoR* of 3.1 (±40%) — generally consistent with the studies summarized in Fig. 1.

An additional statistical test was performed for both the SEAC[4]RS and DAURE campaigns where $f_{pRONO2}$ was calculated using Eq. 1 and the *RoR* value (2.75) to estimate the $R_{pRONO2}$ and alternatively using a fixed $R_{pRONO2}$ of 0.1 (as applied in Kiendler-Scharr, et al. (2016) and several subsequent papers). Correlations of the $f_{pRONO2}$ vs the calibration $R_{NH4NO3}$ were computed with the expectation that a (more) significant correlation for one method would indicate less suitable representation of $R_{pRONO2}$. However, for both campaigns no significant correlations were found which appears to be due to the high variability in sampling compositions from flight-to-flight (SEAC[4]RS) or the large synoptic-timescale trends in composition at similar timescales as the $R_{NH4NO3}$ variability (DAURE). It appears that in order to glean information from this type of statistical test, the ideal scenario would include a large range of (well-captured) calibration $R_{NH4NO3}$ while sampling air with similar composition. The differences in calculated apportionment and concentrations for using the *RoR* method vs fixed $R_{pRONO2}$ will be discussed in a separate manuscript evaluating apportionment uncertainties, and can be quite substantial.

**S3 Detailed summary of prior studies using PMF for $pRONO_2$ separation**

As briefly introduced in Sect. 5.2.1, a few studies have reported results for using PMF of ambient AMS spectra including both the OA and $NO_x^+$ signals to quantify or investigate source associations of $pRONO_2$. Below, we present details and interpretations of those analyses. Additionally, several aspects of the studies are summarized in Table S4.

In the first report of including nitrate ions in PMF, Sun et al. (2012) included HR ions from OA and the major nitrate, sulfate and ammonium ions for measurements collected in New York City during summertime. Eight PMF factors were resolved. Those included two factors which were dominated by $(NH_4)_2SO_4$ or $NH_4NO_3$ together with a mix of organic peaks. The $NH_4NO_3$ factor accounted for 79% of the nitrate; its spectrum was composed of 74% $NH_4NO_3$ with a $NO_x^+$ ratio within 5% of the value measured for pure $NH_4NO_3$, and the associated organic had a relatively low O/C (0.14). The $NH_4NO_3$ factor peaked during the early morning which was shown to be consistent with the temperature-controlled equilibrium of $NH_4NO_3$ with $HNO_3$ and $NH_3$ gases. Most of the $NO_x^+$ not in the $NH_4NO_3$ factor (12%)

was apportioned to a factor characterized as the more oxidized (O/C of 0.48 vs 0.27) of two semi-volatile oxidized organic aerosol (SV-OOA) factors with a $NO_x^+$ ratio equivalent to a *RoR* of 2.6–2.7 (depending on if using the PMF $NH_4NO_3$ factor or pure calibration $NH_4NO_3$ $NO_x^+$ ratio for $R_{NH4NO3}$), indicative of organic nitrates. That factor was attributed to local photochemically-produced SOA, possibly from biogenic VOC (BVOC) oxidation, peaking mid-day. Alternatively, a *RoR* of 3.0–3.1 (depending on if using the PMF or pure calibration for $R_{NH4NO3}$) is calculated by combining the three OOA factors (see Table S1; the other two OOA factors contained only $NO^+$).

Hao et al. (2014) included the HR OA spectra and $NO^+$ and $NO_2^+$ ions in PMF analysis of measurements conducted in a rural forested region with urban influences during fall in Finland. Of the four factors resolved, one factor accounted for 63% of the nitrate, its spectrum was composed of 86% $NO_x^+$ ions with the rest composed of OA ions (O/C = 0.24), and the $NO_x^+$ ratio was within 5% of the value measured with pure $NH_4NO_3$. The rest of the $NO_x^+$ was split between an SV-OOA (28%; commonly referred to as less-oxidized OOA, LO-OOA, in the absence of volatility information; O/C: 0.41), a low-volatility OOA (LV-OOA; 9%; commonly referred to as more-oxidized OOA, MO-OOA, in the absence of volatility information; O/C: 0.74), and hydrocarbon-like OA (HOA; 0.5%) factor. The $NO_x^+$ ratio for the LV-OOA was similar to the $R_{NH4NO3}$, while the SV-OOA factor $NO_x^+$ was nearly all $NO^+$. The *RoR* for the combined non-$NH_4NO_3$ factors was 3.6–3.7 (depending on if using the PMF or pure calibration for $R_{NH4NO3}$). In that study, they explicitly separated the inorganic and organic nitrate concentration time series based on the PMF apportionment of $NO_x^+$ ions according to the $NH_4NO_3$ factor and sum of other factors, respectively. The $NH_4NO_3$ showed a highly-structured time series, on average peaking during morning (likely due in part to effects of temperature and RH) while the $pRONO_2$ was more slowly varying with a fairly flat average diurnal cycle (probably controlled by a combination of boundary layer dynamics, transport, and photochemical production). The strongly contrasting time series as well as similarity of PMF $NH_4NO_3$ $NO_x^+$ ratios to pure $NH_4NO_3$ and *RoR* of PMF $pRONO_2$ to typical values, suggests that the PMF method of separation of the two type of nitrates was likely effective.

In a study focused on $pRONO_2$ in a remote Finnish boreal forest in early spring, Kortelainen et al. (2017) used PMF to separate $pRONO_2$ and $NH_4NO_3$ from AMS measurements. Like Hao et al. (2014), they included the HR OA spectra and $NO^+$ and $NO_2^+$ ions in the PMF analysis. Of the three factors resolved, one was an $NH_4NO_3$ factor, composed of 88% $NO_x^+$ ions, with a $NO_x^+$ ratio identical to the pure $NH_4NO_3$ calibration, and accounting for 65% of the total nitrate on average. The remainder of the $NO_x^+$ was mostly apportioned to the SV-OOA (30%; a.k.a. LO-OOA, O/C: 0.44) with the remainder in the LV-OOA (~5%; a.k.a. MO-OOA, O/C: 0.87). Using the same method as Hao et al. (2014), they compute concentrations of $NH_4NO_3$ from the $NH_4NO_3$ factor time series and the $pRONO_2$ from the sum of the other factors (both OOA). The $pRONO_2$ computed from both OOA factors combined had a $NO_x^+$ ratio equivalent to a *RoR* of 3.5. For the LV-OOA spectrum all the $NO_x^+$ was only present at $NO^+$ and therefore the *RoR* for the SV-OOA $pRONO_2$ would have been 3.0. They observed large $pRONO_2$ spikes from plumes from a nearby sawmill, associated with the SV-OOA factor, that they attributed to terpene emissions from the sawmill reacting with nitrate radicals (formed from the associated elevated gaseous $NO_x$ concentrations). Otherwise, $pRONO_2$ was generally enhanced at night, attributed to BVOC reactions with nitrate radicals. They repeated the PMF analysis after removing the sawmill plumes and resolved similar spectra and time series with the same $NO_x^+$ ratios for the $NH_4NO_3$ factor and combined OOA

factors; however, the spectra for the LV-OOA factor had only $NO_2^+$ and the spectra for the SV-OOA factor had only $NO^+$. That apparent poorer resolution of $pRONO_2$ $NO_x^+$ ratio signature may have been due to the decreased signal-to-noise in the $NO_x^+$ ions associated with $pRONO_2$ in the absence of the strong $pRONO_2$-containing plumes.

Xu et al. (2015a) performed PMF on seven AMS datasets collected at different locations and seasons in the Southeast US, including the HR OA and $NO_x^+$ ions. They compare $NH_4NO_3$ and $pRONO_2$ concentrations calculated with the PMF method (as applied by Hao et al. (2014)) with the $NO_x^+$ ratio method. For the $NO_x^+$ ion ratio method, they cite *RoR*s from isoprene+$NO_3$ SOA and β-pinene+$NO_3$ SOA experiments with *RoR* of ~2 and ~4 as limits, respectively, and then compute two fixed $R_{pRONO2}$ (0.2 and 0.1) based on the average calibration $R_{NH4NO3}$ of all the studies as upper/lower bounds. Given the evidence from our analysis presented in this paper, using fixed $R_{pRONO2}$ that are not referenced to instrument-specific performance likely introduces biases in the apportionment. Such bias was likely substantial in the Xu et al. study, since the calibration $R_{NH4NO3}$ for the campaigns spanned a factor of 1.7. Therefore, for this study, the upper/lower bounds used for the different measurement campaigns represent a wide range of *RoR*s from 1.7–3.4 up to 2.9–5.8. They show that the main uncertainty in the PMF nitrate apportionment was related to the separation of the $NH_4NO_3$ factor. For the two summertime studies, no $NH_4NO_3$ factors were resolved, while for the two "transition" season studies, the $NO_x^+$ ratio ($NO_2^+/NO^+$) for the $NH_4NO_3$ factor was 30–35% lower than for the $NH_4NO_3$ calibration ratio (toward that expected for $pRONO_2$). On the other hand, for wintertime studies, the $NH_4NO_3$ factors resolved had very similar $NO_x^+$ ratios to calibration $R_{NH4NO3}$ (within 5–10%), which is not surprising since the nitrate was dominated by $NH_4NO_3$ during wintertime (as they calculated from both methods). They suggest that the $NH_4NO_3$ factors for the transition periods are likely partially contaminated with $pRONO_2$, thus causing $pRONO_2$ to be underestimated. They also show that the $NH_4NO_3$ factor spectra consisted of only 30–35% nitrate for transition periods and 60–80% in winter. The LO-OOA factors correlated with the $pRONO_2$ (calculated from the $NO_x^+$ ratio method) better than with $pNO_3$, especially for the warmer campaigns. Inspection of the spectra for the different factors shows that the LO-OOA factor had a substantially lower $NO_2^+/NO^+$ ratio than the $NH_4NO_3$ factor, in some cases near zero. Nitrate was distributed among multiple factors such as $NH_4NO_3$, HOA, COA (cooking OA), LO-OOA, OOA (but typically not IEPOX-SOA and MO-OOA) with a range of $NO_x^+$ ratios. BBOA tended to have $NO_x^+$ ratios similar to the $NH_4NO_3$ factor (in two out of three cases), which is likely due to the common presence of $NH_4NO_3$ in biomass burning plumes. Inclusion of the nitrate from the BBOA factor in the $pRONO_2$ calculation, as done in that study, may lead to an overestimate in $pRONO_2$.

For the summer and transition period campaigns, the comparison of the $NO_x^+$ ratio method and PMF method showed large differences. Given the issues with separating a $NH_4NO_3$ factor that comparison provided little insights into further understanding of the $NO_x^+$ ratio method. Consequently, the $NO_x^+$ ratio method limits was used for their analyses. On the other hand, comparisons for the wintertime data suggested that use of the fixed $R_{pRONO2}$ of 0.1 (equivalent to *RoR*=3.4) was most consistent with the PMF results (compared to using $R_{pRONO2}$=0.2, *RoR*=1.7), so for those studies they used the PMF results or a combination of PMF and the $NO_x^+$ ratio method (with $R_{pRONO2}$ of 0.1). In one of the winter studies, the performance of PMF appeared superior due to the often negative $pRONO_2$ concentration calculated with the $NO_x^+$ method — which is not unexpected when $NH_4NO_3$ dominates the nitrate (see later in this

section, and Sect. 5.2). Finally, they conducted PMF separately with only OA ions and with both OA and $NO_x^+$ ions and overall the factor spectra and time series were very similar. That suggests that inclusion of $NO_x^+$ ions did not play a large role in factor determination, beyond of course resolving $NH_4NO_3$ factors in some cases.

In a study conducted in Beijing during a biomass burning (fall) and a coal combustion influenced (winter) period, Zhang et al. (2016) conducted PMF on combined HR OA and $NO_x^+$ ion spectra. PMF was run for the two periods, separately. For both datasets, an $NH_4NO_3$ factor was resolved with spectra comprised of 84–85% $NO_x^+$ ions, and $NO_x^+$ ratios that were within 4–7% of the calibration $R_{NH4NO3}$. Those factors accounted for 77–83% of the total nitrate, on average. Ranges quoted indicate results for the two periods. Four or five other factors were resolved including BBOA or CCOA (coal combustion OA), COA, HOA, OOA (or SV-OOA and LV-OOA). They follow the method of Hao et al. (2014) and calculated concentrations of $NH_4NO_3$ and $pRONO_2$ by equating the $NO_x^+$ in the $NH_4NO_3$ factor to $NH_4NO_3$ and the sum of the $NO_x^+$ in all other factors to $pRONO_2$, yielding average $f_{pRONO2}$ of ~20% for both periods. However, that treatment appears potentially problematic since the $NO_x^+$ ratios in the spectra of the POA factors, that comprised a large amount of the calculated $pRONO_2$, are more similar to $NH_4NO_3$ than $pRONO_2$. For example, HOA has a $NO_x^+$ ratio roughly the same as the $NH_4NO_3$ factor; BBOA and CCOA appear to have only $NO_2^+$. The time series of those factors may have been tightly correlated with some $NH_4NO_3$ production, resulting in PMF apportioning part of the $NH_4NO_3$ to those factors. On the other hand, the OOA factor spectra showed $NO_x^+$ ratios much lower than $NH_4NO_3$, more consistent with $pRONO_2$. Thus, if all the $NO_x^+$ associated with the POA factors was instead assigned to $NH_4NO_3$, the average concentrations of $pRONO_2$ calculated would be a factor of ~2 and ~4 times lower for the biomass burning period and coal combustion periods, respectively.

Combined OA + $NO_x^+$ PMF (HR) was also conducted with data collected in an urban location in southern China (Shenzhen) during four separate seasons (Yu et al., 2019). During the spring, summer and fall seasons, four factors were resolved: HOA, LO-OOA, MO-OOA and a $NH_4NO_3$ factor. During the winter, the same factors and additionally BBOA and COA factors were resolved, however the $pRONO_2$ fraction was too small to accurately apportion, so their analysis focused on only the three warmer seasons. $pRONO_2$ was apportioned as the sum of all of the non-$NH_4NO_3$ factors, with the largest fraction in the LO-OOA factor for all seasons. The total $pRONO_2$ correlated best with the LO-OOA factor with stronger correlations in summer and also during nighttime, an aspect they focus on to support discussions of the importance of nighttime $pRONO_2$ formation processes. The $NO_x^+$ ratios for the $NH_4NO_3$ factors were similar to the calibration ratios (5–10% lower). The $NO_x^+$ ratios for the $pRONO_2$-apportioned factors were very low in most cases (nearly all $NO^+$) with a few cases where ratios were similar to that expected for $pRONO_2$ (see Table S4). They show that the $NO_x^+$ ion apportionment among factors was fairly insensitive (~10–20%) to changing FPEAK over a wide range (-1 to 1), and that increasing to 5 factors had little effect on overall inorganic/organic nitrate apportionment. Inorganic/organic nitrate was also apportioned with the $NO_x^+$ ratio method and compared to the PMF method. Following the method in Xu et al. (2015a), upper and lower limits (for $pRONO_2$) were estimated using *RoR*s of 2.08 and 3.99, respectively. The two methods correlated fairly well (R=0.82, 0.82, 0.72 for $pRONO_2$ and R=0.92, 0.87, 0.86 for $NH_4NO_3$, for summer, spring, autumn), using the upper limit (*RoR* 3.99). However, they showed better average quantitative agreement with the lower limit assumption (*RoR* 2.08; correlations not reported). They

suggest that may have been related to the modestly lower $NO_x^+$ ratios resolved for the $NH_4NO_3$ factors compared to the calibration ratio.

Tiitta et al. (2016) investigated the aerosol composition of logwood combustion in a chamber without aging (thus only POA) and with "dark" aging by $O_3$ (+$NO_x$, $NO_3$ radicals), and photochemical aging (UV light + HONO, thus OH/$NO_x$) (thus POA+SOA). They performed PMF on a combined AMS OA + $NO_x^+$ ions ($NO^+$, $NO_2^+$) spectra time series and observed two POA factors and three SOA factors. One of the two POA factors they identified as more associated with $pRONO_2$ (based on the contribution and ratio of $NO_x^+$ to the spectrum), however both showed prominent $NO_x^+$ peaks in the spectra and had substantially lower $NO_x^+$ ratios than the calibration $NH_4NO_3$ (equivalent *RoR* of 1.8, 2.5). Two of the SOA factors (from $O_3$/$NO_x$/$NO_3$ and from OH/$NO_x$ oxidation) showed prominent $NO_x^+$ ion peaks with ratios consistent with $pRONO_2$ (equivalent *RoR* of 2.6 and 3.1, respectively) while the other (from $O_3$ oxidation) had only a little nitrate (consisting of only $NO_2^+$). While the *RoR*s were generally similar to the *RoR* of 2.75 derived in this study, it is difficult to compute the most representative overall $pRONO_2$ ratio for this study since: 1) an $NH_4NO_3$ factor was not separated (although $NH_4$ was low in POA: ~10% of nitrate in moles), 2) other inorganic nitrate may have been present (although the authors suggest it was negligible), and 3) the average mass contributions of PMF factors are not provided in order to compute combined mass-weighted $NO_x^+$ ratios. However, with dark ($O_3$/$NO_x$/$NO_3$) or UV (OH/$NO_x$) aging, the two SOA factors with *RoR*s of 2.6 and 3.1 grew in and typically dominated the overall contribution to OA mass (individually or combined), and thus provide an approximate range for log burning SOA for our survey (i.e., Fig. 1, Table S1). In that study, $pRONO_2$ concentrations were computed using the $NO_x^+$ ratio method with the measured calibration $R_{NH4NO3}$ (0.4–0.6), and assuming a fixed $R_{pRONO2}$ of 0.1 (thus a *RoR* of 4–6).

Reyes-Villegas et al. (2018) investigated OA sources during "Bonfire Night" and surrounding periods, and $pRONO_2$ concentrations were calculated using the $NO_x^+$ ratio method with the measured calibration $R_{NH4NO3}$ (0.5), and assuming a fixed $R_{pRONO2}$ of 0.1 for $pRONO_2$ (based on the lowest observed $NO_x^+$ ratio per Kostenidou et al. (2015), thus a *RoR* of 5). Since the data were collected with a UMR AMS (C-ToF-AMS), *m/z* 30 and *m/z* 46 were treated as equivalent to $NO^+$ and $NO_2^+$, respectively, which they justify based on the low contribution of other ions at *m/z* 30 in BBOA for prior HR AMS results. Subsequently, they used the calculated $pRONO_2$ time series, together with the standard UMR OA PMF matrix, for conducting constrained PMF (ME-2; (Paatero, 1999; Canonaco et al., 2013)). They separated two factors that they identify as primary and secondary $pRONO_2$ factors. They also show similar separation into primary and secondary $pRONO_2$ based on using the regression slope of total $pRONO_2$ with the BBOA factor during an intense biomass burning event. This hybrid method may have the advantage that separating $pRONO_2$ beforehand may allow for additional separation into primary and secondary $pRONO_2$. On the other hand, prior separation with the $NO_x^+$ method (as opposed to inclusion of the $NO_x^+$ ions in the PMF) may result in loss of some information since the $NO_x^+$ ratios of the resolved $pRONO_2$-containing factors, which can be useful for evaluation, are not determined.

Kim et al. (2018) conducted PMF including signals from OA as well as nitrate, sulfate and ammonium ions for investigation of sources and chemistry of aerosol in Seoul Korea as part of KORUS-AQ. They resolve six factors including four OA (two primary, two secondary) as well two inorganic (nitrate and sulfate, both with ammonium). Both inorganic factors show relatively small contributions from OA. However, they do not attempt to interpret the nitrate contributions to the OA

factors, apportion organic/inorganic nitrate, nor provide adequate information to evaluate the $NO_x^+$ ratios resolved for different factors or factor types.

Zhu et al. (2021) apportioned nitrate using both the OA + $NO_x^+$ PMF (HR) method and the $NO_x^+$ ratio method for a study at a rural site in the North China Plains during summer. BBOA, HOA, OOA, NIA factors were separated and the NIA apportioned to inorganic nitrate and the nitrate in the other three factors to $pRONO_2$. They report that two separate OOA factors (LO-OOA and MO-OOA) were resolved when using only OA ions, but not when including the $NO_x^+$ ions. Of the nitrate apportioned to $pRONO_2$, 11.8%, 85%, and 3.2% was contributed by the HOA, BBOA, and OOA factors, respectively. The $NO_x^+$ ratios for the resolved factors appear to be similar to the $NH_4NO_3$ calibration (~0.34 vs 0.43-0.47) for NIA, much lower for BBOA (~0.02), entirely $NO^+$ for HOA and possibly entirely $NO_2^+$ for OOA. For the $NO_x^+$ ratio method, *RoR*s of 1.4-4.0, based on four literature reports, were used to compute upper and lower limits. Comparison of $pRONO_2$ resolved using the $NO_x^+$ ratio (for the upper limit assumption) vs PMF method showed a slope of 1.2 and $R^2$=0.58. Average $pRONO_2$ concentrations and $fpRONO_2$ for the PMF method were in between the $NO_x^+$ ratio method limits. $pRONO_2$ concentrations computed with the $NO_x^+$ ratio method showed the strongest correlations with the BBOA factor ($R^2$=0.50) and the poorest with the LO-OOA factor ($R^2$=0.04), which they speculate could be due to $pRONO_2$ production from biomass burning VOC reactions.

Xu et al., (2021) also apportioned nitrate using PMF including OA and nitrate ion signals for measurements conducted in the North China Plain. They compared the results to using the $NO_x^+$ ratio method and newly-proposed method using thermal denuder measurements. However, $pRONO_2$ values computed with the PMF method were much lower than the other methods (which showed reasonable agreement with each other). Citing several possible sources of uncertainty of the PMF method for that analysis, they did not focus on further assessments of the PMF method, nor use it for their scientific analysis.

**S4 Expanded details and discussion of new results for PMF separation of $pRONO_2$ and comparison to *RoR* method (briefly summarized in Sect. 5.2.2).**

We conducted PMF on the combined OA and $H_yNO_x^+$ family spectra time series for the same two flights from the SEAC[4]RS campaign as discussed in Sect. 5.1 (RF16, RF18). Unless otherwise specified, PMF analysis was conducted with unconstrained PMF using the PMF Evaluation Tool (PET, v3.01) (Ulbrich et al., 2009). Note that although all the $H_yNO_x^+$ ions that were fit were included in the PMF, the average contributions of all ions other than $NO^+$, $NO_2^+$ (and $N^+$ which is not fit and is fixed as 4% of $NO^+$ and therefore not included in PMF) were <1% of the $H_yNO_x^+$. Moreover, the apportionment of those ions did not show any clear patterns and spread fairly similarly among all factors, likely due to their low signal-to-noise. Therefore, discussions here focus only on the $NO^+$ and $NO_2^+$ ions and nitrate associated with PMF results was reported as the sum of $NO^+$ and $NO_2^+$ (plus 4% of $NO^+$).

Initially, PMF was conducted on 1-s data for both flights. $NH_4NO_3$ factors with $NO_x^+$ ratios similar to calibration $R_{NH4NO3}$ were consistently resolved. However, neither individual factors nor the re-combined non-$NH_4NO_3$ factors showed $NO_x^+$ ratios similar to those expected for $pRONO_2$ (*RoR*~2.75) and in many cases several of the factors contained only $NO^+$ or $NO_2^+$. Generally, most of the non-$NH_4NO_3$ $NO_x^+$ concentrations were apportioned to one or two factors that were associated with biogenic OA for 5–6

factors solutions. Several iterations were conducted to test if better separation of individual factors or recombined factors with $NO_x^+$ ratios representing $pRONO_2$ was possible including: always exploring number of factors up to 12, always varying FPEAK from -1 to +1 (by 0.1 increments), upweighting the $NO_x^+$ ions by a factor of 2 or 10, downweighting the $NO_x^+$ ions by a factor of 2 or 1000 (essentially to remove any weight of the $NO_x^+$ ions in determining the overall OA factor spectra, while still keeping the ions present for assignment to factor spectra), and combining the upweighting/downweighting (or no reweighting) with excluding/including large biomass burning spikes (OA>10–20 μg $m^{-3}$). None of the iterations appeared to produce solutions with substantially improved separation of $NO_x^+$ ratios reflective of $pRONO_2$. Some general behavior included: 1) upweighting $NO_x^+$ ions tended to result in splitting of the $NH_4NO_3$ factor into factors with only $NO^+$ and only $NO_2^+$ at lower threshold of number of factors, 2) downweighting $NO_x^+$ ions by a factor of 2 generally had little effect on the $NO_x^+$ ion apportionment, while aggressive downweighting (×1000) resulted in $NO_x^+$ ions being apportioned among most factors with ratios similar to the average spectrum, 3) increasingly positive FPEAK values tended to result in separate and combined non-$NH_4NO_3$ factors with increasing relative amounts of $NO^+$ (often solely $NO^+$) and the $NH_4NO_3$ factor spectrum becomes an increasingly higher fraction $NO_x^+$ ions, 4) increasingly negative FPEAK values tended to progressively shift separate and combined non-$NH_4NO_3$ factors toward $NH_4NO_3$ $NO_x^+$ ratios, and 5) excluding biomass burning spikes resulted in a more mixed/aged BBOA factor (with smaller $NO_x^+$ contribution) or no BBOA factor at all. Finally, PMF with the 1 Hz data was conducted for OA ion matrix only (excluding $H_yNO_x^+$ ions) which produced very similar factor spectra and time series, as also reported in Xu et al. (2015a).

Additionally, *constrained* PMF was conducted on the 1-s data (ME-2; Paatero, (1999)) using the SoFi software package (Canonaco et al. (2013); v.6.3). One factor was constrained to be purely $NO^+$ and $NO_2^+$ at the ratio of the nearest calibration $R_{NH4NO3}$ or the ratio for the $NH_4NO_3$ factor separated with unconstrained PMF. No downweighting and upweighting of $NO_x^+$ ions was tested, rather only excluding and including large biomass burning plumes was tested. Overall results were similar to unconstrained PMF results, except that when a $NO_x^+$ ratio higher than that resolved with unconstrained PMF was used for the constrained $NH_4NO_3$ factor, all other factors contained only $NO^+$, suggesting that the prescribed $NO_x^+$ ratio for $NH_4NO_3$ was too high. The similarity of the results was not surprising since the unconstrained PMF already appeared to separate out a reasonable $NH_4NO_3$ factor. In situations where unconstrained PMF does poorly at separating an $NH_4NO_3$ factor, like described in Xu et al (2015a) discussed above, constrained PMF with a fixed $NH_4NO_3$ factor, based on offline calibrations, may be an effective approach to better separate nitrates using PMF.

### S4.1 PMF of SEAC[4]RS RF16

Due to the inability of 1-s data to resolve separate or combined factors with $NO_x^+$ ratios similar to expected $pRONO_2$ ratios, PMF was conducted on 1-min data. Results from RF-16 are discussed here first. The main difference, compared to the 1-s analysis, was that the 1-min analysis was effective at separating factors (native individual factors and combined) with $NO_x^+$ ratios similar to a *RoR* of 2.75. Nearly the same iterations were performed as for the 1-s data (i.e. varying number of factors and FPEAK, upweighting (×2, ×10) / downweighting (×2, ×10) $NO_x^+$ ions, and including/excluding large biomass burning plumes). The effects of those iterations on the $NO_x^+$ apportionment (and ratios in profile spectra)

and overall factors were generally similar to those described above for the 1-s runs, with results similar to the 1-min base run or degraded.

### S4.1.1 Exploration of nitrate concentrations and $NO_x^+$ ratios apportionment using PMF (SEAC[4]RS RF16)

The results for the solutions for the FPEAK=0 runs with the standard $NO_x^+$ ions error weighting and unconstrained PMF (with biomass burning plumes included) are described in detail here. The results for the $NO_x^+$ ratios for different number of factors is shown in Fig. S14. For 3-factor solutions and higher, an "$NH_4NO_3$ factor" with a nearly constant $NO_x^+$ ratio ($NO_2^+/NO^+$=0.70 or $NO_2^+/NO_x^+$=0.41), and consistent with the $NH_4NO_3$ offline calibration ratios, is separated. A calibration was performed two days before RF16 and one day afterward with $NO_x^+$ ratios of 0.96 and 0.71, respectively. Given the variability in the $NO_x^+$ ratios measured in offline calibrations during the SEAC[4]RS campaign (Sects. 4 and S2, Figs. S8 and S9e), the PMF-resolved $NO_x^+$ ratio is consistent with the offline calibrations. Also for 3-factor solutions and higher, a biomass burning factor is resolved with a $NO_x^+$ ratio nearly identical to the $NH_4NO_3$ factor, up through the 7-factor solution. With increasing numbers of factors for the biomass burning factor, there is a decrease in the contribution of $NO_x^+$ to the factor spectrum as well as the $NO_x^+$ concentration attributed to the factor time series. This behavior of the $NO_x^+$ ions is consistent with nitrate aerosol in BBOA being dominantly $NH_4NO_3$ (Fig. 3), and PMF apportions it to either the $NH_4NO_3$ or BBOA factor with shifting proportions as the two factors evolve at higher factor solution numbers (e.g., the $NH_4NO_3$ factor spectrum has decreasing organic ion contributions). The remainder of the $NO_x^+$ is distributed among the non-$NH_4NO_3$/non-BBOA factors with a large range of $NO_x^+$ ratios (from all $NO^+$ to all $NO_2^+$), but with most of the $NO_x$ concentration apportioned to LO-OOA factors. However, the $NO_x^+$ ratios of the non-$NH_4NO_3$/non-BBOA factor spectra combined (mass-weighted) for 5-factor solutions and higher is fairly similar to that predicted for a $pRONO_2$ for a *RoR* of 2.75 ($NO_2^+/NO_x^+$=0.203).

The 5-factor solution was identified as the most meaningful solution due to the overall factor solution spectra and time series. The factors separated include $NH_4NO_3$, BBOA, IEPOX-SOA, LO-OOA, and MO-OOA. At higher numbers of factor solutions, in some cases factors split into very similar spectra and/or had time series that were very similar, noisy, or sometimes anticorrelated with each other at high frequency (yielding the results less meaningful). The 5-factor, FPEAK=0 solution spectra are shown in Fig. S15 and are very similar to the factors resolved for other summertime AMS measurements in the SE US (Xu et al., 2015a, 2015b) with the additional $NH_4NO_3$ factor. Like observed in other studies, the $NH_4NO_3$ factor spectrum had a substantial contribution from non-$NO_x^+$ ions. The contribution of $NO_x^+$ to the $NH_4NO_3$ spectrum increased from 19% to 36% from the 5-factor solution to the 12-factor solution (FPEAK=0; Fig. S14), and progressively with increasing FPEAK, up to 92% at FPEAK= +1.0 for the 5-factor solution (not shown). With those shifts, the $NH_4NO_3$ factor retained a similar $NO_x^+$ ratio; however, with increasing FPEAK, the $NO_x^+$ ratios for the combined non-$NH_4NO_3$ / non-BBOA factors shifted to values substantially below expected $pRONO_2$ *RoR*s and decreasing concentrations of $NO_x^+$. Also, with increasing numbers of factor solutions and FPEAK>0, the fraction of $NO_x^+$ attributed to BBOA shifted to the $NH_4NO_3$ factor. However, despite some potentially favorable, "cleaner", factor separations for the $NH_4NO_3$ and BBOA factors, the degradation in the overall factor separations and $NO_x^+$ ratios ruled out their use in this analysis.

The factor time series (including AMS OA and nitrate combined) and average mass fractions are shown in Fig. S16. In addition to the overall low concentrations associated with high altitudes (see Fig. 3), at lower altitudes, the MO-OOA tends to be least variable, the IEPOX-SOA was more variable, and the LO-OOA was the most variable of the secondary factors. Biomass burning was fairly pervasive at small concentrations at lower altitudes and showed very high spikes when intercepting a few concentrated plumes. The $NH_4NO_3$ factor times series was very different than the other factors, is similar to the $NH_4NO_3$ separated with the $NO_x^+$ method discussed in Sect. 5.1, and is further discussed below in this section.

In order to explore the robustness of the $NO_x^+$ ratios for individual and combined factors, 100 bootstrapping or starting seed iterations (Ulbrich et al., 2009) were run for the base case discussed above. Figure S17 shows histograms of the $NO_x^+$ ratios for the bootstrapping and seeding for each factor and the combined non-$NH_4NO_3$ / non-BBOA factors (therefore the three OOA/SOA factors combined). For the seeding runs, the distributions for the $NH_4NO_3$, BBOA, LO-OOA, and combined OOA/SOA factors are very narrow, while the bootstrapping distributions are a little broader for the $NH_4NO_3$ and BBOA factors and substantially broader for the LO-OOA and combined OOA/SOA factors. For both cases the BBOA was indistinguishable from the $NH_4NO_3$ and the IEPOX-SOA and MO-OOA highly variable. The ratios for the IEPOX-SOA are probably not meaningful since the amount of $NO_x^+$ in the spectra (Fig. S14) and the overall contribution to total $NO_x^+$ (Fig. S18) was very small. On the other hand, the MO-OOA spectra showed modest $NO_x^+$ contributions in the factor spectra (Fig. S15a, ~one-third that of LO-OOA) and to the average overall contribution to total $NO_x^+$ (Fig. S18a, half to two-thirds that of LO-OOA) for the bootstrapping runs (lower for seeding, Figs. S15b, S18b). The time series of the $NO_x^+$ concentration apportioned to each factor (Fig. S18a) shows that for the bootstrapping runs, the relative variability in the solution iterations for MO-OOA is quite high compared to the LO-OOA; while the variability for the total (OA + $NO_x^+$) concentrations of those factors is comparable (Fig. S16a). This may indicate that the more aged and mixed-source OOA has more variable $pRONO_2$ contribution and the PMF model of fixed factor profiles does not work well for the $NO_x^+$ ions apportionment. Nonetheless, it can be seen that the average $NO_x^+$ ratio for the combined OOA/SOA factors is similar to the LO-OOA factor (Fig. S17). For the bootstrapping, the average $NO_x^+$ ratios were equivalent to a *RoR* of 3.03 ± 0.54 for LO-OOA (for $NO_2^+/NO_x^+$ between 0.1 and 0.3) and 2.92 ± 0.43 for the combined OOA/SOA factors. For the seeding, the average $NO_x^+$ ratios were equivalent to a *RoR* of 3.00 ± 0.19 for LO-OOA and 3.19 ± 0.14 for the combined OOA/SOA factors.

It is notable that, while the $NO_x^+$ ratios for the LO-OOA factor appear to be representative of $pRONO_2$, there are several bootstrapping runs with much lower $NO_x^+$ ratios and often with only $NO^+$. This may be largely due to the limited S/N in the $NO_x^+$ ions, particularly the lower $NO_2^+$, limiting the robustness of apportionment of those ions to and between OOA factors. However, the apportionment of $NO_x^+$ when considering the combined SOA/OOA factors appears to be substantially improved, as seen by the narrower $NO_x^+$ ratio distributions (Fig. S17) and variability in $NO_x^+$ concentrations time series (Fig. 4 vs Fig. S18).

In order to investigate the relationship between the $NO_x^+$ ratio in the factor profile and $NO_x^+$ concentrations apportioned to a factor time series, $NO_x^+$ concentrations for the LO-OOA from bootstrapping were compared for different $NO_x^+$ ratio ranges. Regression slopes were compared between

the average concentrations using all solutions to those when $NO_2^+/NO_x^+ < 0.1$ or $\geq 0.1$ (which were mostly ~0 and near 0.2, respectively; see Fig. S17). The scatterplots and regression fits are shown in Fig. S19. For $NO_2^+/NO_x^+ < 0.1$ ($\geq 0.1$), $NO_x^+$ concentrations were 69% (123%) that of the average of all solutions. Thus, the low $NO_x^+$ ratio solutions were 56% of the high $NO_x^+$ ratio solutions. This suggests that when the $NO_x^+$ ratio falls well below the expected $pRONO_2$ *RoR*, more total $NO_x^+$ signal is "lost" than just the $NO_2^+$, since a loss of only $NO_2^+$ would yield a value only ~20% lower (i.e. $NO_2^+/NO_x^+ = 0$ vs 0.2), not 44% lower. This exercise suggests that the $NO_x^+$ ratios resolved for factors may be indicative of substantial changes in nitrate apportionment. Consequently, care should be taken when interpreting individual or combined factor apportionment when $NO_x^+$ ratios diverge substantially from expected $pRONO_2$ ratios. This highlights the importance of exploring the variability and robustness of the resolved $NO_x^+$ ratios and apportionment (e.g., bootstrapping, FPEAK). In this particular example, a case could be made that nitrate apportionment to the LO-OOA factor is better represented by the average of the solutions with $NO_x^+$ ratios in an acceptable range (e.g., $NO_2^+/NO_x^+ > 0.1$ or 0.15–0.25).

While the average $NO_x^+$ ratios and the concentrations of nitrate apportioned to $pRONO_2$ vs $NH_4NO_3$ for bootstrapping vs seeding (Fig. S20) is very similar, by all metrics (Figs. S15, S16, S17, S18, S20), the variability of the seeded runs was substantially smaller than for the bootstrapping. This indicates that for this dataset, the starting point of the PMF algorithm had little influence on the resolved solutions. On the other hand, the substantial variability in the bootstrapping results suggests that those may be a better metric of overall robustness. Therefore, we focus the remainder of discussions and results on averages and variability from the bootstrapping analysis.

### S4.1.2 Comparison of PMF method vs *RoR* method for apportionment (SEAC[4]RS RF16)

Comparisons of $NH_4NO_3$ and $pRONO_2$ concentrations using the *RoR* and PMF methods are shown in Fig. 4. As discussed above, for the PMF method $NH_4NO_3$ was calculated as the sum of the $NH_4NO_3$ and BBOA factors and $pRONO_2$ was calculated as the sum of the three SOA factors (LO-OOA, MO-OOA, IEPOX-SOA). Overall, the $NH_4NO_3$ agrees very well between the two methods, which is likely in large part due to the fact that $NH_4NO_3$ often dominated the nitrate. On average, the apportionment of $pRONO_2$ is similar but with notable differences. For much of the flight, $NH_4NO_3$ dominates the $pNO_3$ (~90%), and consequently the $pRONO_2$ computed with the $NO_x^+$ ratio method tends to be fairly noisy due to the measured $NO_x^+$ ratio being near or exceeding the pure $NH_4NO_3$ ratio line. Under those conditions, small variability in the measurement or uncertainties in the bounding ratios can lead to large relative uncertainties in $pRONO_2$. In contrast, under those conditions the PMF-computed $pRONO_2$ concentrations appear to be less noisy in terms of the variability of the averages and standard deviations from the bootstrapping (Fig. 4). This may be due to the additional information and leverage that the other OA ions exert on the separation of the SOA factors which are not strongly affected by the large relative contributions of the $NH_4NO_3$ $NO_x^+$ ions. Similar behavior in $NH_4NO_3$ calculated with the $NO_x^+$ ratios occurs when $pRONO_2 >> NH_4NO_3$, such as around 18:45 during this flight (although not easily visible due to scaling in Fig. 4, top). Large relative variabilities in $pRONO_2$ calculated with the $NO_x^+$ ratios are also apparent when $pNO_3$ is very low, since the $NO_x^+$ ratio noise blows up. In the time series shown in Fig. 4, those points are screened as below detection limit (indicated by different shading) as determined by the detection limit of the $NO_x^+$ ratio. However, those points are mostly below the $pNO_3$ detection limit

and thus still provide useful constraints on both the $pRONO_2$ and $NH_4NO_3$ concentrations, despite the large uncertainties in relative apportionment. During those periods, the PMF-apportioned concentrations show much less variability than the $NO_x^+$ ratio method and are near zero.

The scatterplots in Fig. 4 (bottom left) shows the correlations and regression fits for both nitrate types derived by the two methods. The slope for $NH_4NO_3$ is near unity (1.04) and highly correlated ($R^2$=0.995). For $pRONO_2$, the slopes vary, depending on the fitting method (ODR vs non-ODR), with slopes of 0.86 and 1.30 and $R^2$ = 0.49. The non-ODR fit may be more appropriate if uncertainties in the $NO_x^+$ method dominated over those for PMF. Limiting to data only when $f_{pRONO2} > 0.3$, the slopes are 1.11 and 1.42 (ODR, non-ODR) with an improved correlation ($R^2$ = 0.68). Figure 4 (bottom right) shows the PMF-computed $pRONO_2$ vs the TD-LIF Tot-$RONO_2$, similar to Fig. 3 (bottom left) with the $NO_x^+$ ratio method. The slope is very similar to when using the $NO_x^+$ ratio method, but the correlation is improved (0.72 vs 0.49) or similar to when the $NO_x^+$ ratios method was screened for $f_{pRONO2} > 0.3$ (0.76 vs 0.69). This suggests that the methods perform similarly when $NH_4NO_3$ does not dominate while the PMF method performs better when $NH_4NO_3$ dominates (in this case). However, it is not possible to assess the true accuracy of the PMF separation without an independent determination of $pRONO_2$. While the noise for the PMF method generally appears to be lower than for the $NO_x^+$ method, there may be factors dampening the noise or other biases such as the fact that the PMF model, by nature, apportions a fixed nitrate/OA ratio to each factor. A fixed chemical composition is an approximation since the chemical composition of sources may evolve (such as hydrolysis loss of $pRONO_2$ or gas-particle partitioning) or variable in different air masses sampled. In contrast, the $NO_x^+$ ratio method would not be prone to such effects since it only relies on the information contained in the nitrate ions time series. Scatterplots showing the same information as Fig. 4, except using the seeding results are shown in Fig. S21 with very similar results.

### S4.2 PMF of SEAC[4]RS RF18

Results from a similar analysis and comparisons for the SEAC[4]RS RF18 flight (see Sect. 5.1) are shown in Figs. S22–S28. Overall, the results are similar, with similar factors resolved and similar comparisons between the PMF method and $NO_x^+$ method as well as compared to the Tot-$RONO_2$. However, there were a handful of notable differences in the analysis and results, compared to RF16. For example, the MO-OOA factor comprised a substantially smaller fraction of both OA and $NO_x^+$ concentrations at lower altitudes when OA concentrations were higher, but generally larger contributions when OA was lowest (Fig. S26, S27 vs S16, S18). Overall, $NH_4NO_3$ tended to comprise a smaller fraction and $pRONO_2$ a larger fraction of the nitrate compared to RF16 (Fig. S27 vs S18). Unlike RF16, for RF18 MO-OOA $NO_x^+$ ratios for the bootstrapping grouped around expected $pRONO_2$ ratios (Fig. S25 vs S17). Also unlike RF16, the IEPOX-SOA factor spectrum for RF18 contained a significant $NO_x^+$ contribution (Fig. S24 vs S15a; ~20% that of LO-OOA or MO-OOA, compared to 1% and 4% for RF16), and comprised a substantial fraction of the overall $NO_x^+$ apportionment (Fig. S27 vs S18a; 5–9% compared to 0.3–0.4% for RF16 depending on weighting). While organic nitrate formation is not expected for the low-NO conditions that form IEPOX-SOA, this could be due to coincident presence or formation of isoprene, monoterpene or other VOC-derived nitrates in the presence of some $NO_x$ that PMF cannot separate perfectly. The fact that a lot of the concentration variability is driven by aircraft movement in and out of

the boundary and residual layers may hinder clean separation of some nuances of co-located sources. Finally, inspection of the $NO_x^+$ ratios for different numbers of factors resolved (Fig. S23) and bootstrapping results for the 5-factor solution (Fig. S25) for different FPEAK values showed that using FPEAK = -0.1 produced $NO_x^+$ ratios for the OOA factors much more representative of $pRONO_2$, thus all analysis and comparisons were conducted with the FPEAK = -0.1 (and 5-factor, bootstrapped) solution.

Some trends and statistics for the RF18 analysis that were reported for RF16 are summarized here. For the bootstrapping (FPEAK = -0.1), the average $NO_x^+$ ratios were equivalent to a *RoR* of 2.83 ± 0.64 for LO-OOA and 2.96 ± 0.28 for the combined OOA/SOA factor. As done for RF16, the concentrations of $NO_x^+$ apportionment were compared for bootstrap results when $NO_x^+$ ratios were low/high for the LO-OOA factor. This test was done for FPEAK=0 (rather than FPEAK = -0.1, which was selected for most analyses), since it has a broad range of $NO_x^+$ ratios (unlike FPEAK = -0.1, which is fairly narrow) — see Fig. S25. Using the same high/low criteria ($NO_2^+/NO_x^+$ ≥0.1 vs <0.1 for FPEAK = 0, on average 0.041 vs 0.134), resulted in $NO_x^+$ concentrations for low $NO_x^+$ ratios on average 74% that for high $NO_x^+$ ratios (Fig. S28). Thus, like for RF16, this suggests that solutions resolving lower $NO_x^+$ ratios tend to apportion substantially even less $NO_x^+$ concentration than the amount from the reduction of $NO_2^+$ signal apportionment alone (26% vs ~10%). Again, this results suggests that PMF solutions that do not show $NO_x^+$ ratios expected for $pRONO_2$ may also correspond to time series with biased concentrations, and emphasizes the importance of evaluating the variability and robustness of solutions. In this case, we chose the FPEAK = -0.1 solution instead, due to the narrower distributions in $NO_x^+$ ratios and values consistent with expected $pRONO_2$ ratios for LO-OOA, MO-OOA, and combined OOA/SOA.

Like for RF16, the $NH_4NO_3$ factor progressively "cleans up" with increasingly positive FPEAK. The fraction of the profile spectrum that is $NO_x^+$ ions increases from 21% at FPEAK= -0.1 to 88% at FPEAK= +1.0. However, at higher FPEAK (≥0.2–0.3) overall factor separation degrades, in addition to the loss of $pRONO_2$ $NO_x^+$ ratio signature at FPEAK other than -0.1 (see above and Fig. S25). Also, above FPEAK= +0.1, the amount of $NO_x^+$ concentration assigned to the sum of OOA factors progressively decreases substantially (from 23% at FPEAK= -0.1 to 9% at +1.0). In contrast, going to higher numbers of factors (for FPEAK= -0.1), the fraction of the profile spectra comprised by $NO_x^+$ ions for the $NH_4NO_3$ factor changes little, from 21% at 5 factors to no more than 27% at higher factor numbers (Fig. S23). Moreover, increasing factor numbers does not substantially change the amount of total $NO_x^+$ concentrations apportioned to $NH_4NO_3$ or non-$NH_4NO_3$ / non-BBOA factors. Notably, the $NH_4NO_3$ factor does tend to retain the same $NO_x^+$ ratio with these large variations in FPEAK and number of factors. However, these results suggest that increasing FPEAK to yield "cleaner" $NH_4NO_3$ factors does not appear to be an approach that yields anything meaningful, at least for these datasets. Also, the $NH_4NO_3$ factor resolved had a $NO_x^+$ ratio of 0.55, a bit lower than the calibration performed most closely in time (0.63), the day following the flight after the instrument was turned off and back on. Since the $NH_4NO_3$ calibration $NO_x^+$ ratios were highly variable over this campaign (see Sects. 4 and S2, Figs. S8 and S9e), we do not interpret this difference as meaningful, and thus use the PMF-resolved value for $NO_x^+$ ratio method apportionment for this flight.

## S5 Detailed discussion of comparisons of $pRONO_2$ quantification with AMS and other instruments in the lab and field

In this section, quantitative comparisons of $pRONO_2$ concentrations, as measured by AMS vs other instrumental methods (alternate AMS-based methods, FTIR, TD-LIF/CRDS/CAPS, and FIGAERO-CIMS) are discussed. A few comparisons between non-AMS methods are also discussed. A brief summary is provided in Sect. 5.3 and key details summarized in Table S5.

Fry et al. (2013) compared bulk $pRONO_2$ concentrations measured by AMS ($NO_x^+$ ratio apportionment and *RoR*=2.25 per Farmer et al. (2010)) with those measured by TD-LIF (with a gas-phase denuder; Rollins et al. (2010b)) during the BEACHON-RoMBAS campaign. The two methods showed good agreement with a slope (AMS vs TD-LIF) of 0.94–1.16 (depending on averaging method) and fair correlation ($R^2$ = 0.53). The nitrate was typically dominated by $pRONO_2$; however, they show good inorganic/organic nitrate separation (as demonstrated by close tracking of $pRONO_2$) during an inorganic event.

In contrast, during the SOAS campaign, comparison of four different $pRONO_2$ measurements (AMS $NO_x^+$ ratio, AMS $pNO_3$ minus PILS inorganic nitrate, FIGAERO CIMS with iodide ionization, and gas-denuded TD-LIF) showed some substantial differences (Lee et al., 2016). The sum of the speciated CIMS $pRONO_2$ (nitrate functional groups only, 88 compounds) was correlated with the two bulk AMS-based methods ($R^2$=0.52, 0.67) with slopes of 0.63 and 0.90. However, the TD-LIF measurements were ~2–4 times higher than the AMS-based methods (depending on the period; i.e., TD-LIF/AMS $NO_x^+$ method slope 2.2 or 4.3, both periods with $R^2$=0.74). Possible explanations for the substantial differences between the AMS-based vs TD-LIF methods were investigated (e.g., particle size cut differences, gas-denuder breakthrough, bias in AMS collection efficiency or overall quantification); however, no plausible cause has yet been identified. Importantly, the AMS $pRONO_2$ measurements showed that particle nitrate during SOAS was dominated by $pRONO_2$; therefore, these large differences could not be related to the inorganic/organic apportionment — i.e., assuming all AMS nitrate was $pRONO_2$ would only slightly close the gap. A later modeling study of organic nitrates in the SE US estimated that $pRONO_2$ contributed ~20% to the total $RONO_2$ during SOAS (Zare et al., 2019), which is more consistent with the $pRONO_2$ concentrations measured by the AMS instruments (Ayres et al., 2015).

Similar measurements to Lee et al. (2016), of highly functionalized $pRONO_2$ with FIGAERO CIMS (iodide ionization) as well as with AMS and the $NO_x^+$ ratio method (using a fixed $R_{pRONO2}$ of 0.1), were conducted in rural Germany (Huang et al., 2019). It was shown that the FIGAERO $pRONO_2$ measurements accounted for 47% of the AMS $pRONO_2$ (R=0.52), similar to albeit a bit lower than the equivalent Lee et al. comparison. They note that their CIMS concentrations should be considered lower limits due to their calibration method used since: 1) a collisional limit sensitivity from literature was applied which itself is an upper limit on sensitivity, and 2) they suspected the collision limit applied may have also been too high for their instrument. Additionally, it appears that the mass concentrations of the total organic nitrate molecules measured by the CIMS (not just the nitrate functionality, as was done for Lee et al. (2016)) were compared to the AMS nitrate group only mass concentrations. Therefore, given that the average molecular weight of the CIMS-measured nitrates were ~250 g $mol^{-1}$, and di-nitrates were a small contribution, the CIMS-measured nitrate functional group mass concentration, may have been ~4

times smaller (250/62) than the total molecular concentration that was compared to AMS (thus accounting for ~10% of the AMS organic nitrate). Chen et al. (2020) also reported comparisons of FIGAERO-CIMS ($I^-$) and AMS field measurements (SE US). The fractions of the total organic signal that were organic nitrate molecules were compared for each respective instrument, yielding 12.3±10.8% for the CIMS and 5-18% for the AMS. Assumptions required for the comparison included the average molecular weight of the AMS-measured organic nitrate molecules (220 g $mol^{-1}$), $R_{pRONO2}$ fixed at 0.1-0.2, and constant sensitivity of all organic nitrates measured by CIMS. Additionally, the average N/C ratios for the CIMS total signal was shown to be in the center of the range estimated from the AMS total organic signal (including nitrate functional groups) across the diurnal cycle. However, comparison of the estimated O/C and H/C elemental ratios showed substantial differences (~10-20%), likely reflecting bias in the CIMS toward more oxygenated compounds.

Comparisons of AMS vs TD-LIF $pRONO_2$ observations in the boundary layer during the KORUS-AQ aircraft campaign are reported in Kenagy et al. (2021). TD-LIF measurements used in the analysis and comparisons were corrected for particle losses in the aircraft sampling inlet, including charge losses to non-conductive tubing as well as inertial and diffusion losses. Net inlet losses were typically ~20-60% by aerosol volume. AMS measurements used in the analysis and comparisons were screened for $f_{pRONO2}$>0.2 due to higher uncertainty and noise under those conditions. The inlet sampling corrections to the TD-LIF showed substantial improvements in agreement of the two methods, with an AMS vs TD-LIF slope without corrections, 3.12, decreasing to 1.89 after corrections.

Quantitative comparison of $pRONO_2$ concentrations formed during chamber experiments investigating SOA formed from reaction of terpenes (α-pinene and Δ-3-carene) with nitrate radicals (those described in Sect. S1.2) as measured by AMS and (gas-denuded) TD-CRDS (a similar method to TD-LIF but with cavity ring-down spectroscopy $NO_2$ detection (Paul et al., 2009; Thieser et al., 2016)) showed good average agreement, albeit with substantial scatter (Keehan et al., 2020) (AMS vs TD-CRDS slope = 1.06-1.14; $R^2$ = 0.73). In that analysis, specific *RoR* were determined for the α-pinene and Δ-3-carene SOA (3.12, 3.78, cf. Table S1 here) from dry experiments and used for apportionment, since experiments with elevated RH showed possible indications of inorganic nitrate formation (e.g. $NH_3$ gas from chamber walls reacting with $HNO_3$ generated from $N_2O_5$ injections). However, the apportionment of possible inorganic nitrate had a relatively small effect (~10%) on the average comparison slope (and slightly improved correlation), since $pRONO_2$ dominated the nitrate overall. Similarly, Eris et al. (2018) compared bulk $pRONO_2$ concentrations (for SOA formed from isoprene and monoterpenes reaction with OH, $O_3$, $NO_3$ in a chamber) measured with AMS and gas-denuded TD-CAPS (Cavity Attenuated Phase Shift Spectroscopy for $NO_2$ detection) and reported "quantitative agreement" which we assume to mean within combined instrumental uncertainties or within ~50%.

Bruns et al. (2010) compared the N/H elemental ratios as measured by FTIR vs AMS for SOA formed in a chamber from reaction of isoprene and monoterpenes with nitrate radicals and found ratios 3–4 times higher N/H for FTIR. They discuss some possible explanations for the difference including: 1) ionization of intact organic nitrates producing an organic cations and neutral $NO_x$ fragments in the AMS, 2) evaporation of organic nitrate in the vacuum region of the AMS, or 3) artifacts from uptake of gas-phase organic nitrates as collected organic mass increases or volatilization of organic products that don't contain organic nitrates during collection for FTIR analysis (on an impactor). While such

cation/neutral bias during electron ionization (EI) (1) may occur (as they show by performing AMS software-based elemental analysis on the NIST EI spectrum of hydroxy ethyl nitrate and compute a N/H 2.5 times lower than the elemental formula), the thermal lability of organic nitrates and propensity to decompose to $NO_2$ during vaporization in the AMS (as also pointed out by those authors) suggests that this would not have a major effect on organic nitrate quantification. Regarding large losses due to evaporation in the AMS vacuum chamber (2), such effects are likely too slow to be significant. For example, Shingler et al. (2016) show that for liquid particles, losses as large as half the mass are expected to occur only for the highest volatility organic compounds expected to be present in OA on timescales of at least hundreds of milliseconds. In the AMS, the particles spend only a few milliseconds in the vacuum chamber prior to vaporization. The authors suggest the FTIR collection artifacts (3) did not appear to be a major factor based on an observation of invariant nitrate/carbonyl functional group ratios (as measured by FTIR) over a 2-hour collection period where SOA concentration varied 20-fold on the collection impactor.

Another possibility that may lead to an underestimate in the N/H (or N/C) ratio when N is dominated by organic nitrates, is application of an incorrect relative ionization efficiency for the organic component. While application of an RIE of 1.4 is recommended for ambient OA quantification, RIE for single species and simpler mixtures can be substantially larger (more than a factor of 2) (Jimenez et al., 2016; Xu et al., 2018). Thus, a factor of two larger RIE for organic and unchanged RIE for nitrate (assuming it largely decomposes prior to ionization) would lead to a factor of two underestimation of N/H, N/C, or nitrate fraction of OA if applying the default ambient RIE (which most likely was done for that study). Such an effect could explain their agreement of N/H between FTIR and AMS for the standard compound they analyzed (isosorbide 5-mononitrate, $C_6H_9NO_6$) if the ionization efficiency of that compound is similar to that of ambient OA.

Liu et al. (2012) showed a comparison of $pRONO_2$ as measured by FTIR vs AMS for SOA formed in a chamber experiment from photooxidation of 1,2,4-trimethylbenzene (TMB), with FTIR measuring 2.28 times AMS ($R^2$=0.98, with no dependence on humidity (for <1–85% RH). Speculating on the FTIR vs AMS differences, they state: “Possible explanation for the large slope include: (1) ON [organic nitrate] groups are fragmented by electron impact ionization and do not have a uniform probability of carrying the positive charge necessary for detection (Bruns et al., 2010), or the related point (2) the true relative ionization efficiency of ON molecules is lower than the value of 1.1 used to calculate nitrate mass, or (3) ON groups dissociated (during ionization processes) to form other nitrogen-containing fragments (e.g., $C_xH_yO_zN^+$ in Figure 2b) that were small (compared to $NO^+$ and $NO_2^+$) and caused the scatter in Figure 2c.” Possibility 1 is discussed above and possibility 3 would not lead to large average differences. A comparison of the RIE for nitrate from $pRONO_2$ compounds vs $NH_4NO_3$ has not been directly tested (beyond the more convoluted instrument comparisons discussed in this section). However, again under the assumption that $RONO_2$ largely decomposes to $NO_2$ (and NO) upon vaporization, a much lower ionization efficiency does not seem likely. Possible reasons for a positive bias in FTIR quantification was not discussed. While a good agreement between total OA measured by FTIR and SMPS (R=0.9, slope 1.05) was observed, a similar comparison of AMS and SMPS is not reported (nor discussion of AMS calibration, collection efficiency applied, etc.), so it is difficult to assess the general quantification accuracy of AMS measurements within a factor of 2 during those experiments.

During a study in Bakersfield California, measurements of $pRONO_2$ using FTIR and (gas-denuded) TD-LIF were compared (Rollins et al., 2013). After applying an average correction factor for differences in particle sampling size cuts (1.0/2.5 μm = 0.83, based on FTIR OA measurements), the TD-LIF/FTIR linear fit showed a slope of 1.38 and offset of +0.068 μg $m^{-3}$ (R=0.72). For concentrations measured (<0.2 μg $m^{-3}$), the offset was relatively large such that the average TD-LIF/FTIR ratio was substantially >2 and a fit line constrained through the origin was probably >2. As the authors note, possible reasons for the differences were scrutinized, yet the differences remain unexplained.

**Abbreviations/Glossary/Nomenclature**

| | |
|---|---|
| $NH_{4\_Bal}$ | Ammonium Balance = molar ratio of $NH_4/(NO_3+2SO_4)$ |
| ACSM | Aerosol Chemical Speciation Monitor (Aerodyne). UMR and lower sensitivity, typically used for routine or long-term air quality monitoring. Uses quadrupole MS (sometimes referred to as Q-ACSM). |
| AMS | Aerosol Mass Spectrometer. Refers to Aerodyne models cable of particle size-resolved chemical measurements. |
| BBOA | Biomass Burning OA (separated by PMF) |
| BVOC | Biogenic Volatile Organic Compounds; e.g., isoprene, monoterpenes |
| CIMS | Chemical Ionization Mass Spectrometry |
| Closed | Mode or signal observed in AMS when particle beam is blocked (background) |
| COA | Cooking OA (separated by PMF) |
| Collection Efficiency (CE) | The efficiency that particles are detected in the AMS (0–1). The dominant factor in reduced CE is due to particle bounce at the vaporizer. |
| C-ToF (AMS) | Compact Time-of-Flight AMS (Aerodyne). Nominal spectral resolution of ~600 and typically used only for UMR analysis. |
| Diff | Raw "closed" spectra subtracted from "open" spectra. HR fitting done after raw spectra subtraction. |
| EI | Electron Ionization (formally known as Electron Impact ionization) |
| FIGAERO | Filter Inlet for Gases and AEROsols. |
| FMS mode | Fast MS mode. Data acquisition mode where the particle beam is unblocked for an extended period (1+ minutes) to collect high-frequency data (1–10 Hz) and |

| | |
|---|---|
| | backgrounds (closed) measured intermittently for short periods. Used for aircraft studies discussed here. |
| $f_{NH4NO3}$ | $NH_4NO_3/pNO_3$. I.e. fraction of AMS nitrate that is apportioned to particle-phase ammonium nitrate. Also denoted as $NH_4NO_{3,frac}$ in a few places per previous work. See Eq. 3 |
| $f_{pRONO2}$ | $pRONO_2/pNO_3$. I.e. fraction of AMS nitrate that is apportioned to particle-phase organic nitrate. Also denoted as $RONO_{2,frac}$ in other studies. See Eqs. 1,2 |
| HOA | Hydrocarbon-like OA (separated by PMF) |
| HR | High-Resolution. Refers to AMS instrument models and peak-fitting with nominal spectral resolutions of ~2000–4000 (see "V-mode" and "W-mode"). |
| HR-AMS, HR-ToF-AMS | High-Resolution (Time-of-Flight) AMS (Aerodyne) |
| IE | Ionization Efficiency. The efficiency of detection of ions from particles that vaporize on the AMS vaporizer. |
| IEPOX-SOA | IEPOX-derived SOA (separated by PMF). From low-NO oxidation of isoprene. |
| LO-OOA | Less-oxidized OOA (separated by PMF), sometimes equated with SV-OOA. |
| LV-OOA | Low-Volatility OOA (separated by PMF), sometimes equated with MO-OOA. |
| ME-2 | Multi-linear Engine (2). PMF solver algorithm where factor time series and profiles can be constrained. Implemented with SoFi Software. |
| MO-OOA | More-oxidized OOA (separated by PMF), sometimes equated with LV-OOA. |
| MS mode | "Mass-Spec" mode. Data acquisition mode where particle beam is alternatively blocked (closed mode) and transmitted (open mode), typically every 5–10 s, in order to quantify non-size-resolved chemical composition. |
| $NH_4NO_3$ | Always refers to particle-phase ammonium nitrate here. |
| $NO^+$, *m/z* 30 | Aerosol signal from $NO^+$, sometimes approximated from *m/z* 30 for UMR. |
| $NO_2^+$, *m/z* 46 | Aerosol signal from $NO_2^+$, sometimes approximated from *m/z* 46 for UMR. |
| $NO_x^+$ ratio | Ratio of aerosol-phase $NO_2^+$ and $NO^+$. Unless otherwise specified, the convention used here is always $NO_2^+/NO^+$. |
| O/C, H/C | Oxygen-to-carbon and hydrogen-to-carbon ratios for OA estimated with AMS. |
| OA | Organic Aerosol (particle-phase organic species) |

| | |
|---|---|
| OFR | Oxidation Flow Reactor. Flow reactor where gas/particle sample flow exposed to oxidants. Processed ambient outflow sampled by AMS here. |
| OmC | "Open" minus "Closed" signal (HR fitting done first and then subtracted). |
| OOA | Oxygenated OA (separated by PMF) |
| Open | Mode or signal observed in AMS when particle beam is not blocked. |
| PMF | Positive Matrix Factorization. Implemented with "PET" software. |
| $pRONO_2$ | Particle-phase organic nitrate. Concentrations here are expressed in mass concentrations of the nitrate functional group ($-ONO_2$) only. |
| PToF mode | Particle-time-of-flight mode. Size-resolved chemical sampling mode. |
| Q-AMS | Quadrupole AMS (UMR). |
| $R_{ambient}$ | $NO_x^+$ ratio measured for ambient mixed nitrate aerosol sampled with AMS. Applied in Eq. 1. Also referred to as $R_{meas}$ or $R_{obs}$ (measured, observed) in other studies. |
| $R_{NH4NO3}$ | $NO_x^+$ ratio observed for calibration with pure $NH_4NO_3$. Applied in Eq. 1. |
| RIE | Relative Ionization Efficiency. The relative detection efficiency of a chemical species, referenced to that of nitrate (measure with $NH_4NO_3$ aerosol). |
| $RONO_2$ | Organic nitrate (any organic molecule containing a nitrate functional group) |
| *RoR* | "Ratio-of-Ratios". $R_{NH4NO3}/R_{pRONO2}$ for $pRONO_2$ (or more generally can be relative ratios of any other nitrate pairs). |
| $R_{pRONO2}$ | $NO_x^+$ ratio observed for pure $pRONO_2$. Applied in Eq. 1. Measured in isolated studies or inferred as $R_{NH4NO3}/RoR$. Also referred to as $R_{RONO2}$ in other studies. |
| S/N | Signal-to-Noise ratio |
| SOA | Secondary Organic Aerosol |
| SV-OOA | Semi-Volatile OOA (separated by PMF), sometimes equated with LO-OOA |
| TD-LIF | Thermal Dissociation – Laser Induced Fluorescence. Different classes of reactive nitrogen gas/aerosol (such as $RONO_2$) are separately quantified by selectively thermally decomposing molecules to $NO_2$ (which is detected). |
| ToF-ACSM | Time-of-Flight Aerosol Chemical Speciation Monitor. Higher sensitivity and spectral resolution (~600) than Q-ACSM. Uses compact ToF (Aerodyne). |

| | |
|---|---|
| $pNO_3$ | Total nitrate (concentration) quantified by AMS. |
| Tot-$RONO_2$ | Total $RONO_2$ concentration (gas + particle). Measured by TD-LIF here. |
| UMR | Unit-Mass-Resolution. Refers to AMS (or related) instrument models (or peak-fitting analysis) where only unit *m/z* can be (or are) resolved. |
| V-mode | Mode for HR-ToF-AMS with spectral resolution of ~2000 (higher-sensitivity) |
| W-mode | Mode for HR-ToF-AMS with spectral resolution of ~4000 (lower-sensitivity) |

DC3, SEAC$^4$RS, KORUS-AQ (or KORUS), SOAR, MILAGRO, DAURE, BEACHON-RoMBAS (or BEACHON), SOAS, GoAmazon (IOP1, IOP2) are field campaigns used in this analysis (see Sect. S1.1, Table S3).

780

**SI Tables**

**Table S1.** Summary of sources, values, calculations, and details for $pRONO_2$ and $NH_4NO_3$ $NO_x^+$ ratios and Ratio-of-Ratios included in Fig. 1. Numbers in bold indicate values directly reported in literature sources (or from this study) while otherwise the values were calculated here. Details relevant to specific calculations (beyond direct calculations using other numbers in each row of the table) are described in footnotes. For completeness, footnote "ee" lists a few earlier published studies that were not included in the characterization of the *RoR* in this study and the rationale (which includes the Bruns et al. (2010) data which are shown in Fig. 1 and this table but not included in averages or correlations).

| **$pRONO_2$ Source** | **Reference** | ***RoR*** | ***RoR* Uncertainty** | **$pRONO_2$** | | **$NH_4NO_3$** | |
|---|---|---|---|---|---|---|---|
| | | | | **$NO_2^+/NO^+$** | **$NO^+/NO_2^+$** | **$NO_2^+/NO^+$** | **$NO^+/NO_2^+$** |
| ***Chamber SOA*** | | | | | | | |
| Δ-3-carene SOA ($NO_3$) | Bruns et al. (2010) | 5.8 | 2.2[g] | 0.071 | **14** | 0.42 | **2.4** |
| Δ-3-carene SOA ($NO_3$) (2014[y]) | Kang et al. (2016) | **3.31** | **0.17[h]** | **0.184** | **5.4** | **0.61** | **1.64** |
| Δ-3-carene SOA ($NO_3$) (2015[y]) | Kang et al. (2016) | **3.12** | N/A | **0.263** | **3.8** | **0.82** | **1.22** |
| Δ-3-carene SOA ($NO_3$) (2015[y], high OA[z]) | Kang et al. (2016) | **2.56** | **0.33[i]** | **0.39** | **2.56** | **1.00** | **1.00** |
| α-pinene SOA ($NO_3$) | Bruns et al. (2010) | 4.6 | 1.6[g] | 0.091 | **11** | 0.42 | **2.4** |
| α-pinene SOA ($NO_3$) (2014[y]) | Kang et al. (2016) | **3.75** | **0.45[j]** | **0.162** | **6.2** | **0.61** | **1.64** |
| α-pinene SOA ($NO_3$) (2015[y]) | Kang et al. (2016) | **3.78** | N/A | **0.217** | **4.6** | **0.82** | **1.22** |
| α-pinene SOA ($NO_3$) (2015[y], high OA[aa]) | Kang et al. (2016) | **3.05** | **0.45[k]** | **0.269** | **3.71** | **1.00** | **1.00** |
| α-pinene SOA ($NO_3$) ($RO_2$+$NO_3$) | Takeuchi et al. (2019) | **2.86** | 0.19[l] | 0.118 | **8.44** | 0.337 | **2.97** |
| α-pinene SOA ($NO_3$) ($RO_2$+$HO_2$) | Takeuchi et al. (2019) | **3.07** | N/A | 0.116 | **8.60** | 0.357 | **2.80** |
| α-pinene SOA ($OH/NO_x$) | Takeuchi et al. (2019) | **2.12** | 0.065[m] | 0.167 | **6.00** | 0.353 | **2.84** |
| β-pinene SOA ($NO_3$) | Fry et al. (2009) | 3.70 | N/A | 0.100 | **10** | **0.37** | 2.7 |
| β-pinene SOA ($NO_3$) | Bruns et al. (2010) | 4.2 | 1.0[g] | 0.10 | **10** | 0.42 | **2.4** |

| | | | | | | | |
|---|---|---|---|---|---|---|---|
| β-pinene SOA ($NO_3$) ($RO_2$+$NO_3$) | Boyd et al. (2015) | **3.2** | N/A | 0.154 | **6.5** | 0.49 | 2.03 |
| β-pinene SOA ($NO_3$) ($RO_2$+$HO_2$) | Boyd et al. (2015) | **4.8** | N/A | 0.116 | **8.6** | 0.56 | 1.79 |
| β-pinene SOA ($NO_3$) ($RO_2$+$NO_3$) | Takeuchi et al. (2019) | **2.48** | N/A | **0.140** | **7.13** | **0.348** | **2.87** |
| β-pinene SOA ($OH/NO_x$) | Takeuchi et al. (2019) | **1.64** | N/A | **0.199** | **5.02** | **0.327** | **3.06** |
| limonene SOA ($NO_3$) | Fry et al. (2011) | 2.33 | 0.22[n] | **0.15** | 6.7 | **0.35** | 2.9 |
| limonene SOA ($NO_3$) | Bruns et al. (2010) | 6.3 | 1.9[g] | 0.067 | **15** | 0.42 | **2.4** |
| isoprene SOA ($NO_3$) | Rollins et al. (2009) | 2.24 | N/A | **0.156** | 6.41 | **0.35** | 2.86 |
| isoprene SOA ($NO_3$) | Bruns et al. (2010) | 2.1 | 0.50[g] | 0.20 | **5.0** | 0.42 | **2.4** |
| isoprene SOA ($OH/NO_x$), LV[bb] | Schwantes et al. (2019) | 3.24 | 0.26[o] | 0.164 | 6.1 | 0.53 | 1.88 |
| isoprene SOA ($OH/NO_x$), 2MGA[bb] | Schwantes et al. (2019) | 3.04 | 0.24[o] | 0.175 | 5.7 | 0.53 | 1.88 |
| benzene SOA ($OH/NO_x$) | Sato et al. (2010) | 2.07 | 0.34[p] | 0.249 | **4.02** | 0.514 | **1.95** |
| monoalkylbenzenes SOA ($OH/NO_x$) | Sato et al. (2010) | 2.30 | 0.34[p] | 0.224 | **4.47** | 0.514 | **1.95** |
| dialkylbenzenes SOA ($OH/NO_x$) | Sato et al. (2010) | 2.75 | 0.50[p] | 0.187 | **5.35** | 0.514 | **1.95** |
| trialkylbenzenes (TMB) SOA ($OH/NO_x$) | Sato et al. (2010) | 2.73 | 0.44[p] | 0.189 | **5.31** | 0.514 | **1.95** |
| 3-methylfuran SOA ($NO_3$) | Joo et al. (2019) | **1.38** | 0.01[q] | 0.190 | **5.25** | 0.263 | **3.8** |
| Alkanol SOA ($OH/NO_x$) | Liu et al. (2019)[cc] | **2.18** | **0.13**[r] | **0.473** | **2.11** | **1.03** | **0.97** |
| biomass burning SOA, PMF ($O_3/NO_x$ /$NO_3$) | Tiitta et al. (2016) | 3.12 | N/A | 0.128 | **7.8** | **0.40** | **2.5** |
| biomass burning SOA, PMF ($OH/NO_x$) | Tiitta et al. (2016) | 2.56 | N/A | 0.156 | **6.4** | **0.40** | **2.5** |
| ***Isolated pRONO$_2$ (from chamber SOA or standard)*** | | | | | | | |
| isosorbide 5-mononitrate (standard) | Bruns et al. (2010) | 6.3 | N/A | 0.067 | **15** | 0.42 | **2.4** |

| | | | | | | | |
|---|---|---|---|---|---|---|---|
| oleic acid, hydroxynitrate (HN), ($NO_3$) | Farmer et al. (2010) | 3.03 | 0.23[s] | 0.220 | **4.55** | 0.68 | **1.50** |
| oleic acid, carbonylnitrate (CN), ($NO_3$) | Farmer et al. (2010) | 2.67 | 0.31[s] | 0.250 | **4.00** | 0.68 | **1.50** |
| oleic acid, HN/CN oligomers ($NO_3$) | Farmer et al. (2010) | 1.85 | 0.30[s] | 0.360 | 2.78 | 0.68 | **1.50** |
| 1-tetradecene, 1-hydroxy-2-nitrate ($OH/NO_x$) | Farmer et al. (2010) | 1.17 | 0.36[s] | 0.570 | **1.75** | 0.68 | **1.50** |
| 1-tetradecene, 2-hydroxy-1-nitrate ($OH/NO_x$) | Farmer et al. (2010) | 2.30 | 2.32[s] | 0.290 | **3.45** | 0.68 | **1.50** |
| 1-tetradecene, dihydroxynitrate ($OH/NO_x$) | Farmer et al. (2010) | 2.67 | 2.31[s] | 0.250 | **4.00** | 0.68 | **1.50** |
| 1-pentadecene, hydroxynitrate ($NO_3$) | This Study[dd] | **1.89** | N/A | **0.408** | **2.45** | **0.77** | **1.30** |
| 1-pentadecene, carbonylnitrate ($NO_3$) | This Study[dd] | **2.62** | N/A | **0.294** | **3.41** | **0.77** | **1.30** |
| ***Ambient (instrument comparisons or PMF)*** | | | | | | | |
| ambient AMS $NO_x^+$ ratio method vs TD-LIF (pine forest, summer) | Fry et al. (2013) | **2.12[a]** | 0.44[t] | 0.139 | 7.17 | **0.295** | 3.39 |
| ambient IC-AMS vs AMS $NO_x^+$ ratio method (SEUS, summer) | Xu et al. (2015a) | 2.73[b] | 0.53[u] | 0.125 | 8.00[b] | 0.341 | **2.93** |
| ambient PMF (NYC, summer) | Sun et al. (2012) | 3.04[c] | 0.04[v] | 0.093 | 10.8[c] | 0.282 | **3.55[c]** |
| ambient PMF (boreal, fall) | Hao et al. (2014) | 3.65[d] | 0.06[w] | 0.096 | **10.4[d]** | 0.351 | **2.85[d]** |
| ambient PMF (boreal, spring) | Kortelainen et al. (2017) | 3.54 | N/A | 0.118 | **8.5[e]** | 0.42 | **2.4[e]** |
| ambient PMF (SEUS, summer, RF16) | This Study | **2.92** | **0.04[x]** | **0.240** | **4.2** | **0.70[f]** | **1.43** |
| ambient PMF (SEUS, summer, RF18) | This Study | **2.96** | **0.03[x]** | **0.182** | **5.5** | **0.54[f]** | **1.85** |

790 *RoR* and $pRONO_2$ or $NH_4NO_3$ $NO_x^+$ ratio footnotes:

*(If no footnote, then values simply tabulated from reported $NH_4NO_3$ and pure $pRONO_2$ $NO_x^+$ ratios and RoR calculated or provided)*

[a]Estimated by calculating *RoR* consistent with a 1:1 fit of AMS vs TD-LIF $pRONO_2$ (Fig. 11b in Fry et al. (2013)).

[b]Estimated by calculating $R_{pRONO2}$ consistent with a 1:1 fit between AMS-PILS-IC vs AMS $NO_x^+$ ratio methods (Fig. 11 in Xu et al. (2015a)).

[c]Calculated from concentration-weighted combined PMF factors (three OOA factors only: LO-OOA, MO-OOA, LV-OOA) and $NH_4NO_3$ from offline $NH_4NO_3$ calibration and $NH_4NO_3$ PMF factor ("$NO_3$-OA") (Tables 1, 2 in Sun et al. (2012))

[d]$R_{pRONO2}$ reported for concentration-weighted combination of the three non-$NH_4NO_3$ PMF factors (SV-OOA, LV-OOA, HOA although HOA contribution was very small) and average of $R_{NH4NO3}$ from offline $NH_4NO_3$ calibration and $NH_4NO_3$ PMF factor ("NIA")

[e]$R_{pRONO2}$ reported for combination of the two non-$NH_4NO_3$ PMF factors (SV-OOA, LV-OOA). Offline $NH_4NO_3$ calibration and $NH_4NO_3$ PMF factor ("NO-factor") $NO_x^+$ ratios were identical.

[f]$R_{NH4NO3}$ from PMF $NH_4NO_3$ factor.

<u>*RoR* Uncertainty footnotes:</u>

*(If N/A then RoR represents single measurement or statistics not available)*

[g]Standard error (1σ) calculated by propagating 2σ values reported for repeats chamber experiments of $pRONO_2$ (n=2) and $NH_4NO_3$ (n=3) $NO^+/NO_2^+$ ratios.

[h]Standard error calculated for *RoR*s of 11 chamber experiments.

[i]Standard error calculated for *RoR*s of 2 chamber experiments.

[j]Standard error calculated for *RoR*s of 4 chamber experiments.

[k]Standard error calculated for *RoR*s for 3 chamber experiments.

[l]Standard error calculated for *RoR*s of 2 chamber experiments.

[m]Standard error calculated for *RoR*s of 2 chamber experiments.

[n]Standard error calculated from reported standard deviation of $R_{pRONO2}$ for 2 chamber experiments.

[o]LV or 2MGA indicate experiments under conditions resulting in SOA formation via low-volatility or 2-methyl glyceric acid product formation pathways, respectively. All values used and calculated are taken from Fig. S8 in Schwantes et al. (2019) which contains values for four LV and six 2MGA experiments. $NH_4NO_3$ ratios were calculated from the five high RH experiments where large (and overwhelming) concentrations of inorganic nitrate were formed from $HNO_3$ partitioning to particles; these values were taken to be more representative of the corresponding instrument response in lieu of the typical instrument response quoted in the text for $NH_4NO_3$ $NO^+/NO_2^+$ (2.4).

[p]Standard error calculated from reported $pRONO_2$ and $NH_4NO_3$ *m/z*30-to-*m/z*46 ratios for 2–3 separate chamber experiments (and range of measured $NH_4NO_3$ values).

[q]Standard error calculated from reported range of 4 experiments and approximating standard deviation as one-fourth of the range.

[r]Standard error calculated from 3 experiments with different OA seeds (squalene, sucrose, and oleic acid)

[s]Standard error calculated from reported standard errors of $pRONO_2$ and $NH_4NO_3$ $NO_2^+/NO^+$ ratios for 3 or more repeat measurements.

[t]Calculated as combined accuracy for TDLIF (±25%) (Fry et al., 2013) and AMS (±34%) (Bahreini et al., 2009; Middlebrook et al., 2012) particle nitrate concentrations (accuracy uncertainties first divided by two to scale from 2σ to 1σ for consistency with other 1σ uncertainties reported here).

[u]Calculated as combined accuracy for PILS-IC (±10%) (Weber et al., 2001; Xu et al., 2015a) and AMS (±34%) (Bahreini et al., 2009; Middlebrook et al., 2012) particle nitrate concentrations (AMS accuracy uncertainty first divided by two to scale from 2σ to 1σ for consistency with other 1σ uncertainties reported here).

[v]Calculated as range for using $NO_x^+$ ratio from offline $NH_4NO_3$ calibration vs $NH_4NO_3$ PMF factor ("$NO_3$-OA").

[w]Calculated as range for using $NO_x^+$ ratio from offline $NH_4NO_3$ calibration vs $NH_4NO_3$ PMF factor ("NIA").

[x]PMF Bootstrapping standard error for 100 iterations.

Other footnotes:

[y]For Kang et al. (2016) values, 2014 and 2015 denote the year they were conducted which were done with two different AMS instruments, but with the same SOA production method.

[z]High OA: >200 μg $m^{-3}$. For other Kang et al. (2016) Δ-3-carene SOA ($NO_3$), concentrations of OA were 10–20 μg $m^{-3}$.

[aa]High OA: 25–75 μg $m^{-3}$. For other Kang et al. (2016) α-pinene SOA ($NO_3$), concentrations of OA were 5–10 μg $m^{-3}$.

[bb]Standard errors calculated from the 4 LV or six 2MGA experiments (including propagation of errors from 5 experiments representing $NH_4NO_3$ ratios).

[cc]Alkanol SOA was produced from a mixture of C6, C8, C9, C10, and C12 n-alcohols oxidized by OH at high-NO conditions according to the methods described in Krechmer et al. (2017), but with different organic seeds (Liu et al., 2019). Data included here are from the average (and standard error) of results for experiments with squalene, sucrose, and oleic acid seeds under dry conditions (RH<1%).

[dd]Measurements of isolated compounds separated by HPLC from SOA formed in a chamber from oxidation of 1-pentadecene by $NO_3$ radicals. Same chamber, separation, and sampling methods as described in Farmer et al. (2010). For the hydroxynitrate, the $NO_x^+$ ratio is from the period of the initial rise in concentrations when OA<20 μg $m^{-3}$, since OA concentrations reached ~500 μg $m^{-3}$ at the peak concentration and the $NO_x^+$ ratio drifted up by 25%. OA concentration for the carbonylnitrate measurement was ~85 μg $m^{-3}$.

[ee]Published studies excluded from characterization of the *RoR* in this study and rationale: **Alfarra et al.** (2006) reported UMR *m/z* 46 / *m/z* 30 ratios for 1,3,5 trimethylbenzene (TMB) and α-pinene (+OH/$NO_x$) SOA (0.13, 0.20, respectively) but did not report corresponding $R_{NH4NO3}$. **Liu et al.** (2012) reported $NO_x^+$ ratios for 1,2,4 TMB +OH/$NO_x$ SOA (0.11) but did not report corresponding $R_{NH4NO3}$. **Sato et al.** (2012) reported for 1,3,5 TMB (+OH/$NO_x$) SOA that "The $NO^+/NO_2^+$ ratio observed was 3.8–5.8, higher than that for inorganic nitrates", but $R_{NH4NO3}$ was not explicitly reported, so is not clear what the "inorganic nitrate" refers to and if it was actually measured with their instrument. **Rollins et al.** (2010a) reported $NO_x^+$ ratios for hydroxy nitrates synthesized from butane, α-pinene, limonene, and caryophyllene and reported a large range of values (0.19–1.01), however associated $R_{NH4NO3}$ was not reported. Additionally, two-thirds of the nitrogen observed in the AMS spectrum was at non-$NO_x^+$ peaks, mostly as reduced ions ($NH_x^+$, $C_xH_yN_z^+$), which is very atypical, since those ions are generally observed at no more than trace amounts for isolated organic nitrates or SOA containing organic nitrates (e.g., Farmer et al., 2010; Boyd et al., 2015). It is unclear if standards were impure, contaminants

became concentrated in the aerosol during particle generation and evaporation/drying, possibly the AMS was functioning abnormally, or some other explanation for the atypical spectra. Consequently, we recommend interpretation of that large range in $NO_x^+$ ratios with caution. Finally, the **Bruns et al.** (2010) data were not included in reported averages or fitted lines reported in this table, the text, or figures due to the large range in variability of repeat measurements and also because the Particle Time-of-Flight (PToF) acquisition mode was used to conduct most experiments as a way to attenuate very large particle concentrations. It is not clear if using a different time sequence of impacting and blocking the particle beam on the vaporizer will affect the observed $NO_x^+$ ratios.

**Table S2.** Summary of sources, values, calculations, and details for inorganic nitrates and nitrites and $NH_4NO_3$ $NO_x^+$ ratios and Ratio-of-Ratios. Numbers in bold indicate values directly reported in literature sources (or measured in our laboratory), while otherwise the values were calculated here. See Fig. S4 for graphical representation and comparison to $pRONO_2$ of these *RoR*s.

| Compound | Reference | *RoR* | *RoR* Uncertainty | Nitrate or Nitrite | | $NH_4NO_3$ | |
|---|---|---|---|---|---|---|---|
| | | | | $NO_2^+/NO^+$ | $NO^+/NO_2^+$ | $NO_2^+/NO^+$ | $NO^+/NO_2^+$ |
| $NaNO_3$ | Alfarra (2004) | 10.8 | N/A | 0.0342 | **29.2** | 0.37 | **2.7** |
| $NaNO_3$ | Bruns et al. (2010) | 33 | 8.1[a] | 0.0125 | **80** | 0.42 | **2.4** |
| $NaNO_3$ | Hu et al. (2017) | 58 | N/A | **0.006** | 170 | **0.35** | 2.9 |
| $NaNO_3$ | This study[b] | 7.6 | 0.7 | **0.0340 (0.0019)** | **29.4 (1.7)** | **0.2585 (0.0164)** | **3.88 (0.25)** |
| $Ca(NO_3)_2$ | Alfarra (2004) | 16.9 | N/A | 0.0219 | **45.6** | 0.37 | **2.7** |
| $Mg(NO_3)_2$ | Alfarra (2004) | 3.93 | N/A | 0.0943 | **10.6** | 0.37 | **2.7** |
| $KNO_3$ | Drewnick et al. (2015) | 9.7 | N/A | 0.036 | **28** | 0.35 | **2.9** |
| $KNO_3$ | This study[b] | 40.7 | 4.9 | **0.0141 (0.0014)** | **71.7 (7.85)** | **0.5694 (0.0281)** | **1.76 (0.09)** |
| $NaNO_2$ | Bruns et al. (2010) | 290 | N/A | 0.00142 | **700** | 0.42 | **2.4** |
| $KNO_2$ | This study[b] | 28.9 | 4.9 | **0.0103 (0.0016)** | **99.8 (15.4)** | **0.2913 (0.0200)** | **3.45 (0.23)** |
| 4-nitrocatechol | This study[c] | 3.35 | 0.81 (0.21) | **0.246 (0.052)** | **4.25 (0.84)** | **0.795 (0.119)** | **1.29 (0.23)** |

[a]Standard error (1σ) calculated by propagating 2σ values reported for repeated chamber experiments of $NaNO_3$ (n=11) and $NH_4NO_3$ (n=3) $NO^+/NO_2^+$ ratios.

[b]Performed in our laboratory with the aircraft HR-AMS. Values in parentheses for the $NO_x^+$ ratios are standard deviations of ~5-20 minutes of 1 Hz resolution data for the duration of the one-time measurements, and reflect experimental/instrument noise and substantial drifts in some cases. The uncertainties for those *RoR* are the standard deviations from propagating standard deviations of the $NO_x^+$ ratios in quadrature.

[c]See Fig. S5 for details. The uncertainties for the $NO_x^+$ ratios (parenthesis) are standard deviations of the averages from each individual calibration. Uncertainties for the *RoR* is the standard deviation (1σ) and standard error (parenthesis) of the separately-calculated *RoR*s for each calibration (n=15).

**Table S3.** Summary of field campaigns from which data is used in this analysis. See Sect. S1.1 for additional details.

| Name | Location | Season, Year | Type | Reference(s) |
|---|---|---|---|---|
| SOAR-1 | Riverside, California | Summer, 2005 | Urban, ground | Docherty et al. (2011) |
| MILAGRO | Mexico City | Late winter / early spring, 2006 | Urban (megacity), ground | Molina et al. (2010), Aiken et al. (2009, 2010) |
| DAURE | Montseny, Spain | Late winter / early spring, 2009 | Rural, urban-influenced, ground | Minguillón et al. (2011), Pandolfi et al. (2014) |
| BEACHON-RoMBAS | Colorado Rocky Mts., pine forest | Summer, 2011 | Rural, ground | Ortega et al. (2014), Fry et al. (2013), Palm et al. (2017) |
| DC3 | Continental U.S. | Spring 2012 | Focus on deep convective cloud chemistry, aircraft | Barth et al. (2015), Nault et al. (2016) |
| SOAS | Rural Alabama, mixed forest | Summer, 2013 | Rural, semi-polluted, ground | Carlton et al. (2018), Hu et al. (2016) |
| SEAC$^4$RS | Continental U.S., especially SE US | Late summer, 2013. Special focus on RF16/18 (11/16 Sept) in SE US | Many foci, aircraft | Toon et al. (2016), Fisher et al. (2016) |
| GoAmazon | Central Amazonia | Wet season (IOP1), dry season (IOP2), 2014 | Rural/remote. Sometimes urban downwind. | Martin et al. (2016, 2017), de Sá et al. (2018, 2019), Palm et al. (2018) |
| KORUS-AQ | South Korea and Seoul | Spring, 2016 | Urban (megacity) + regional survey, aircraft | Nault et al. (2018) |

**Table S4.** Summary of results for studies using PMF for $pRONO_2$ separation with AMS (using OA and nitrate ions as input). See Sects. 5.2.1, 5.2.2, and 5.2.3 for summaries and Sects. S3, S4 for details and discussions of these studies.

| Reference | Sample description | No. fact.[a] | $R_{NH4NO3}$ comp[b] | $f_{pRONO2}$[c] | $pRONO_2$ factors[d] | *RoR*[e] | $NO_x^+$ ratio meth.[f] |
|---|---|---|---|---|---|---|---|
| Sun et al. (2012)[g] | New York City, summer | 8 | 3% lower | 21% | MO-SV-OOA (12%)[h], NOA (4%)[h], LO-SV-OOA (2%)[h] | MO-SV-OOA (2.6-2.7), ∑OOA (3.0-3.1) | No |
| Hao et al. (2014) | Semi-polluted rural Finland, fall | 4 | 3% lower | 37% | SV-OOA (28%), LV-OOA (9%) | ∑OA (3.6-3.7) | No |
| Xu et al. (2015a) | Southeast US, summer (2 sites) | 3,4 | Not resolved | 100% | LO-OOA, possibly others | LO-OOA (~2.5) | Yes |
| Xu et al. (2015a) | Southeast US, winter (3 sites) | 3,6,6 | within 10% | 10%, 11%, 19% | LO-OOA, possibly others | LO-OOA (>10, nearly all $NO^+$) | Yes |
| Xu et al. (2015a) | Southeast US, transition (2 sites) | 6,7 | 30-35% lower | 33%, 39% | LO-OOA, possibly others | LO-OOA (~5) | Yes |
| Zhang et al. (2016) | Beijing, fall, biomass burning-influenced period | 6 | 4% lower | 23% | SV-OOA (8%), HOA (6%)[i], LV-OOA (5%), BBOA (4%)[i] | SV-OOA (~5), LV-OOA (~2.5) | No |
| Zhang et al. (2016) | Beijing, winter, coal combustion –influenced period | 5 | 7% lower | 17% | HOA (10%)[i], OOA (4%), CCOA (2%)[i] | OOA ($NO_x^+$ was $NO_2^+$) | No |
| Kortelainen et al. (2017) | Remote Finnish boreal forest, spring | 3 | Same | 35% | SV-OOA (30%), LV-OOA (5%) | SV-OOA (3.0), ∑OOA (3.5) | No |
| Yu et al. (2019) | Urban southern China (Shenzhen), spring | 4 | 4% lower | 12% | LO-OOA (6%) HOA (4%) MO-OOA (2%) | HOA (3.9), others (>10, nearly all $NO^+$) | Yes |

| | | | | | | | |
|---|---|---|---|---|---|---|---|
| Yu et al. (2019) | Urban southern China (Shenzhen), summer | 4 | 9% lower | 43% | LO-OOA (22%) HOA (12%) MO-OOA (9%) | LO-OOA (4.7), MO-OOA (2.1), HOA (>10, nearly all $NO^+$), ∑OA (5.0) | Yes |
| Yu et al. (2019) | Urban southern China (Shenzhen), fall | 4 | 6% lower | 16% | LO-OOA (7%) HOA (5%) MO-OOA (4%) | All (>10, nearly all $NO^+$) | Yes |
| Zhu et al. (2021) | North China Plains, summer | 4 | 21-26% lower | 9.3% | BBOA (8) HOA (1.1%) OOA (0.3%) | BBOA (~20) Others all $NO^+$ or $NO_2^+$ | Yes |
| This study | Southeast US, late summer (aircraft, RF16) | 5 | 1% lower[j] | 14%, (22%)[k] | LO-OOA (9, 12%)[k] MO-OOA (5, 9%)[k] | LO-OOA (3.03±0.54)[h], ∑OOA (2.92±0.43)[l] | Yes |
| This study | Southeast US, late summer (aircraft, RF18) | 5 | 13% lower[j] | 29%, (55%)[k] | LO-OOA (13, 18%)[k] MO-OOA (5, 28%)[k] IEPOX-SOA (5, 9%)[k] | LO-OOA (2.83± 0.64)[l], ∑OOA (2.96±0.28)[l] | Yes |
| Tiitta et al. (2016) | Wood burning emissions, oxidized with $O_3$, $NO_3$, OH, $NO_x$ in laboratory | 5 | Not resolved | N/A[m] | N/A[m] | POA2 (2.5)[n], SOA2 (2.6)[n], SOA3 (3.1)[n] | No |
| Reyes-Villegas et al. (2018)[o] | Manchester UK, "Bonfire Night", fall | 6 | N/A | N/A | Primary and secondary $pRONO_2$ | N/A | No[p] |

[a]Number of factors resolved with PMF.

[b]Comparison of the $NO_x^+$ ratio ($NO_2^+/NO^+$) for $NH_4NO_3$ factor resolved with PMF vs the calibration $NH_4NO_3$ $NO_x^+$ ratio.

[c]Average fraction of total nitrate apportioned to $pRONO_2$ using PMF apportionment method.

[d]$pRONO_2$ factors comprising >85% of non-$NH_4NO_3$ nitrate concentration. % contributed to total nitrate indicated in parentheses when available.

[e]Ratio-of-Ratios for non-$NH_4NO_3$ factors where $NO_x^+$ ratios indicative of $pRONO_2$ were resolved. ∑OOA and ∑OA indicate the mass-weighted sum of all OOA (and other SOA) or OA (non-$NH_4NO_3$) factors, respectively.

[f]Was the $NO_x^+$ ratio method also used for nitrate apportionment and compared to PMF method apportionment?

[g]Sulfate and ammonium ions also included.

[h]More-oxidized and less-oxidized of two SV-OOA factors; "Nitrogen-enriched" OA

[i]HOA $NO_x^+$ ratios very similar to $NH_4NO_3$. BBOA and CCOA factors had only $NO_2^+$ (no $NO^+$). However, nitrate from all OA factors were apportioned as $pRONO_2$. CCOA = Coal-Combustion OA

[j]$NH_4NO_3$ calibration $NO_x^+$ ratios were atypically variable during this campaign (see Sects. 4 and S2, Figs. S8, S9e). These comparisons are for the calibrations performed most closely in time, the day following the flight after the instrument was powered off and back on.

[k]Second % is the average fraction in the time series (not mass weighted). Other $f_{pRONO2}$ in table are mass-weighted.

[l]"Uncertainties" for these *RoR* are the standard *deviation* of 100 bootstrapping runs (standard *error* is 10 times smaller)

[m]Not apportioned with PMF method. Apportioned with $NO_x^+$ ratio method.

[n]POA2 is a primary OA factor associated with $pRONO_2$. SOA2 and SOA3 are secondary factors from $O_3$/$NO_x$/$NO_3$ and OH/$NO_x$ oxidation, respectively.

[o]$pRONO_2$ concentrations were separated first with the $NO_x^+$ ratio method. Then PMF performed with OA ions combined with $pRONO_2$ concentrations to separate different $pRONO_2$ sources.

[p]The secondary/primary $pRONO_2$ apportionment was compared between the combined $pRONO_2$ + OA PMF method (see footnote "o") and another apportionment method using ratios of $pRONO_2$ vs BBOA factor during distinct plume events. UMR data used (all other studies used HR).

**Table S5.** Summary of instrument comparisons of total $pRONO_2$ concentrations in the field and laboratory. A summary is presented in Sect. 5.3 and details and discussions of the comparisons are provided in Sect. S5.

| Reference | Instruments compared | Sample description | Slope ($R^2$) | Notes |
|---|---|---|---|---|
| ***Field (outdoor ambient)*** | | | | |
| Fry et al. (2013) | AMS (*RoR*) vs TD-LIF | Montane pine forest in US, summer | 0.94-1.16 (0.53) | Typically nitrate was dominated by $pRONO_2$, however instruments tracked well during $NH_4NO_3$ plumes. |
| Lee et al. (2016) | AMS (*RoR*) vs AMS (AMS-IC) | Semi-polluted rural SE US, summer | 1.15 (0.72) | Nitrate usually $pRONO_2$-dominated (same for following two entries). |
| Lee et al. (2016) | AMS (*RoR*) vs TD-LIF | Semi-polluted rural SE US, summer | 0.23, 0.45 (0.74) | Two distinct slopes were observed for different periods (with same $R^2$). |
| Lee et al. (2016) | AMS (*RoR*) vs FIGAERO-CIMS ($I^-$) | Semi-polluted rural SE US, summer | 1.11 (0.67) | FIGAERO-CIMS used iodide-adduct CI and was the sum of 88 compounds. |
| Huang et al. (2019) | AMS (fixed $R_{pRONO2}$=0.1) vs FIGAERO-CIMS ($I^-$) | Rural Germany, summer | 2.13 (0.27) | Reported as CIMS vs AMS (slope =0.47, R=0.52). CIMS considered lower limit, based on calibration assumptions. Considering only the nitrate functionality for the CIMS for direct comparison of nitrate functional group concentration, the CIMS vs AMS slope may have been ~0.1. |
| Chen et al. (2020) | AMS (fixed $R_{pRONO2}$=0.1-0.2) vs FIGAERO-CIMS ($I^-$); nitrate/organic fraction and N/C. | Rural SE US, late summer to mid-fall | 5-18% vs 12.3±10.8% | Percents in slope column are the organic nitrate molecule fraction of total organic measured. Additionally, the N/C agreed ~1:1 ± ~30-50%, for the range of nitrate computed for the AMS (for assumed $R_{pRONO2}$ range). |

| | | | | |
|---|---|---|---|---|
| Kenagy et al. (2021) | AMS (*RoR*) vs TD-LIF | Korean Peninsula, spring (aircraft) | 1.89 | Screened for $f_{pRONO2}$ (AMS) > 0.2 and TD-LIF corrected for particle losses in aircraft sampling inlet. |
| Rollins et al. (2013) | TD-LIF vs FTIR | Bakersfield, CA, summer | 1.38 (0.52) | Relatively large offset in fit; average TD-LIF/FTIR ratio >2. |
| ***Laboratory*** | | | | |
| Keehan et al. (2020) | AMS vs TD-CRDS | SOA from α-pinene and Δ-3-carene + $NO_3$ radicals | 1.06-1.14 (0.73) | Range of slopes is for ODR fitting without and with y-intercept fixed to zero when plotting TD-CRDS vs AMS (0.88, 0.94) respectively; but reported here in the slope column as AMS vs TD-CRDS for consistency in this table. |
| Eris et al. (2018) | AMS vs TD-CAPS | SOA from terpenes and isoprene + OH, $O_3$, $NO_3$ | "good quantitative agreement" | No peer-reviewed publication available at this time. Assumed to be within ~50% |
| Liu et al. (2012) | AMS vs FTIR | SOA from TMB + $OH/NO_x$ | 2.28 (0.98) | Inadequate information provided on AMS quantification and calibration to assess factor of 2 differences. |
| Bruns et al. (2010) | AMS (N/C ratio) vs FTIR (N/C ratio) | SOA from terpenes + $NO_3$ radical | FTIR N/C ~3–4 times AMS | Multiple possible factors may have led to large difference (see Sect. S5). |

## Supplementary Figures

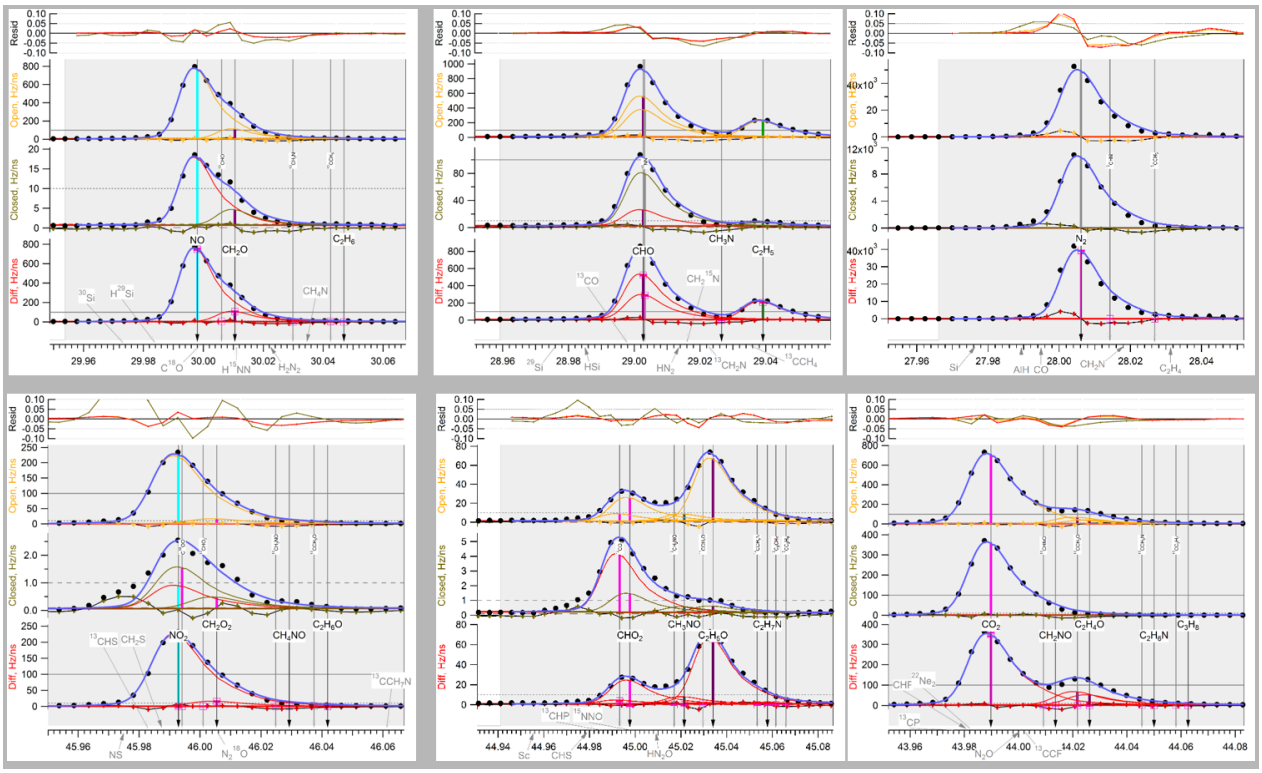


**Figure S1.** High-resolution peak fitting example for *m/z* 30, 29, 28, 46, 45, 44 for SOA produced from reaction of Δ-3-carene with nitrate radicals (see Sect. S1.2). Lower three panels (Open, Closed, Diff): acquired data (black dots), individual peak fits (red, gold, and orange curves), and sums of all ions fits (blue curves). Ion formulae in black were fit and grey formulae were not. Top panel: Residuals for Open, Closed, Diff color-coded according to the y-labels on the lower panel.

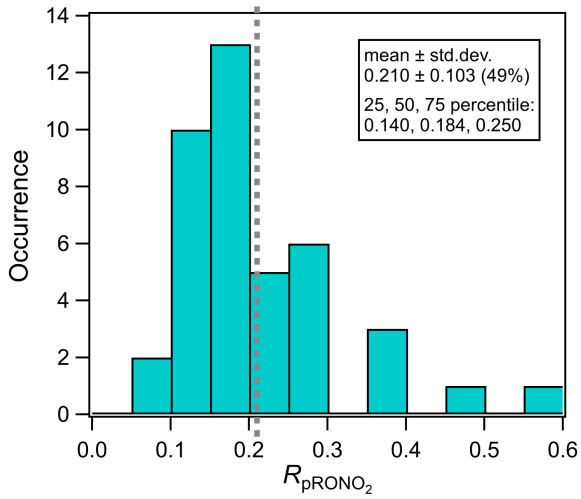


**Figure S2.** Histogram and mean of $pRONO_2$ $NO_x^+$ ratios ($R_{pRONO2}$) for studies in Fig. 1. The relative standard deviation (and interquartile range) is double that of the Ratio-of-Ratios (*RoR*) as shown in Fig. 1. The tighter distribution for the *RoR* in Fig. 1 than for $R_{pRONO2}$ here reflects a substantial degree of correlation between $R_{pRONO2}$ and $R_{NH4NO3}$ and supports using the *RoR* method for estimating $R_{pRONO2}$.

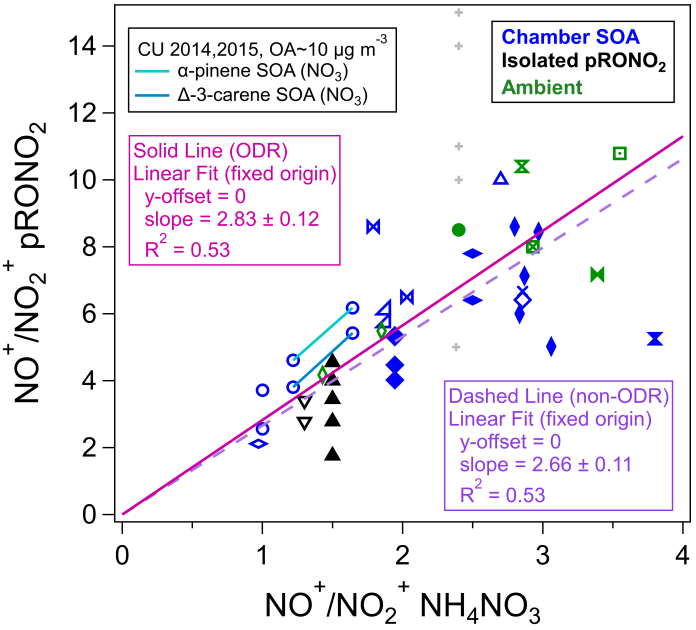


**Figure S3**. Same as lower right panel in Fig. 1, except axes are swapped and $NO_x^+$ ratios are inversed ($NO^+/NO_2^+$). Plotting this way (compared to Fig. 1), emphasizes slightly different data and outliers and gives more weight to points with higher $NO^+/NO_2^+$. In this representation the $R_{NH4NO3}$ is placed on the x-axis, and thus a non-ODR fit may be appropriate under the assumption that most uncertainty is contributed by the $pRONO_2$ ratios. Thus both ODR and non-ODR fits are shown (constraining the y-intercept to zero since unconstrained intercept was not significant). Compared to Fig. 1, slopes (also equivalent to a *RoR*) are slightly higher (and bracket the average *RoR*, 2.75), and the degree of correlation is the same.

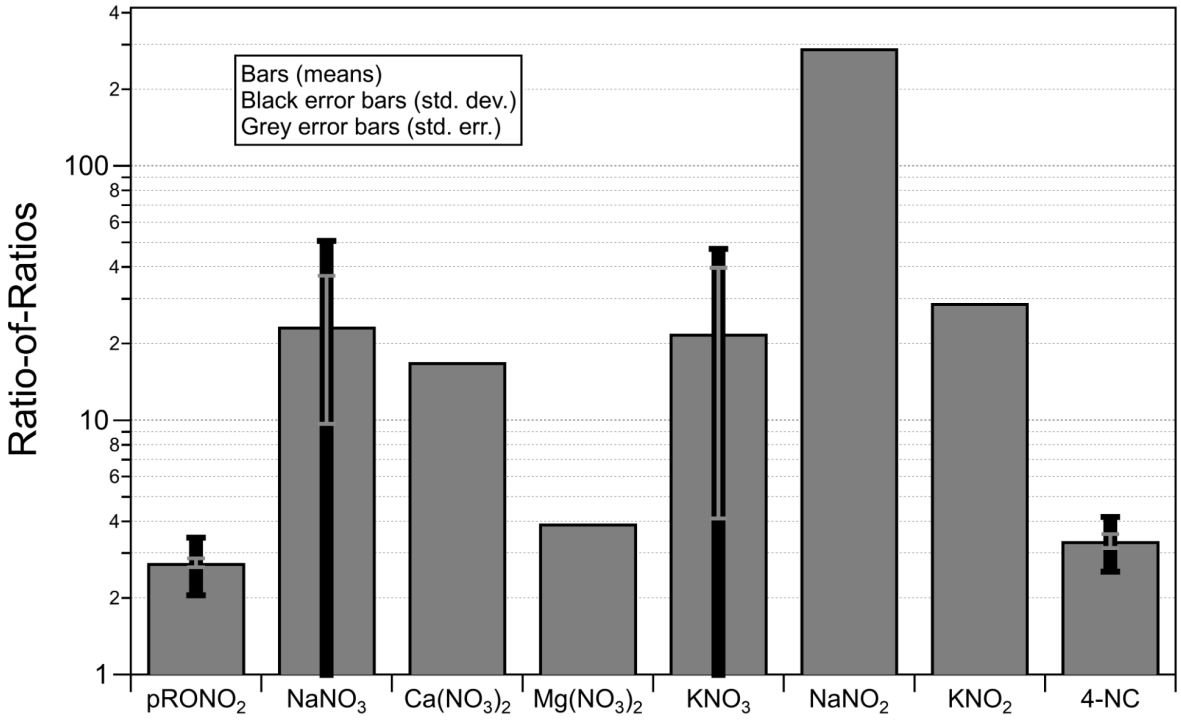


**Figure S4.** Ratios-of-Ratios (always referenced to the measured $NH_4NO_3$ ratio) reported for nitrate and nitrite compounds reported in the literature and this study. The value shown for $pRONO_2$ is from the survey conducted in this paper (as mean ± standard deviation/error). Sources and details for all other compounds are shown in Table S2. The values shown for $NaNO_3$ and $KNO_3$ are statistics for all values reported in different sources. Statistics for 4-nitrocatechol (4-NC) are for multiple measurements during a 2-month campaign with the same instrument.

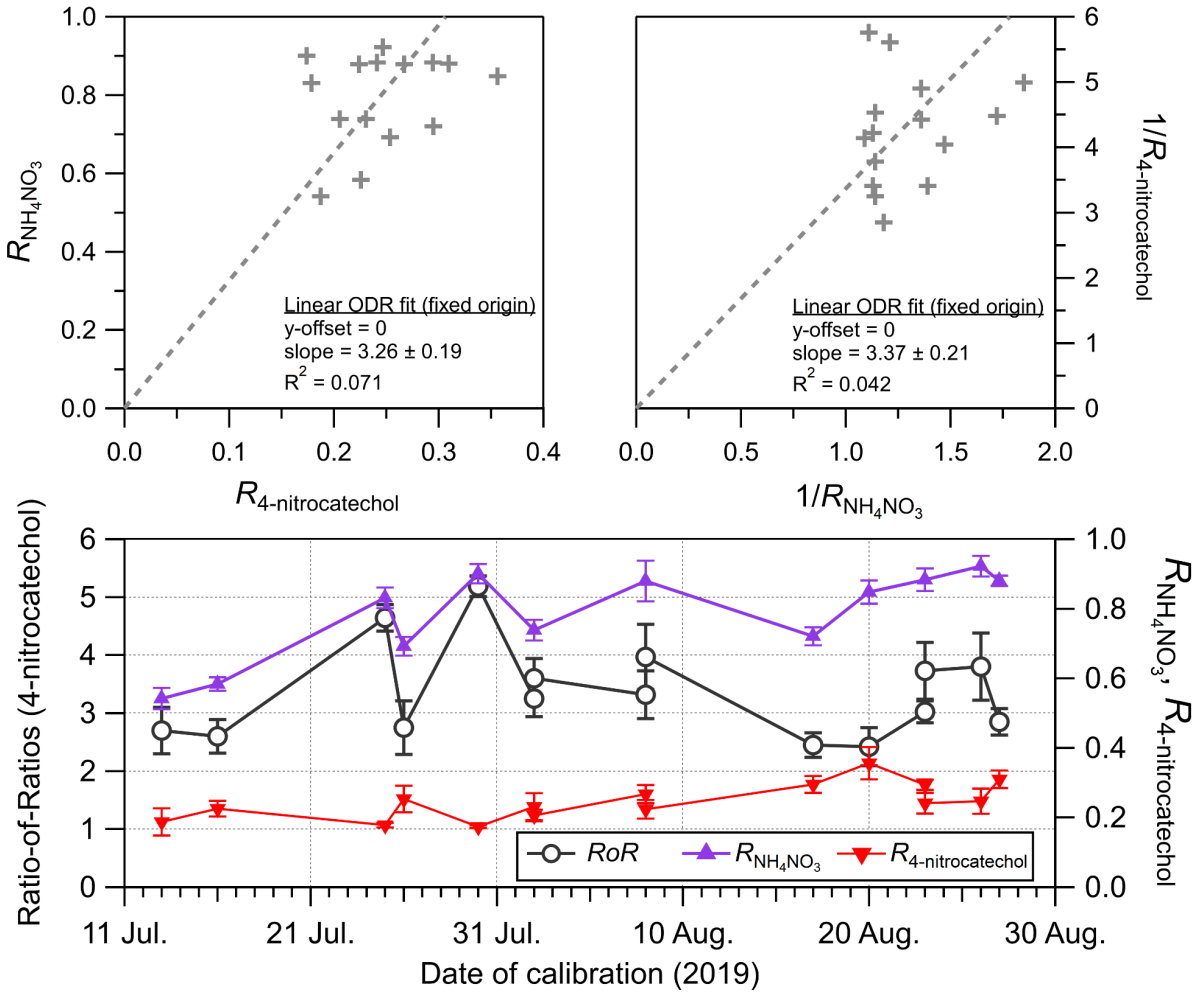


**Figure S5.** $NO_x^+$ ratios for 4-nitrocatechol and $NH_4NO_3$ and the corresponding *RoR* for 4-nitrocatechol measured on board the NASA DC-8 during the FIREX-AQ biomass burning study (Pagonis et al., 2021). Calibrations were performed during pre-flight, post-flight, and ground-service days. Pre-flight/post-flight calibrations pairs are shown on three days (Aug. 2, 8, 23), and with all cases post-flight *RoR* were measured higher due to higher measured $R_{4\text{-nitrocatechol}}$ values (since $R_{NH4NO3}$ was only measured post-flight and applied to both calculations of the $RoR_{4\text{-nitrocatechol}}$). Therefore, it is not clear if that pattern was due to actual shifts in $RoR_{4\text{-nitrocatechol}}$ or if there were corresponding shifts in $R_{NH4NO3}$. Scatter plots are shown for both the standard $R_{NH4NO3}$ vs $R_{4\text{-nitrocatechol}}$ format (as $NO_2^+/NO^+$, top left) and as inverse ratios (top right). Linear fits with a y-intercept fixed to zero represent the average *RoR* (3.28 ± 0.19 and 3.37 ± 0.21, respectively). However there was no significant correlation, likely due to a combination of the limited range of $R_{NH4NO3}$, experimental uncertainty, and some variability in the *RoR* for nitrocatechol.

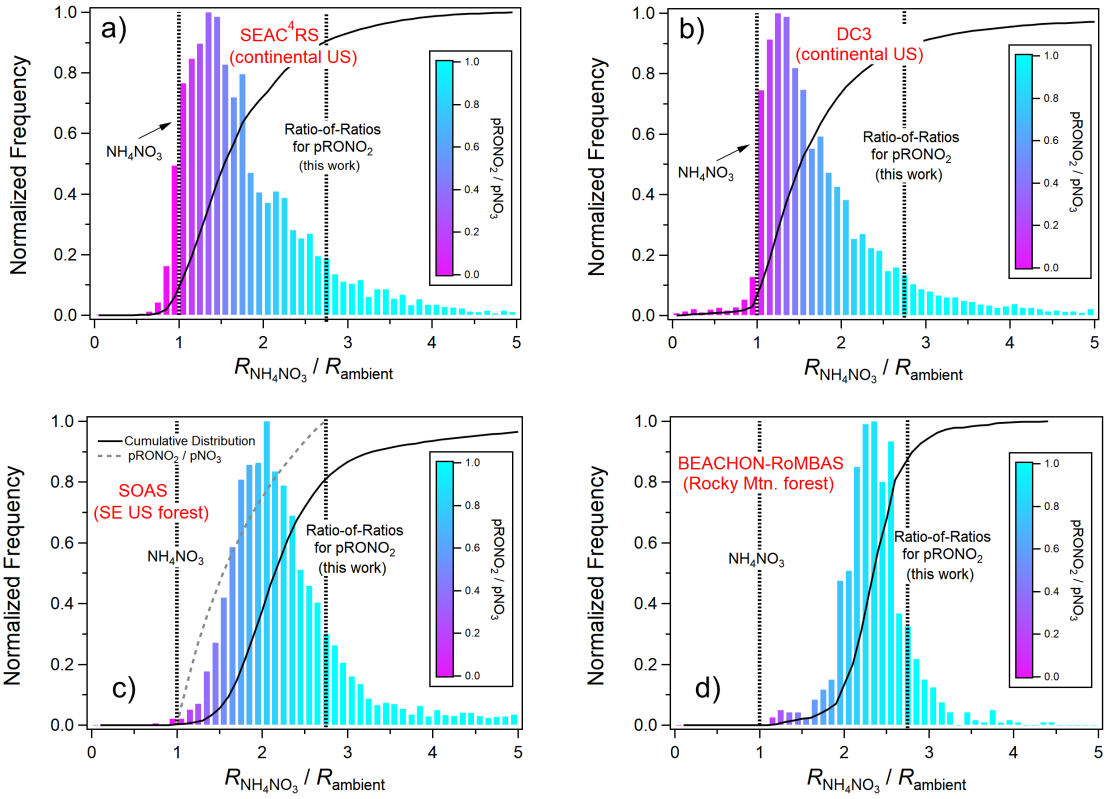


990 **Figure S6**. Standard frequency histograms (*not* weighted by mass concentration) for the same data as shown in Fig. 2. See Fig. 2 capture for additional details.

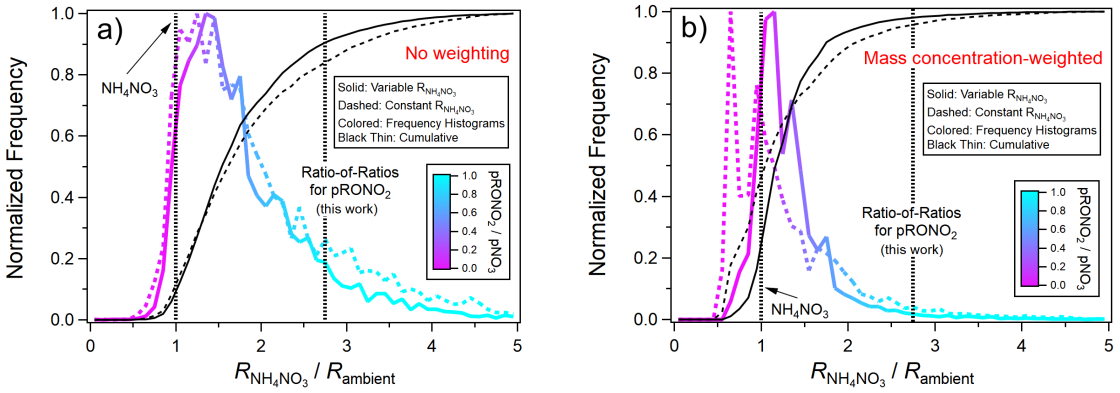


**Figure S7**. Histograms using the same data as shown in Figs. 2 and S6 for SEAC[4]RS, except two versions of the histograms are shown: calculated with a campaign-average $R_{NH4NO3}$ ("constant") vs flight-specific 995 $R_{NH4NO3}$ ("variable" as in Figs. 2 and S6). Panel a) shows standard frequency distributions and panel b) shows mass concentration-weighted distributions. The calibration $R_{NH4NO3}$ for SEAC[4]RS showed large variability between flights (Fig. S8 and S9e). There is substantial narrowing of the distributions using the flight-specific $R_{NH4NO3}$ for the non-weighted distributions (panel a). The most prominent differences for the mass concentration-weighted distributions are largely due to data with high $NH_4NO_3$ concentrations 1000 where the $R_{ambient}$ were beyond the campaign-averaged $R_{NH4NO3}$ ("constant"), resulting in much more of the distribution below 1. These differences support the importance of applying time-varying calibration ratios, when applicable (see Sect. 4)

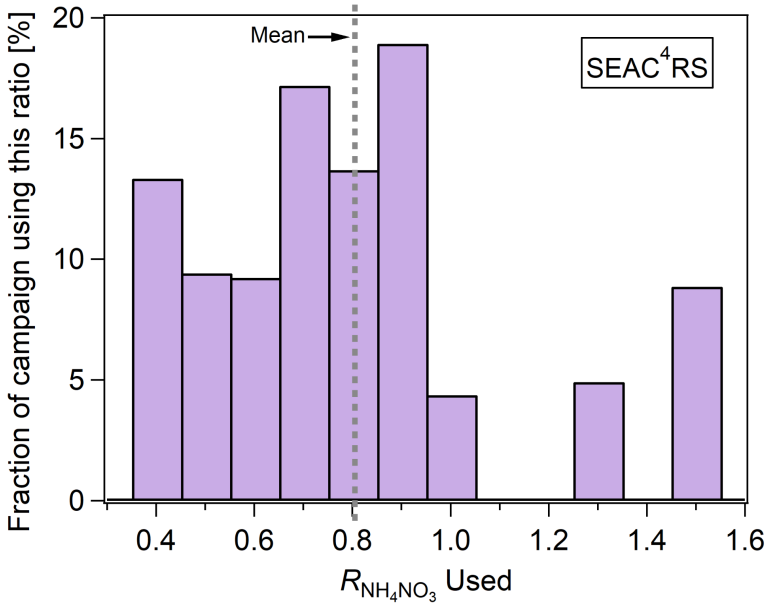


**Figure S8.** Frequency distribution of $NH_4NO_3$ calibration $NO_x^+$ ratios ($R_{NH4NO3}$) applied to ambient nitrate apportionment for SEAC[4]RS campaign. Mean value is also shown, which was used for the "constant" $R_{NH4NO3}$ calculation shown in Fig. S7.

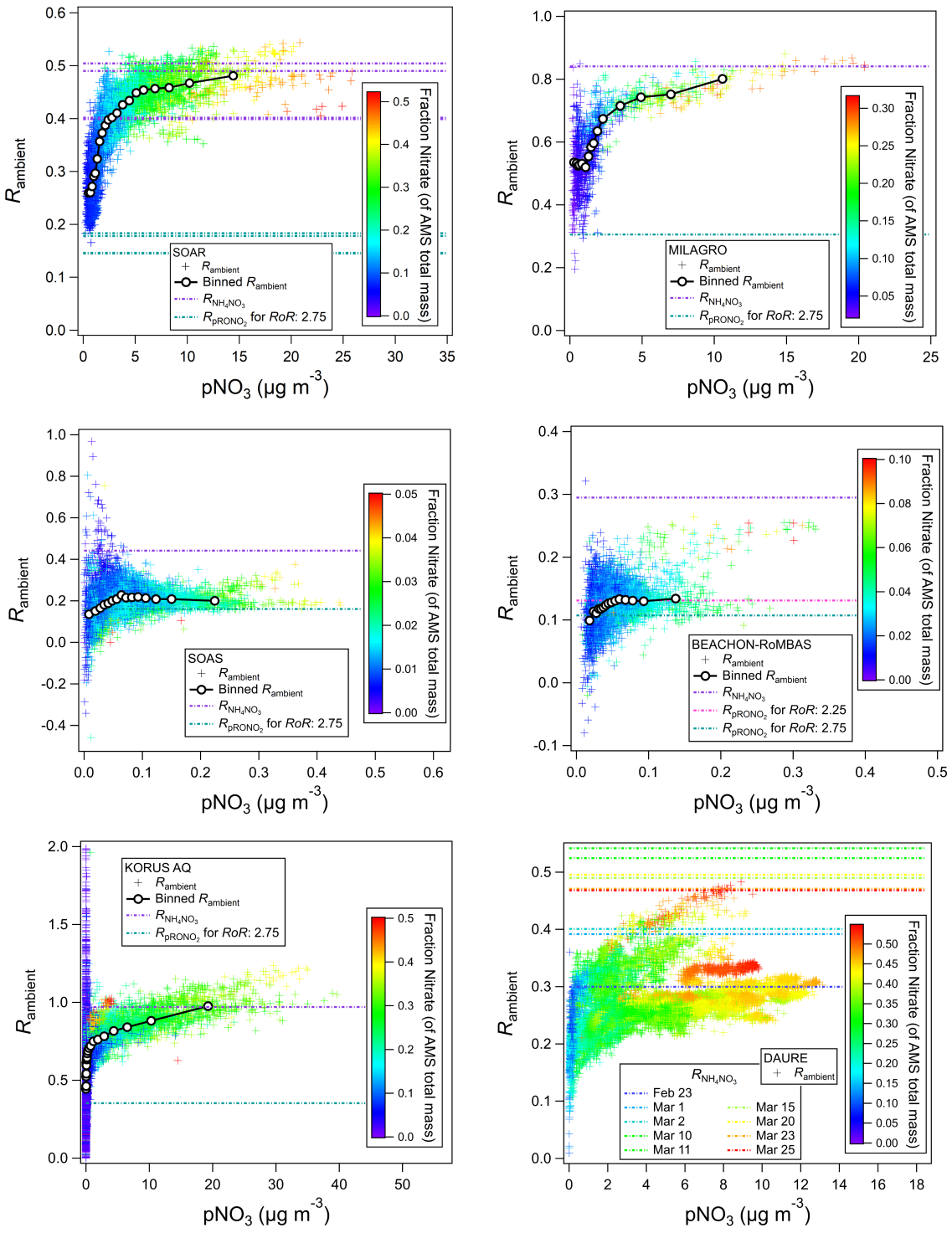


**Figure S9a.** $R_{ambient}$ vs pNO$_3$ for six different campaigns (indicated in legends), colored by mass fraction nitrate, and overlaid with quantile averages. Horizontal lines are shown for calibration $R_{NH4NO3}$ (multiple in some cases) and the corresponding estimated $R_{pRONO2}$ ratios (using $RoR$ = 2.75). Data is not detection limit thresholded, and quantiles are means except for BEACHON-RoMBAS and KORUS-AQ which are medians (to reduce impact of outliers).

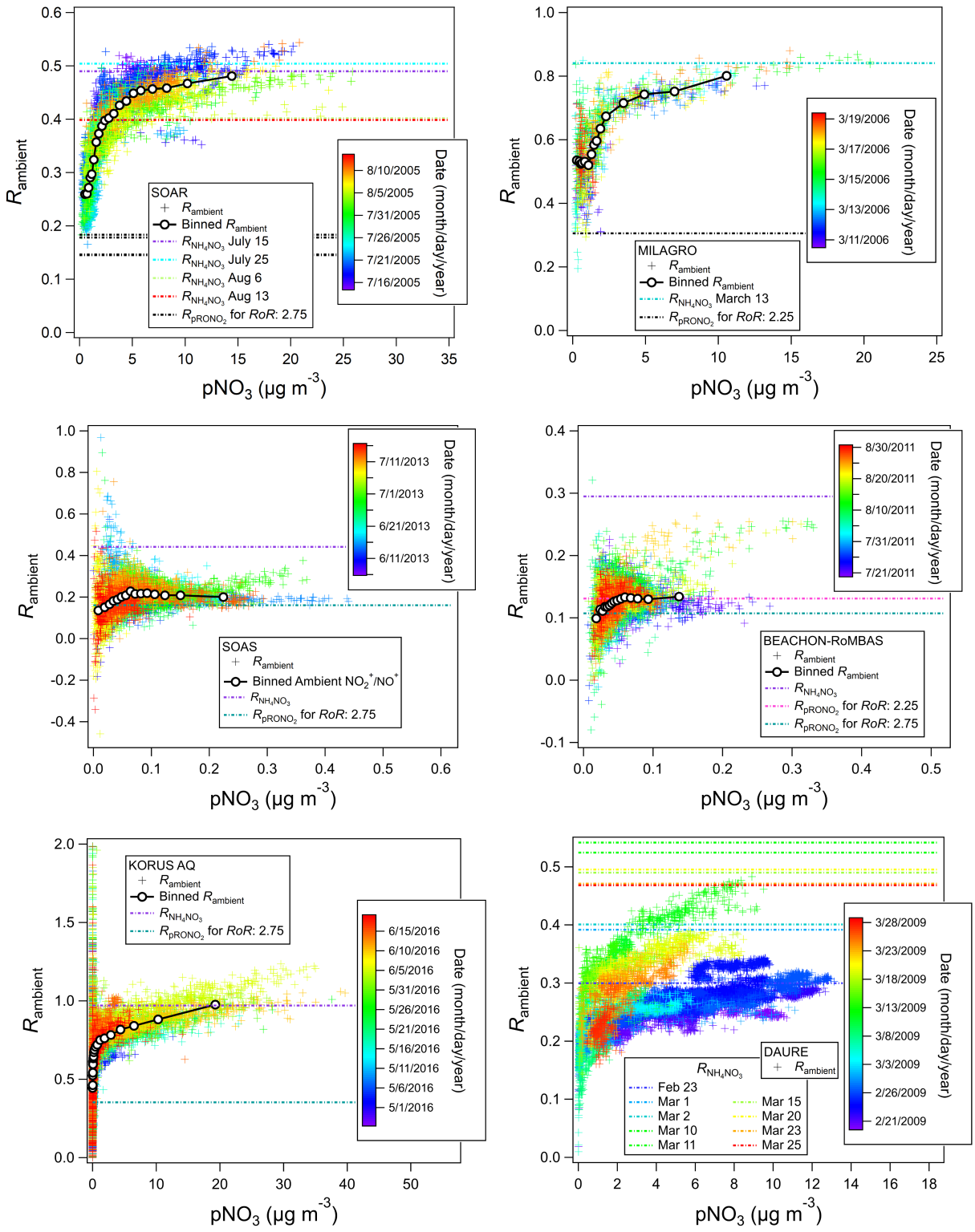


**Figure S9b.** Same as Fig. S9a except colored by data collection time during campaign.

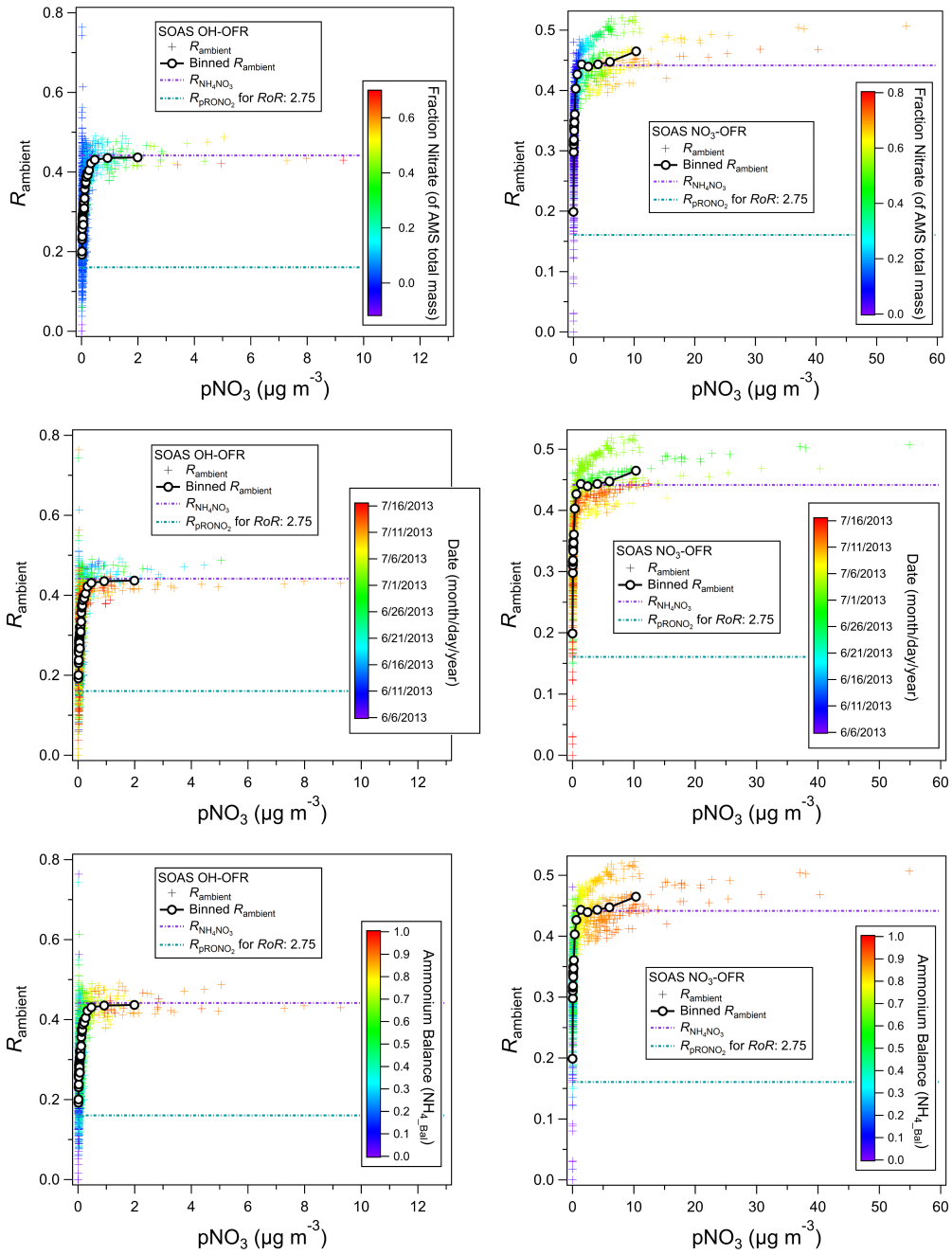


**Figure S9c.** $R_{ambient}$ vs $pNO_3$ for SOAS campaign for oxidation flow reactor (OFR) measurements using OH (left column) and $NO_3$ (right column) radicals as oxidants. Each of the three rows contains the same data, but colored by different measures: mass fraction of AMS mass that is aerosol nitrate (top row), time (middle row), and $NH_{4\_Bal}$ (bottom row) as indicated in colorbar legends. Data is overlaid with quantile averages (medians). $NH_{4\_Bal}$ is calculated as the molar ratio of $NH_4/(NO_3+2\times SO_4)$. Values approaching unity suggests full ion balance of sulfate and nitrate by ammonium and little contribution of organic nitrate or organic sulfate. Lower values suggest acidic particles and/or the presence of substantial organic nitrate or organic sulfate. Horizontal lines are shown for calibration $R_{NH4NO3}$ and corresponding estimated $R_{pRONO2}$ (from $RoR$ = 2.75).

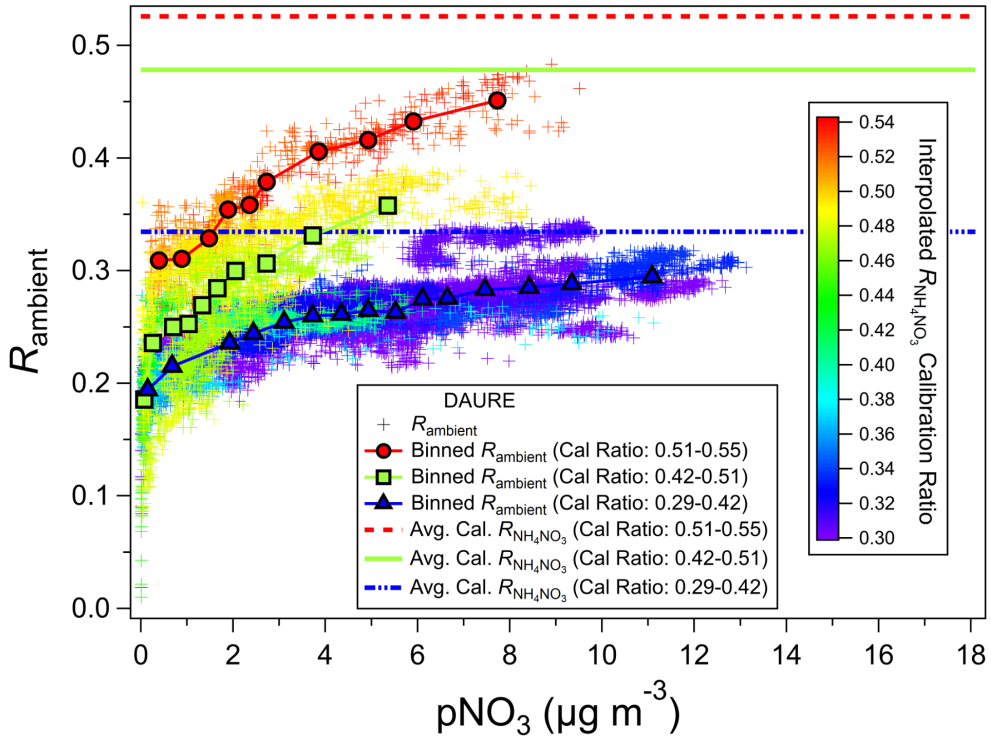


1035 **Figure S9d.** $R_{ambient}$ vs $pNO_3$ for DAURE campaign, colored by time-dependent calibration $R_{NH4NO3}$ (calculated by linear interpolation of measured ratios during $NH_4NO_3$ calibrations). Binned averages (means) for three calibration ratio ranges are shown as well as corresponding averages of applied calibration $R_{NH4NO3}$ (horizontal lines).

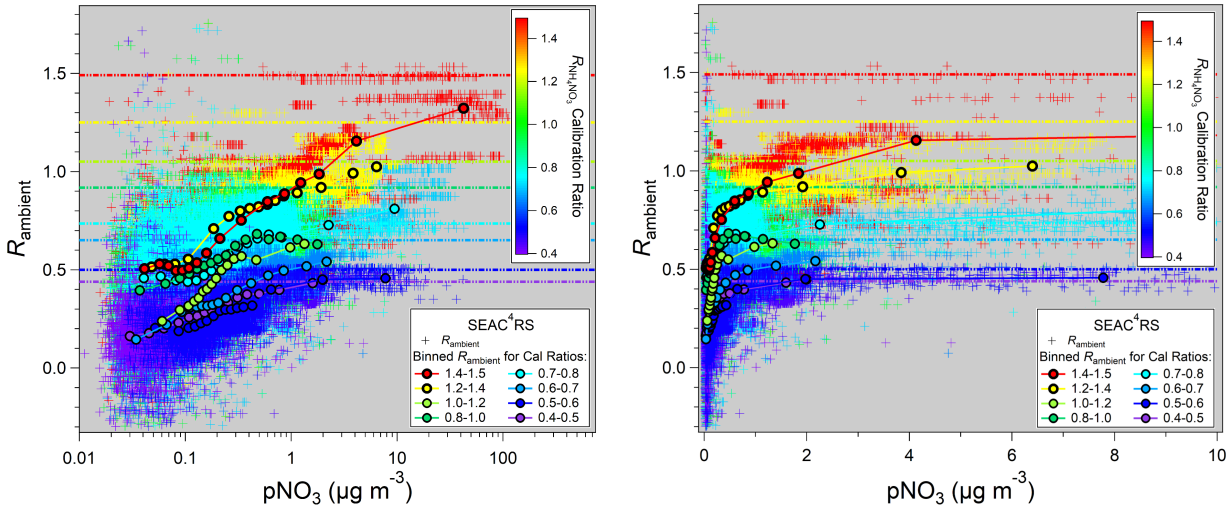


1040

**Figure S9e.** $R_{ambient}$ vs $pNO_3$ for SEAC[4]RS campaign (log left, linear right), colored by flight-dependent calibration $R_{NH4NO3}$. Binned averages (means; 15 quantiles & 98–100% by $pNO_3$) for seven $R_{NH4NO3}$ calibration ratio ranges are shown, as well as corresponding averages of applied calibration ratios (horizontal lines, in color matching binning). Grey background is used for better contrast of light colors.

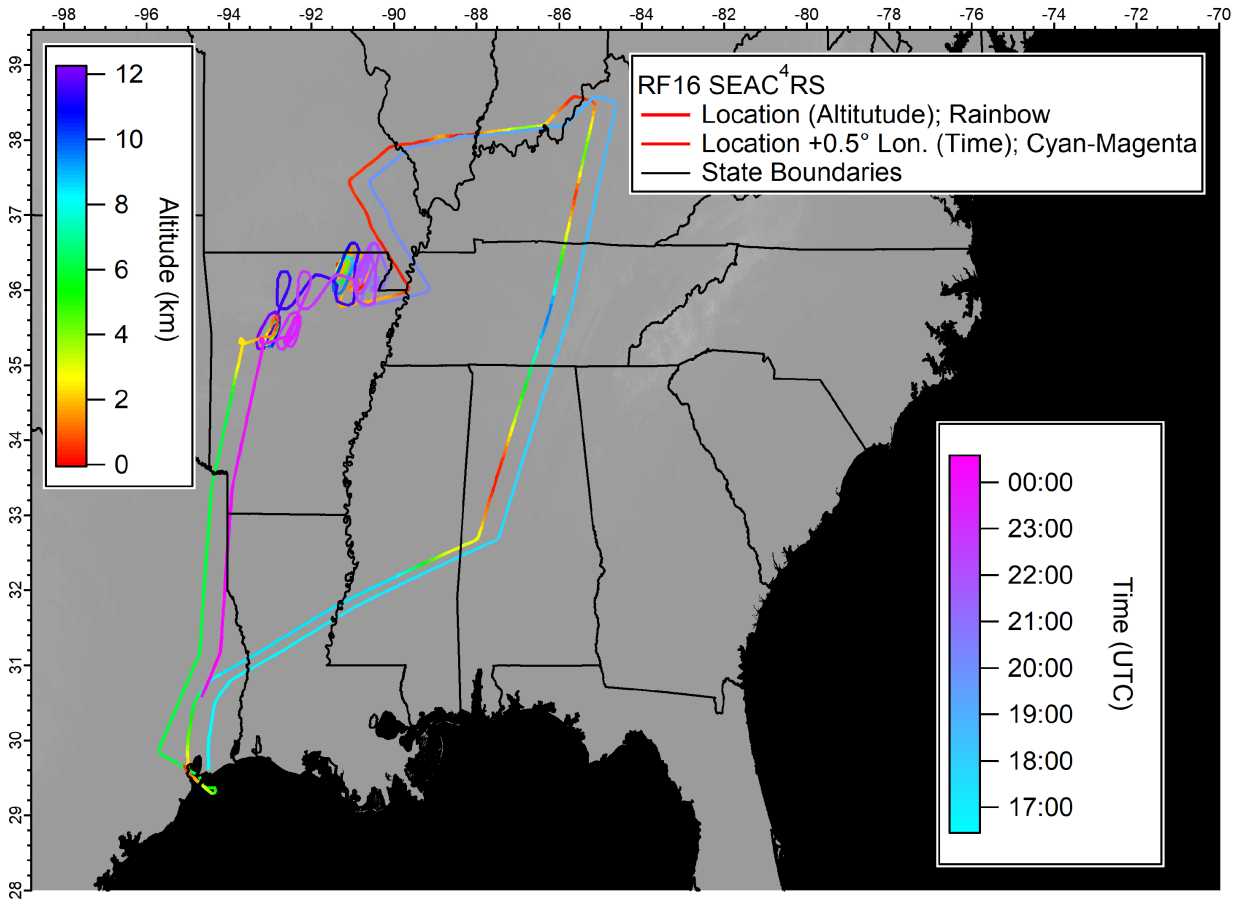


**Figure S10**. Flight track for SEAC4RS RF16 (11 Sept, 2013) over the SE US, colored by altitude and time (offset +0.5 degrees in longitude). Flight description (locations and sources sampled): The aircraft flew from Houston northeast to the Ohio River Valley partly at higher altitude with dips to low altitude in the region where the SOAS campaign was conducted in west-central Alabama, in central Kentucky, and at the Ohio River Valley, then flew to western Missouri (Ozark Mts) and the Mississippi River Valley (low altitudes), then northern Arkansas (range of altitudes), then returned south to Houston (at altitude). A range of source influences were sampled during different periods of the flight and can be approximately separated as follows for the low-level legs (<500 m) when pRONO$_2$ tended to be elevated: 16:40–17:00: (biogenic including isoprene-related and especially monoterpenes, low anthropogenic); 17:30 (biogenic and anthropogenic such as NO$_x$, NO$_y$, CO, aromatics); 17:45–18:00 (biogenics and anthropogenics; 18:20–19:30 (mixed anthropogenic and biogenic with varying proportions); 19:45–20:00 (mixed biogenic and anthropogenic with two large agricultural biomass burning spikes at 19:53–19:54 and 19:59–20:00 showing large spikes in $NH_4NO_3$, acetonitrile, and $f_{60}$); 20:15–20:30 (mixed biogenic and anthropogenic); 22:25–22:55 (mixed biogenic, anthropogenic). During low-level legs, OA was typically ~7-15 μg m$^{-3}$, but exceeded 80 μg m$^{-3}$ during the biomass burning plumes, and was 0.1–0.3 μg m$^{-3}$ in the free troposphere (see Fig. S11, top).

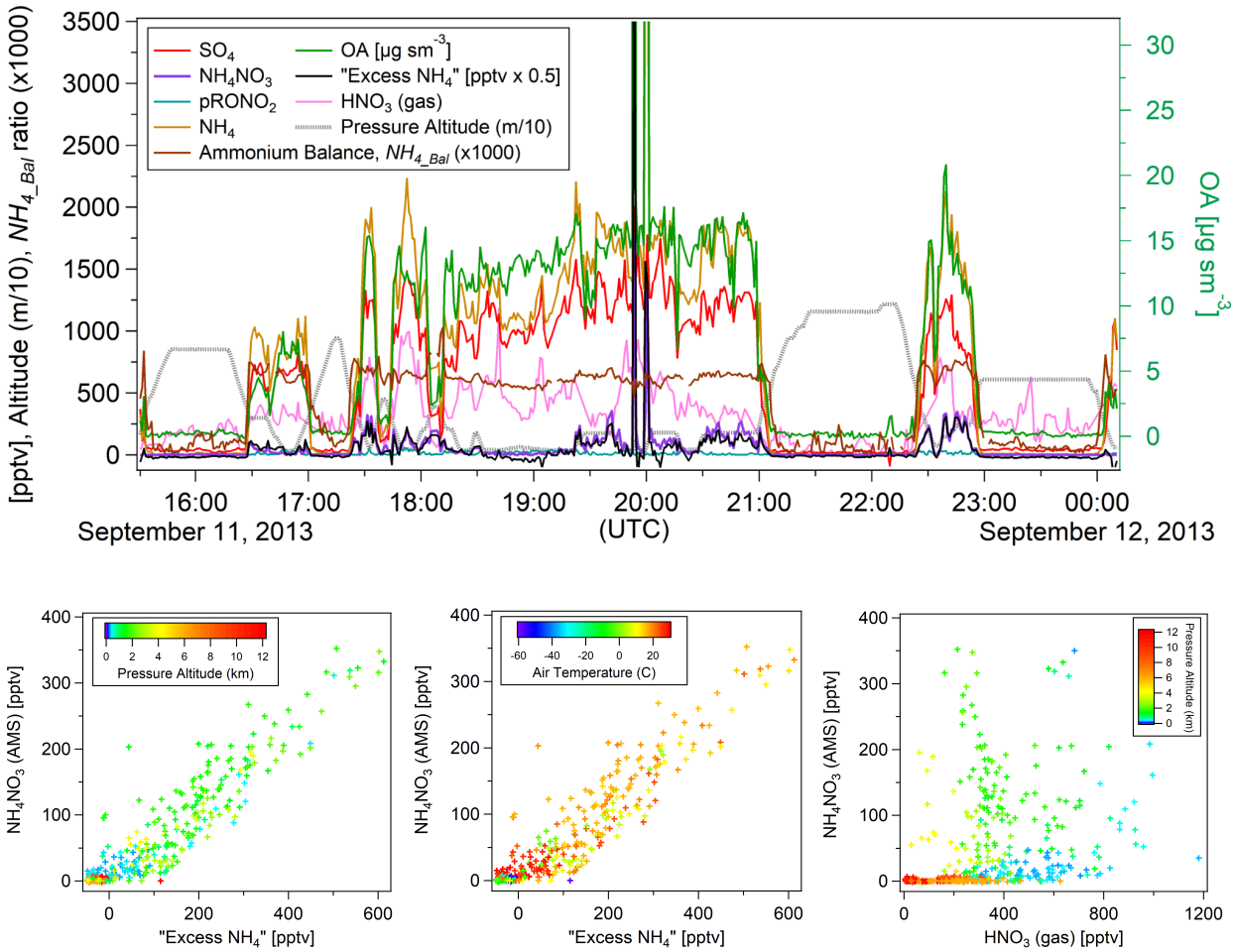


**Figure S11.** (top) Time series of $SO_4$, $NH_4$, $NH_4NO_3$, $pRONO_2$, "Excess $NH_4$", OA, $HNO_3$(gas), altitude, and ammonium balance ($NH_{4\_Bal}$, molar ratio of $NH_4$/ ($NO_3$+2$SO_4$)) for SEAC$^4$RS RF16 flight (same flight as shown in Fig. 3). "Excess $NH_4$" was calculated by subtracting the AMS-measured molar concentrations of $NH_4$ - 1.2 x $SO_4$ as an indicator of possible changes in the $NH_4$ related to $NH_4NO_3$ concentrations (see Sect. 5.1). All concentrations shown are in parts-per-trillion (pptv) mixing ratio unless otherwise indicated (i.e., OA). (bottom) Scatterplots of $NH_4NO_3$ vs. "Excess $NH_4$" (colored by altitude or air temperature) and vs $HNO_3$ gas (colored by altitude).

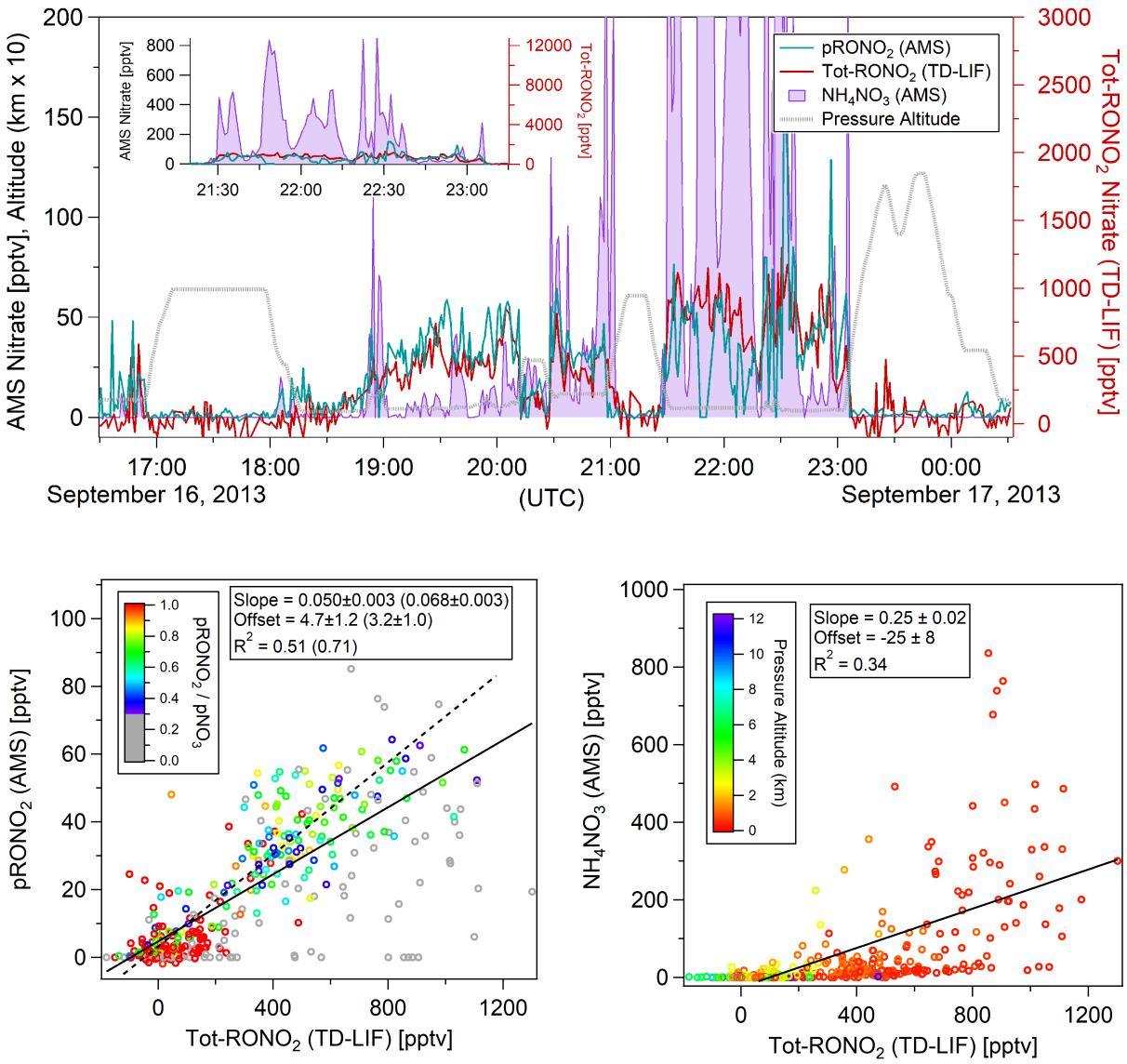


**Figure S12a.** Comparisons of AMS $pRONO_2$ and $NH_4NO_3$ with TD-LIF total (gas+particles) organic nitrate (Tot-$RONO_2$) during a SEAC[4]RS flight (RF18) in the Southeast US (1-min averages). The time series (top) and scatterplots of $pRONO_2$ (bottom left) or $NH_4NO_3$ (bottom right) vs Tot-$RONO_2$ are shown. $R_{NH4NO3}$ (constrained by calibrations and PMF), a *RoR* of 2.75, and Eqs. 2/3 were used to apportion the AMS nitrate. Linear least-squares lines are orthogonal distance regression (ODR). For the $pRONO_2$ vs Tot-$RONO_2$ plot (bottom left), and additional line (dotted) and fits (parentheses) are shown for data including only when $f_{pRONO2}$ is greater than 0.3 (and datapoints with $f_{pRONO2}$<0.3 are greyed). Figure S13 shows the flight track and timing of different source types sampled.

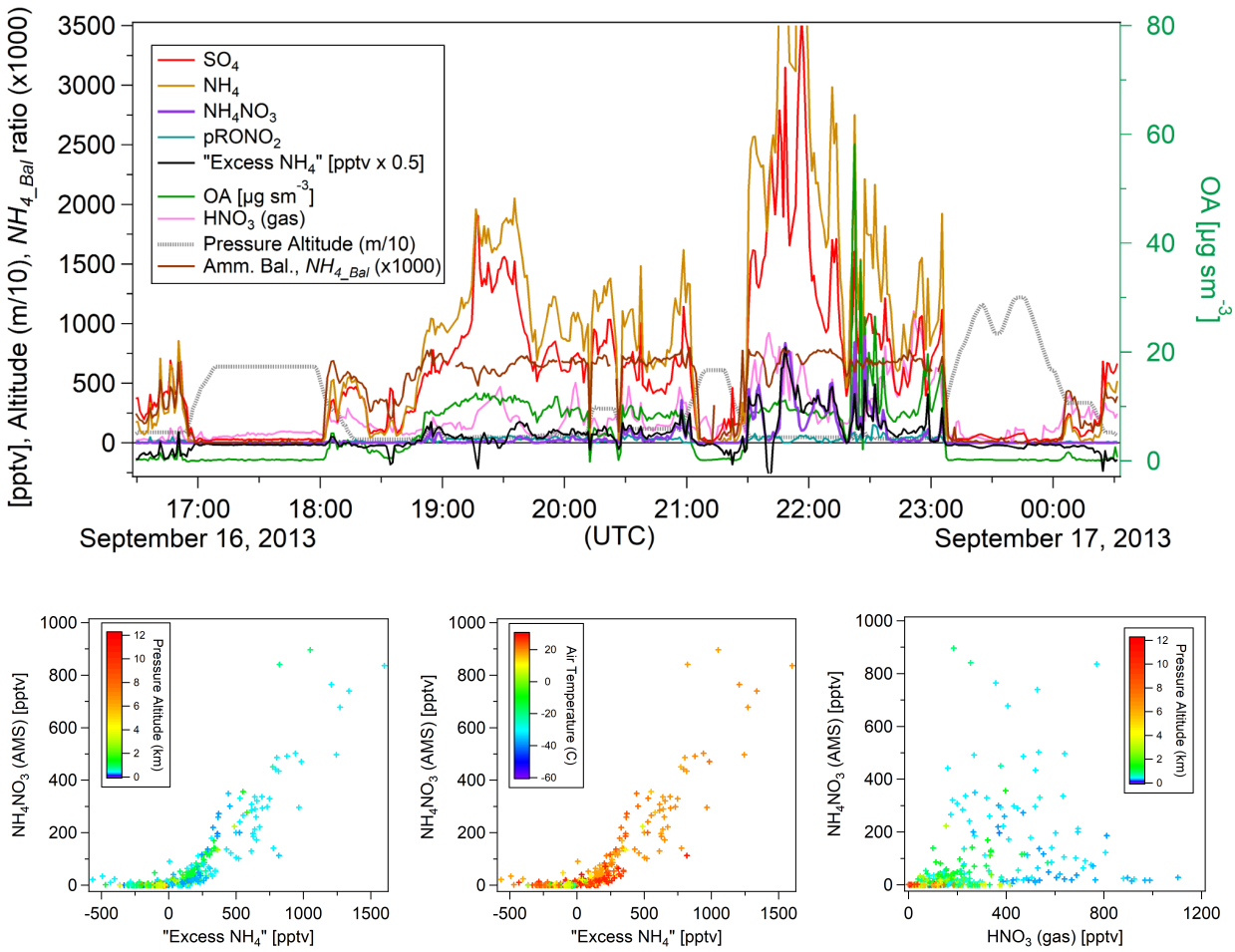


**Figure S12b.** Same as Fig. S11, except for RF18 (same flight as shown in Fig. S12a).

1090

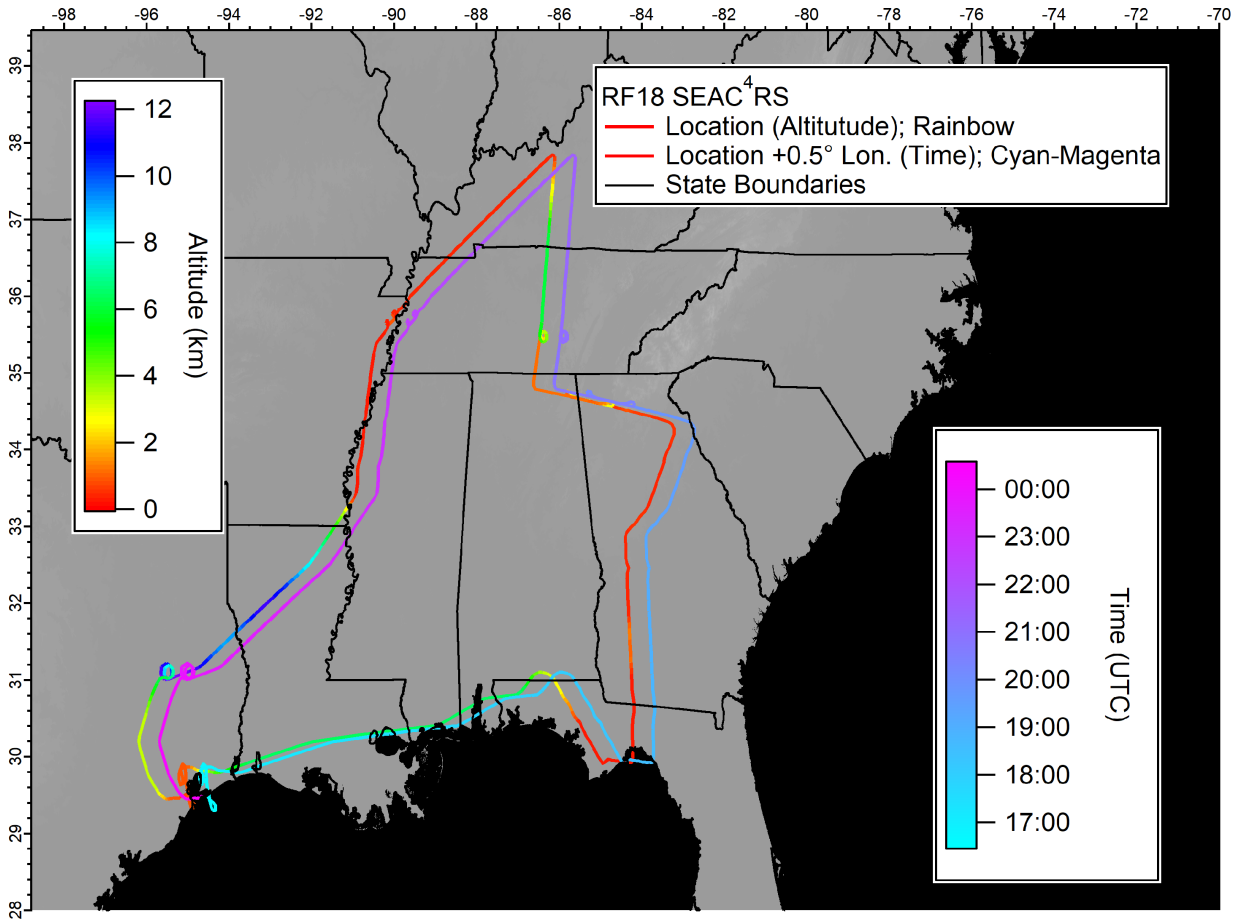


**Figure S13**. Flight track for SEAC4RS RF18 (16 Sept, 2013) over the SE US, colored by altitude and time (offset +0.5 degrees in Longitude). Flight description (locations and sources sampled): The aircraft flew from Houston east just inland along the Gulf Coast to the Florida panhandle (mostly at high altitude), north and northwest to the Ohio River Valley (mostly at low altitude), southwest to and south along the Mississippi River Valley (at low altitude), and then returned to Houston (mostly at high altitude). A range of source influences were sampled during different periods of the flight and can be approximately separated as follows for the low-level legs: 18:00–19:00 (strongly biogenic including isoprene-related and especially monoterpenes, low anthropogenic); 19:00–20:15 (elevated/decreasing monoterpenes, increasing isoprene-related, elevated anthropogenic such as aromatics, $NO_x$, $NO_y$); 20:30–21:00 (elevated isoprene-related biogenics and anthropogenics); 21:30–22:10 (lower biogenics, elevated anthropogenics); 22:20–23:10 (episodic concentrated agricultural biomass burning). During low-level legs, OA was typically ~5–10 μg $m^{-3}$, but exceeded 50 μg $m^{-3}$ during the biomass burning plumes, and was 0.1–0.3 μg $m^{-3}$ in the free troposphere (see Fig. S12b, top).

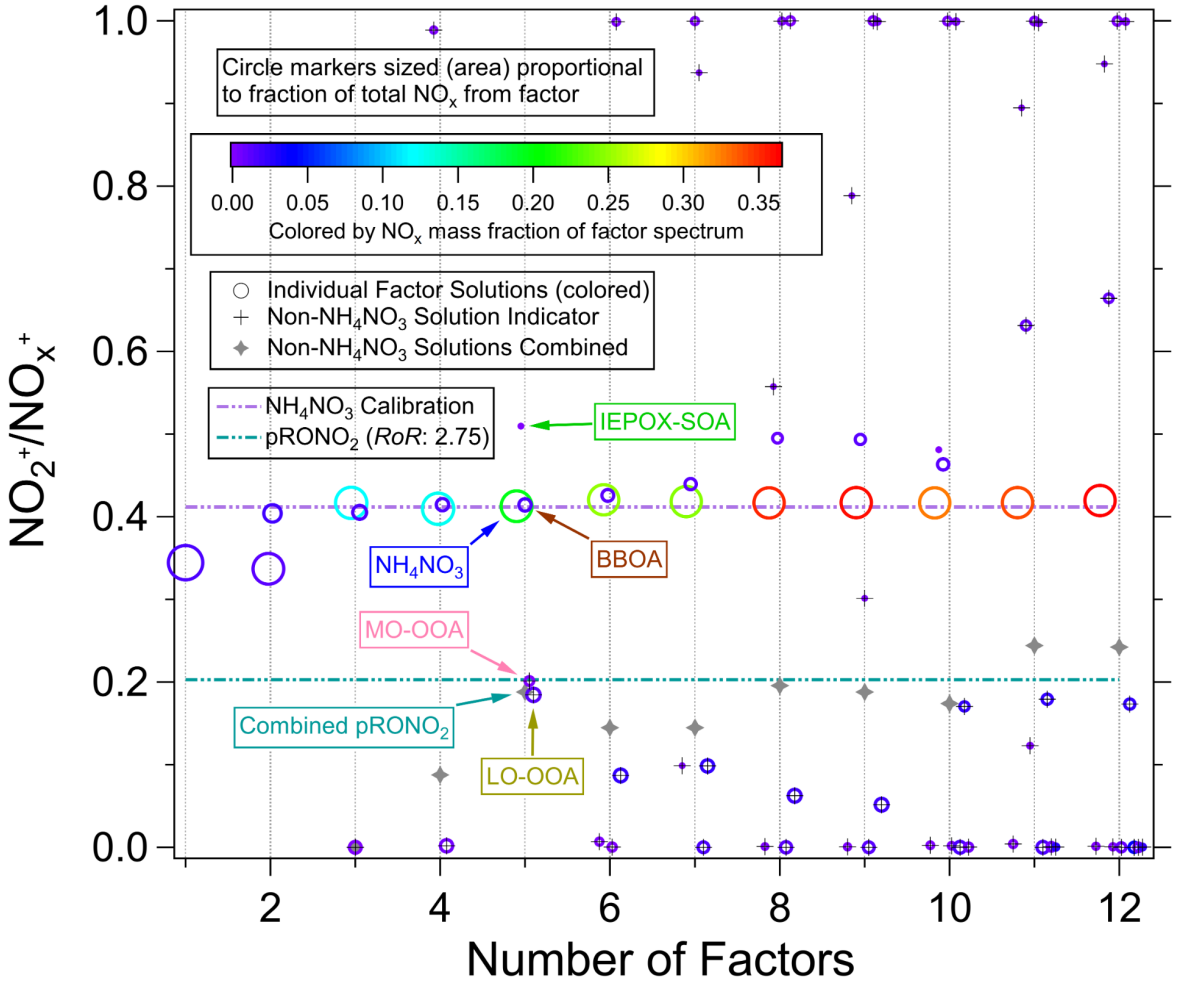


**Figure S14.** $NO_x^+$ ratios for individual and combined factors for PMF solutions for SEAC[4]RS RF16 vs number of factor solutions (FPEAK=0). Circles are sized by the fraction of the total $NO_x^+$ concentration apportioned to each individual factor and colored by the fraction of the spectrum from $NO_x^+$ ions. The individual factors that are not associated with $NH_4NO_3$ (generally a "$NH_4NO_3$ factor" and BBOA-related factors are and those not are defined as outside -20%/+50% of the calibration $NH_4NO_3$ $NO_2^+/NO_x^+$ for this plot) are indicated and their combined (mass-weighted) ratio is also shown. The largest circles with high $NO_x^+$ fraction in the spectrum are the $NH_4NO_3$ factors and generally the factors with similar $NO_x^+$ ratio are BBOA. The points not associated with $NH_4NO_3$ that have the largest contribution to total $NO_x^+$ concentration are typically LO-OOA. Factor assignments are indicated for the 5-factor solution, which was used in the analyses discussed in the manuscript. Note that in this figure rather than represent $NO_x^+$ ratios as used throughout this paper ($NO_2^+/NO^+$), instead $NO_2^+/NO_x^+$ is used. This allows the full range from entirely $NO^+$ to entirely $NO_2^+$ to be shown on a compact scale, since $NO_2^+/NO^+$ blows up as the limit of entirely $NO_2^+$ is approached. The relationship between the two ratios is: $NO_2^+/NO_x^+ = 1/(1+1/(NO_2^+/NO^+))$ or $NO_2^+/NO^+ = 1/(1/(NO_2^+/NO_x)-1)$.

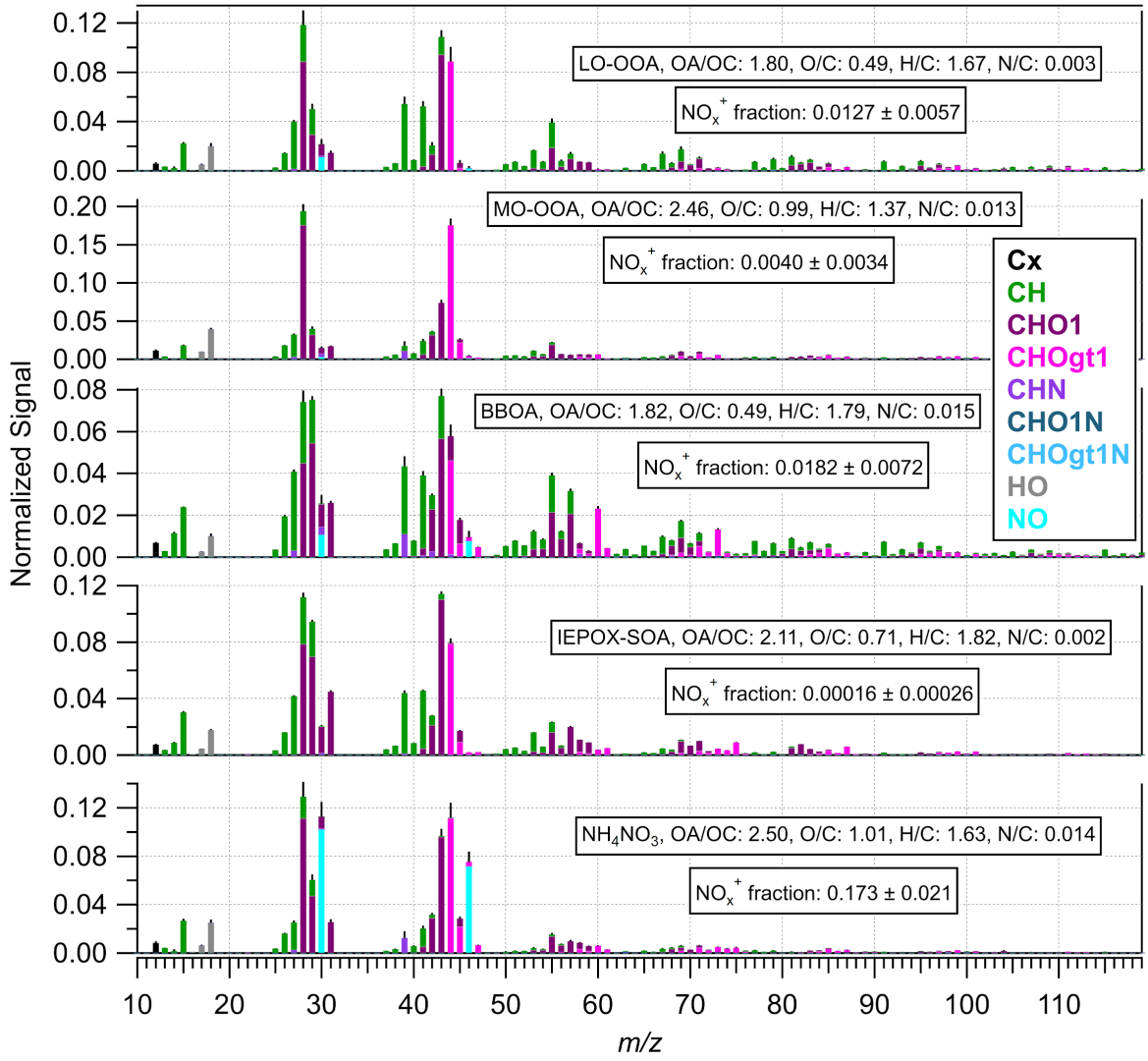


**Figure S15a.** PMF factor spectra for SEAC[4]RS RF16 (FPEAK=0). The spectra are averages from 100 *bootstrapping* (Ulbrich et al., 2009) iterations (with standard deviations propagated to the UMR sum shown in thin black vertical lines). The contributions from different ion families are colored and stacked at nominal *m/z*. The "1" or "gt1" denote that one or greater-than-one nitrogen or oxygen is associated with an ion family. The "NO" ion family contains all $H_yNO_x^+$ calculated in the HR analysis, although ions other than $NO^+$ and $NO_2^+$ are too small to be visible. "$NO_x^+$ fraction" is the fraction of the total signal from $NO^+$ and $NO_2^+$ ions. Elemental ratios (Aiken et al., 2008; Canagaratna et al., 2015) are also indicated where N/C ratios do not include $H_yNO_x^+$ ions (as is typically reported for AMS analysis).

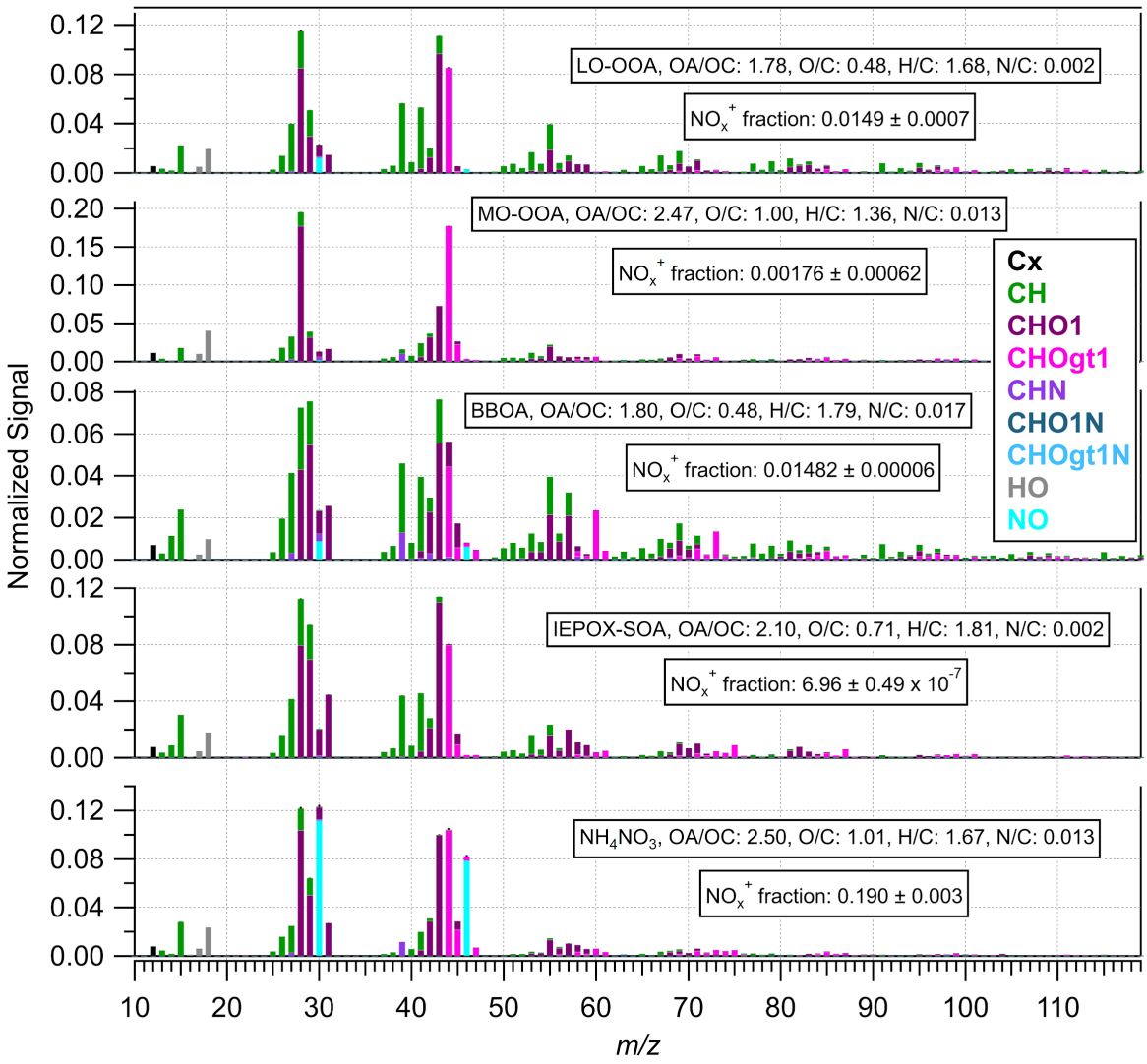


1135 **Figure S15b.** Same as Fig. S15a except averages and standard deviations are from 100 starting *seed* iterations (Ulbrich et al., 2009).

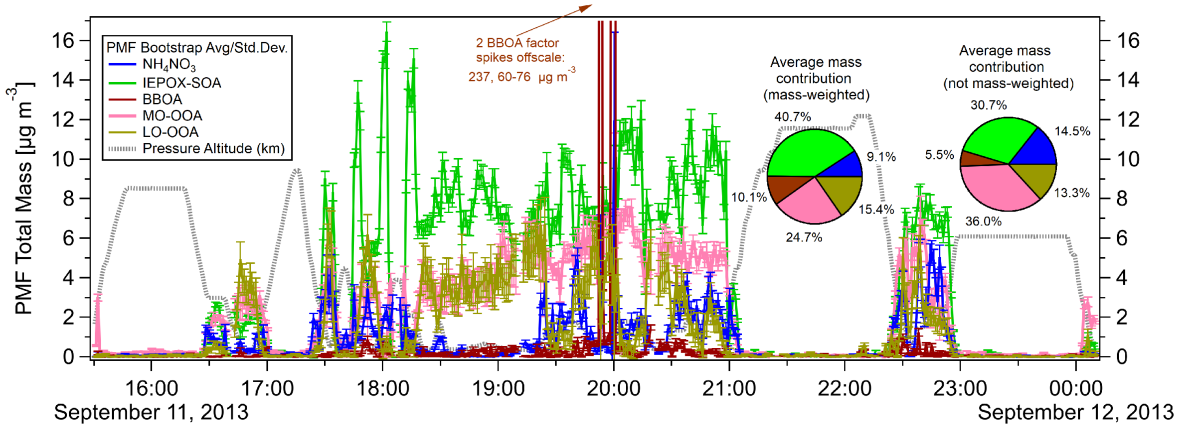


**Figure S16a.** Time series of PMF factors (total signal: OA + nitrate) for SEAC[4]RS RF16 (FPEAK=0). Averages and standard deviations for each point in the time series as well as the all-flight averages (shown as pies) were computed from 100 *bootstrapping* run

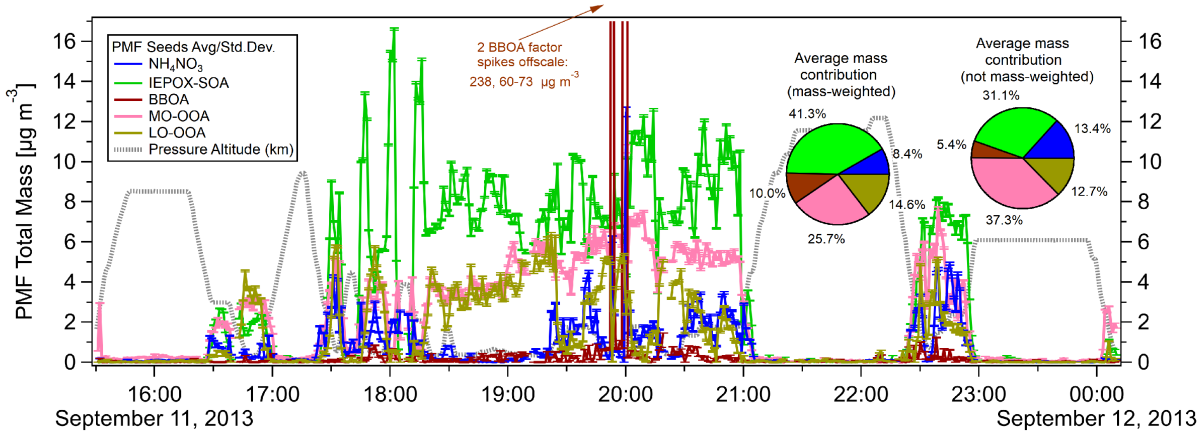


**Figure S16b.** Same as Fig. S16a, except using 100 *seed* runs (rather than *bootstrapping*)

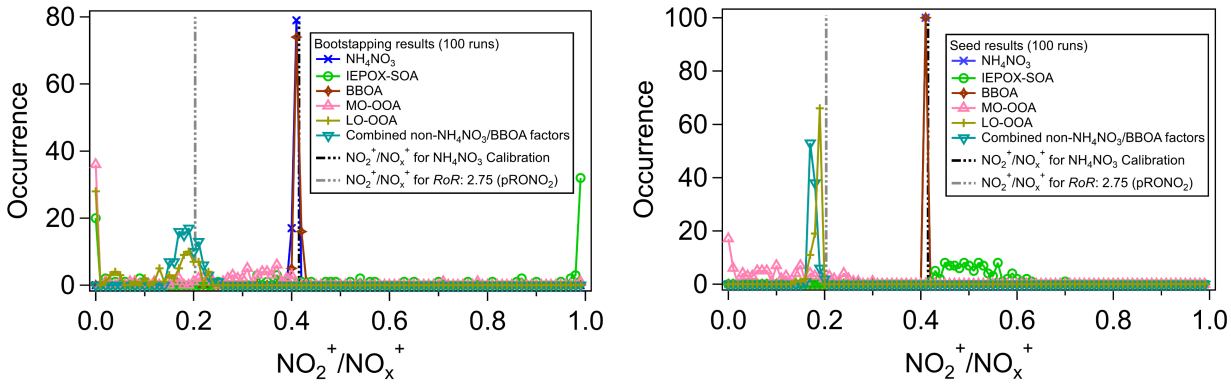


**Figure S17.** Histograms of $NO_x^+$ ratios for individual and combined PMF factors for SEAC[4]RS RF16 (FPEAK=0) for 100 bootstrapping (left) or seeding (right) iterations. Vertical lines are shown for the calibration $R_{NH4NO3}$ and the $R_{pRONO2}$ using a *RoR* referenced to the $NH_4NO_3$ factor ratio. Note that in this figure rather than represent $NO_x^+$ ratios as used throughout this paper ($NO_2^+/NO^+$), instead $NO_2^+/NO_x^+$ is

used in order that the full range from all $NO^+$ to all $NO_2^+$ can be displayed on a compact scale (see Fig. S14 caption for more details).

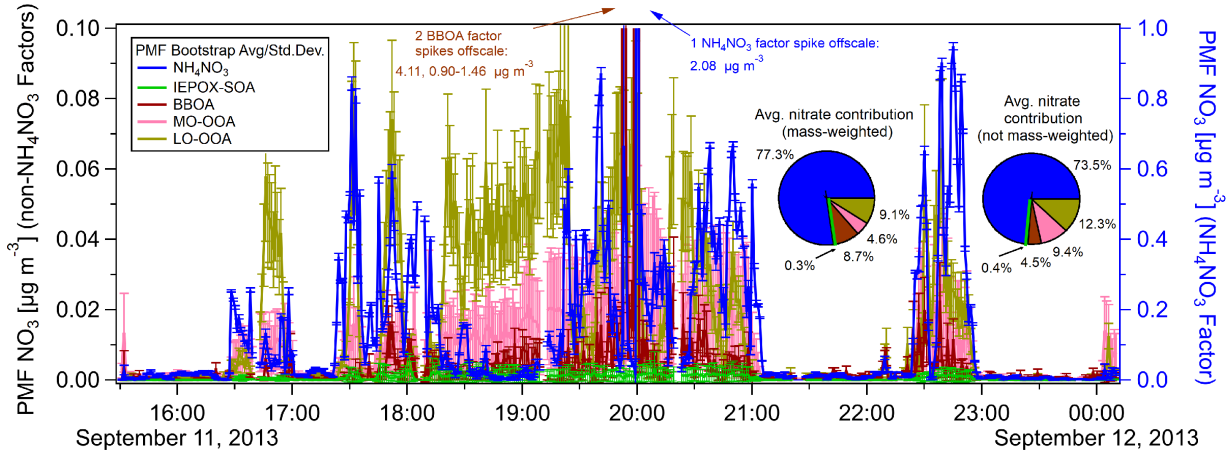


**Figure S18a.** Time series of nitrate component of PMF factors for SEAC[4]RS RF16 (FPEAK=0). Averages and standard deviations for each point in the time series as well as the all-flight averages (shown as pies) were computed from 100 *bootstrapping* runs. For aircraft sampling altitude see Fig. S16.

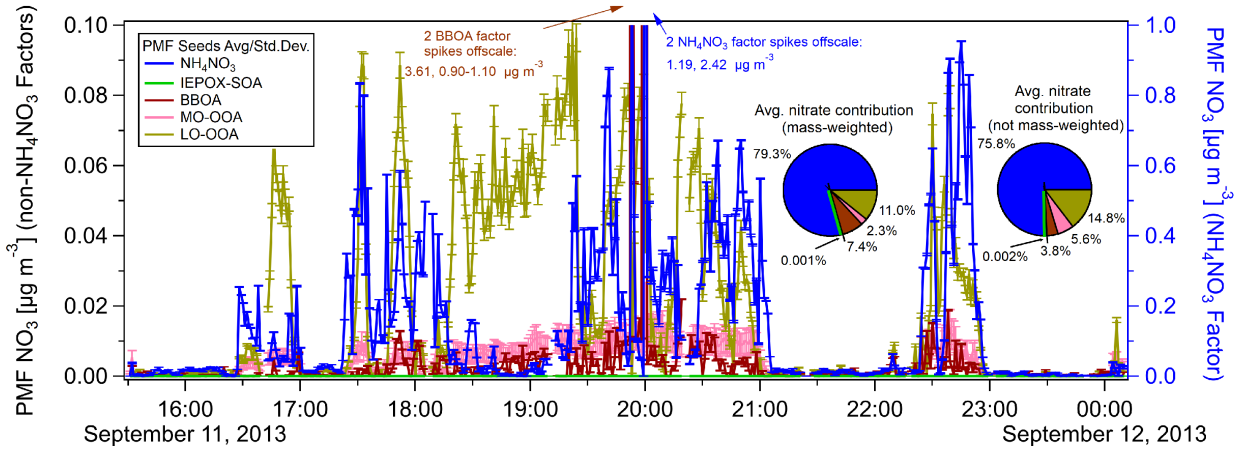


**Figure S18b.** Same as Fig. S18a, except using 100 *seed* runs (rather than *bootstrapping*). For aircraft sampling altitude see Fig. S16.

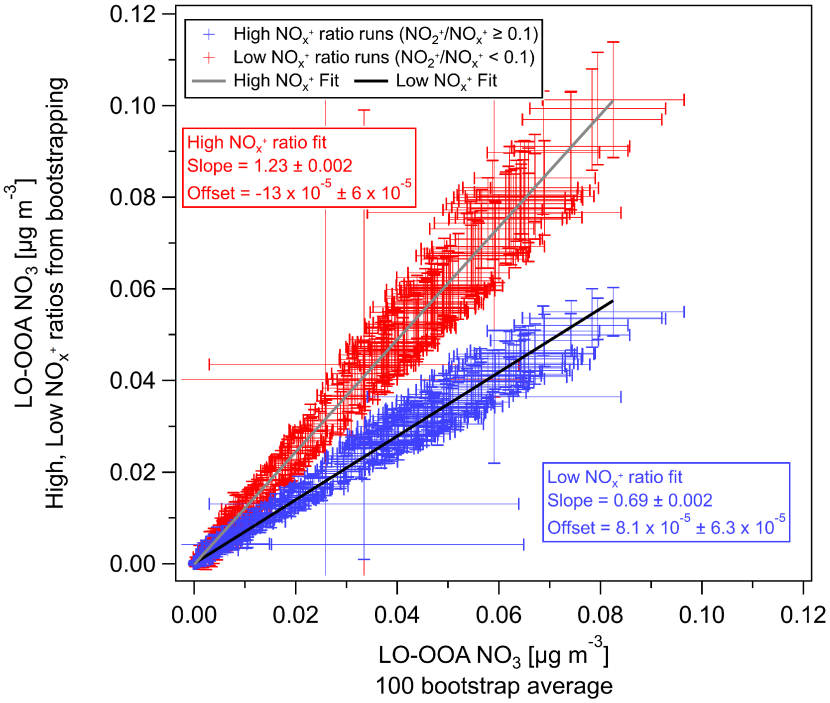


**Figure S19.** Nitrate concentrations apportioned to the PMF LO-OOA factor for different ranges of $NO_x^+$ ratios (in the factor spectra) vs the average of all runs for 100 bootstrapping runs (SEAC[4]RS RF16). The averages and standard deviations for the different subsets are shown for each time point.

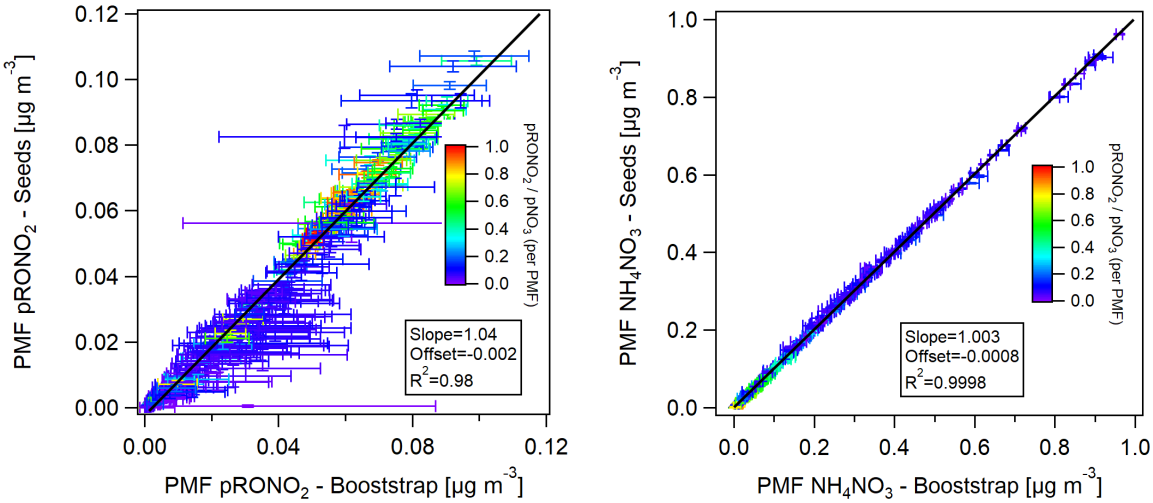


**Figure. S20.** Comparison of bootstrapping vs seeding nitrate apportionment concentrations for SEAC[4]RS RF16 (averages and standard deviations for 100 runs shown for each time point).

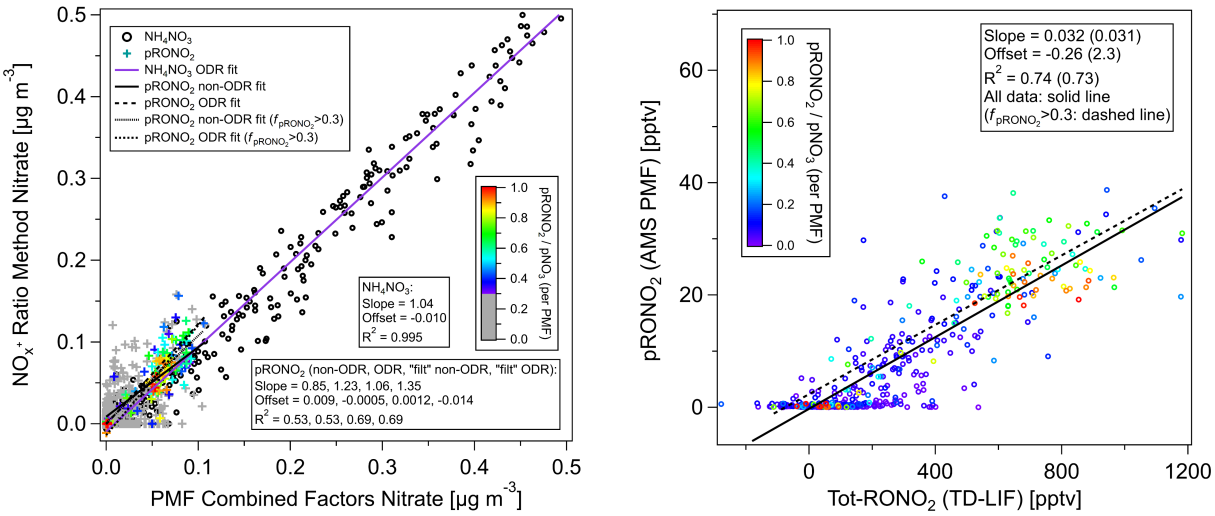


**Figure S21.** Equivalent plots to bottom panels in Fig. 4 except averages of seed runs (rather than bootstrapping).

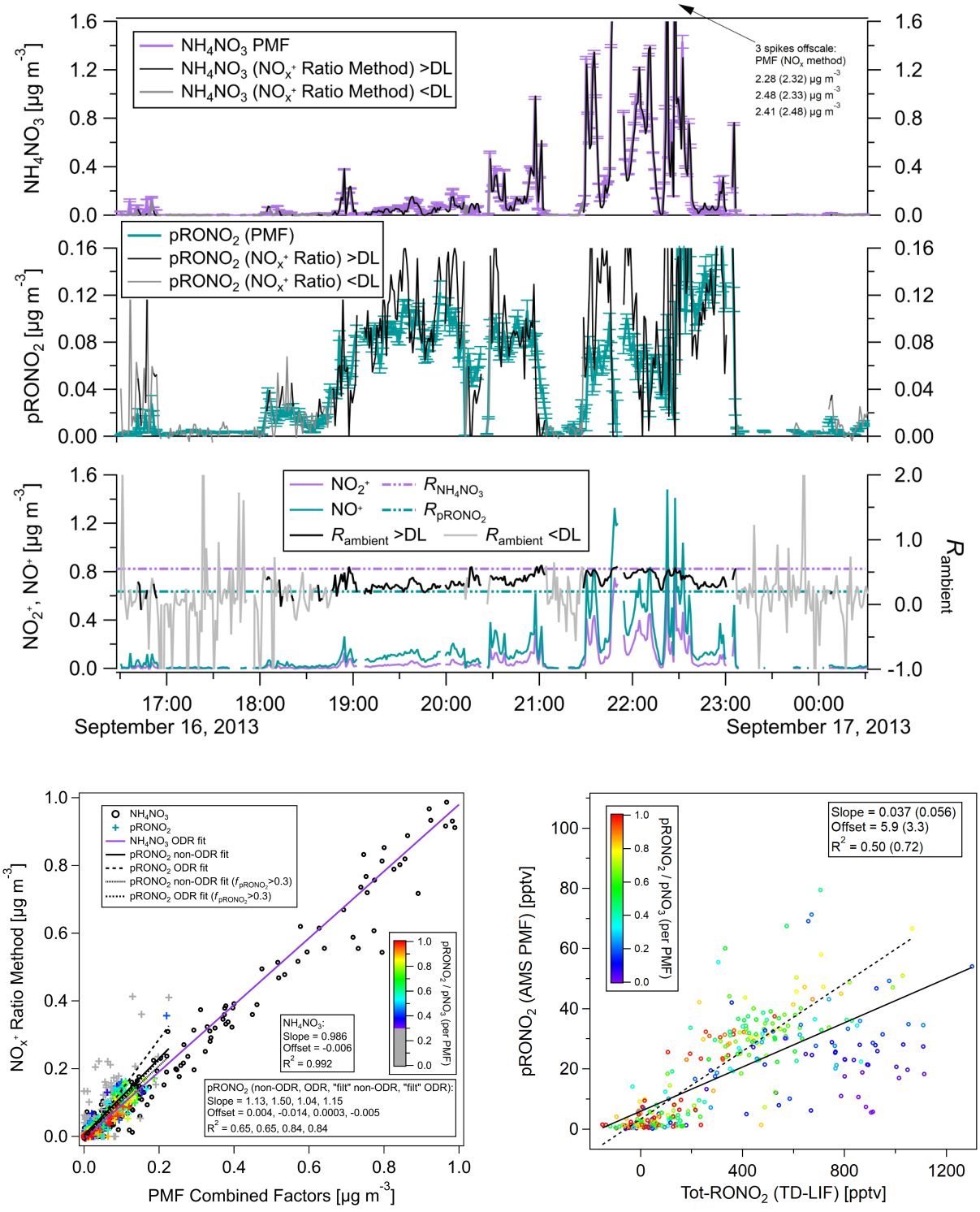


**Figure S22.** Same as Fig. 4 except for SEAC[4]RS RF18 (rather than RF16).

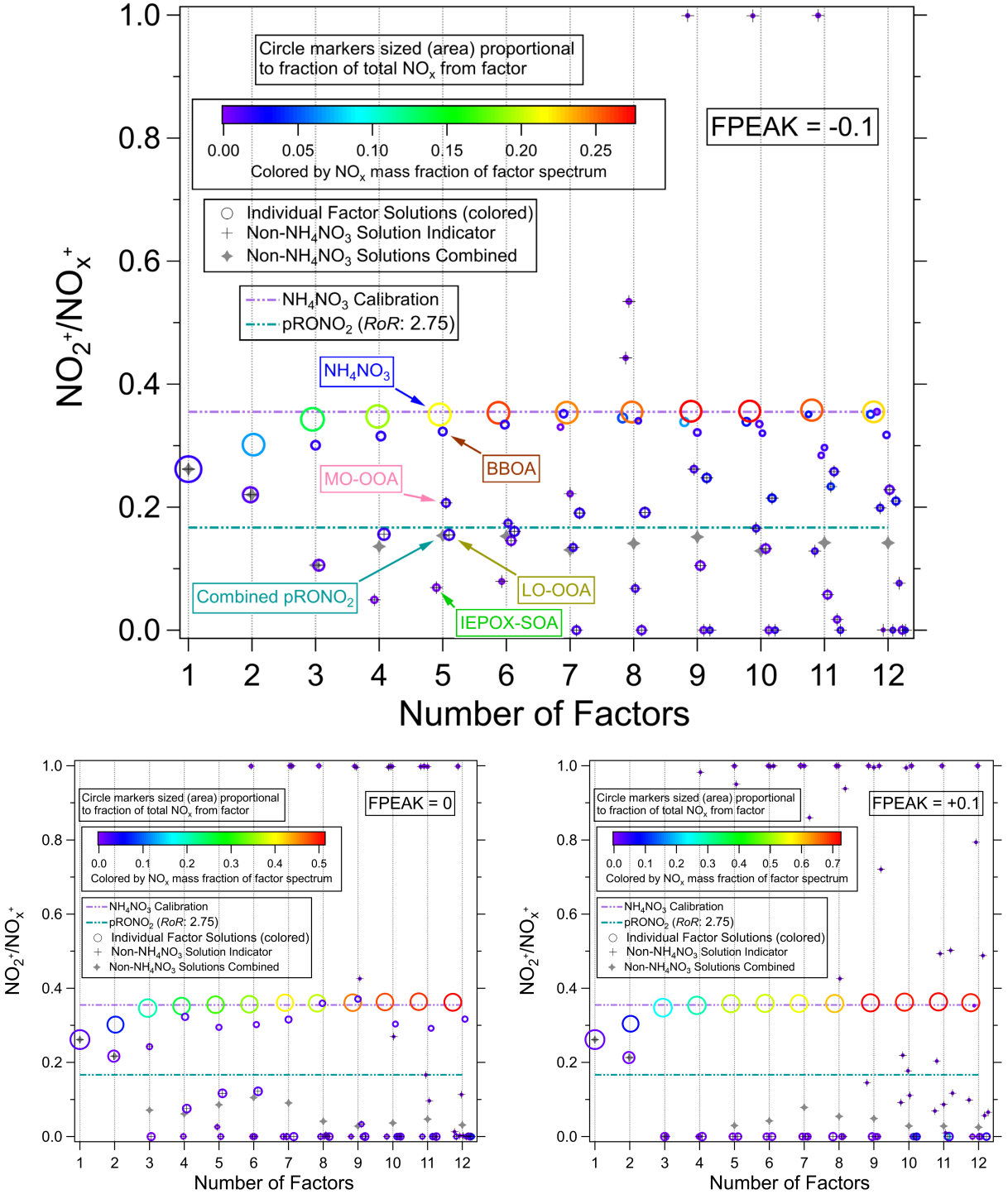


**Figure S23.** Same as Fig. S14 except for SEAC[4]RS RF18 (instead of RF16) and also showing results for three different FPEAK (-0.1, 0, +0.1), since the FPEAK = -0.1 (5-factor) solution was used all for analyses and comparisons (see Sect. S4.2). Factor assignments are indicated for the 5-factor solution with FPEAK = -0.1.

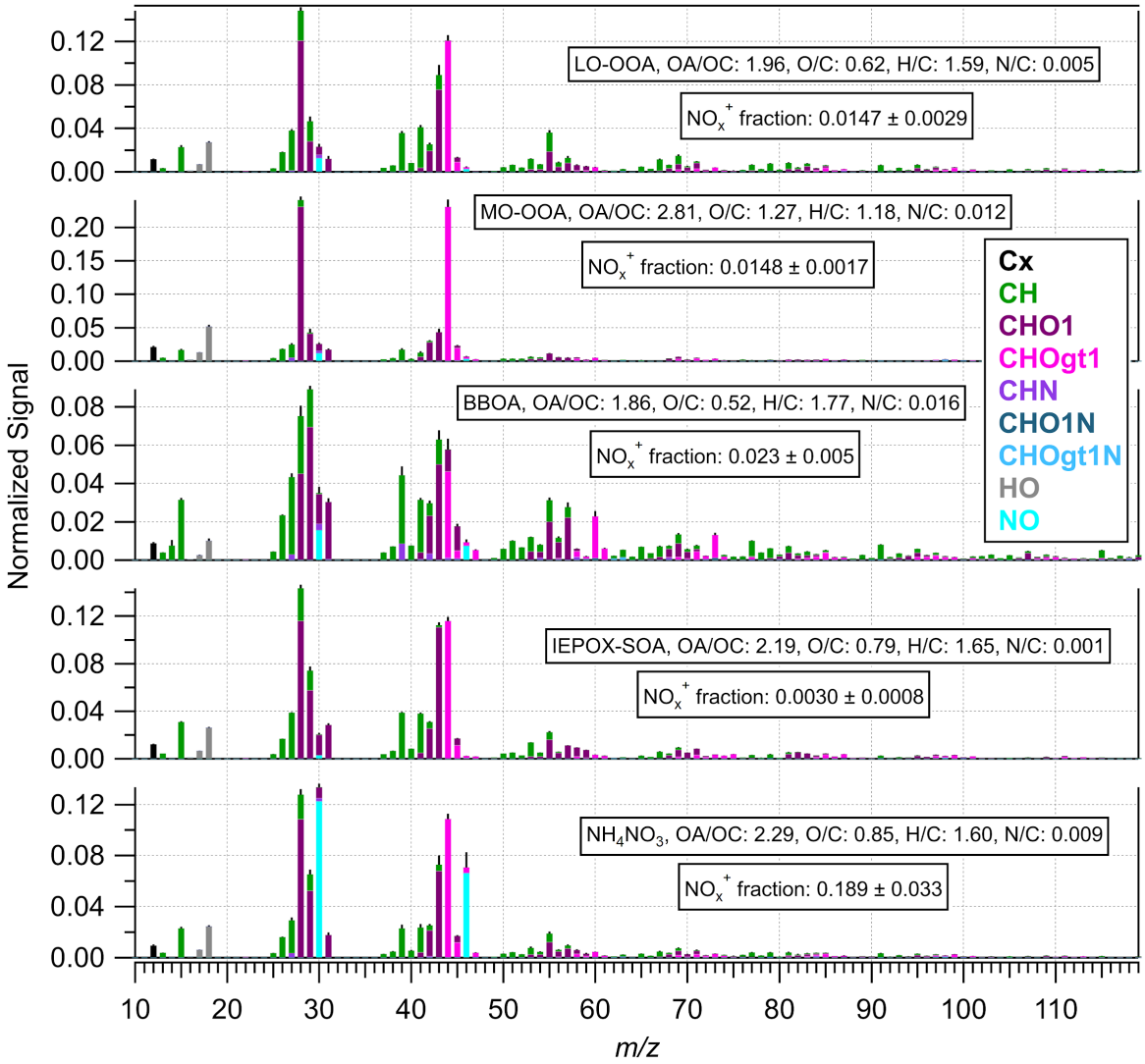


**Figure S24.** PMF Factor spectra for SEAC[4]RS RF18 (FPEAK= -0.1). The spectra are averages and from 100 bootstrapping iterations. See caption for Fig. S15a (showing same results for RF16) for additional details.

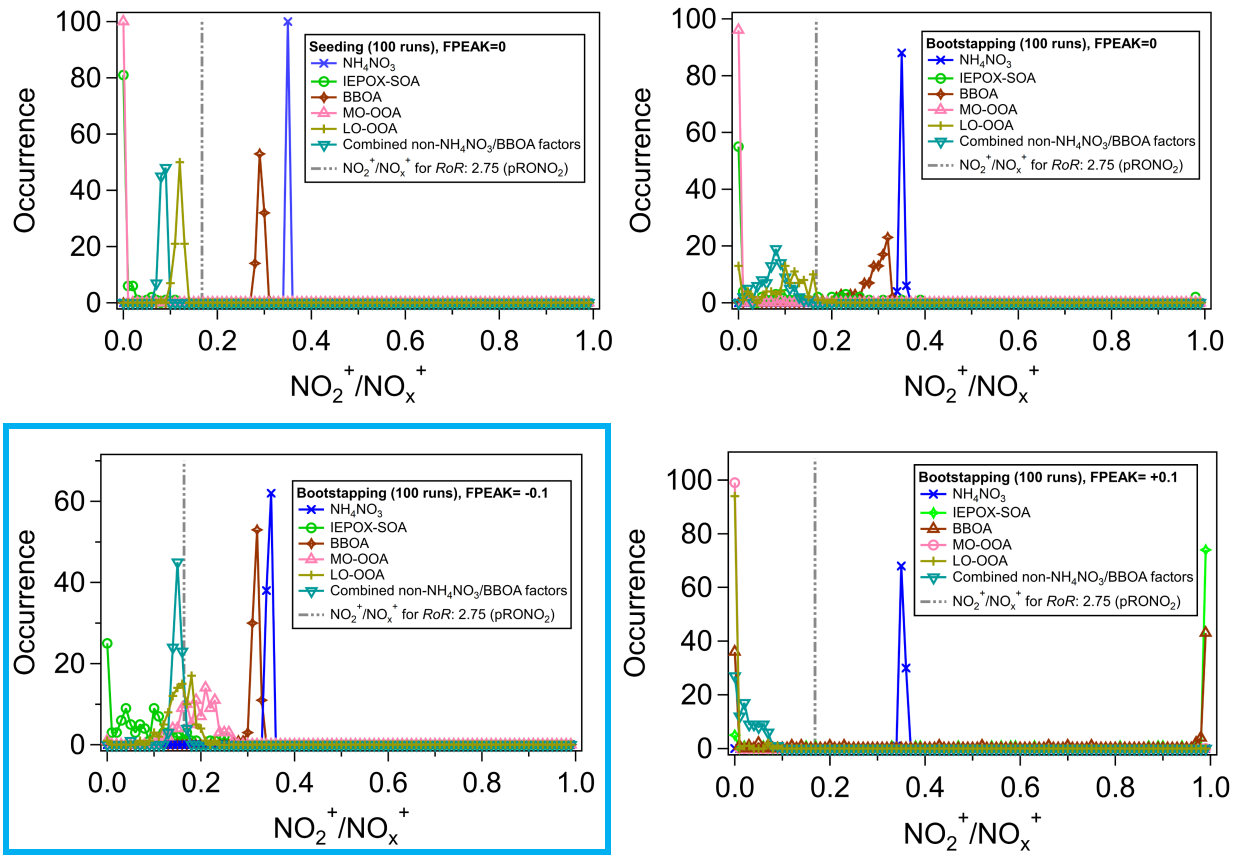


**Figure S25.** Histograms of $NO_x^+$ ratios for individual and combined PMF factors for SEAC[4]RS RF18 for 5-factor solutions with: (top left) seeding, FPEAK = 0; (top right) bootstrapping, FPEAK = 0; (bottom left) bootstrapping, FPEAK = -0.1; (bottom right) bootstrapping, FPEAK = +0.1 (see Fig. S14, S17 captions for more details on $NO_x^+$ ratio scale). The vertical line indicates the $R_{pRONO2}$ using a *RoR* referenced to the $NH_4NO_3$ factor ratio. The FPEAK = -0.1 solution (highlighted with blue border) was used in all analyses and comparisons (see Sect. S4.2).

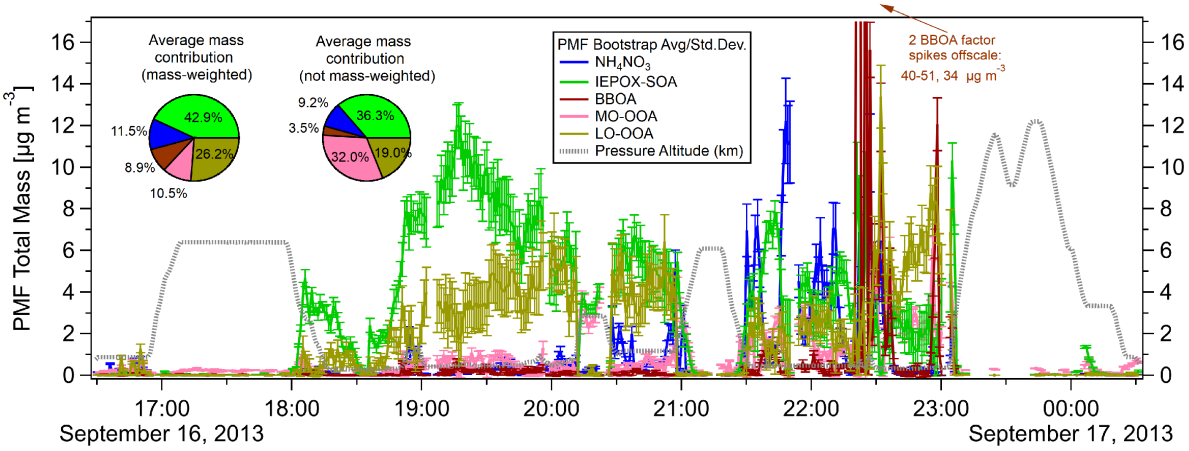


**Figure S26.** Time series of PMF factors (total signal, OA + nitrate) for SEAC[4]RS RF18 (FPEAK = -0.1). Averages and standard deviations for each point in the time series as well as the all-flight averages (shown as pies) were computed from 100 bootstrapping runs.

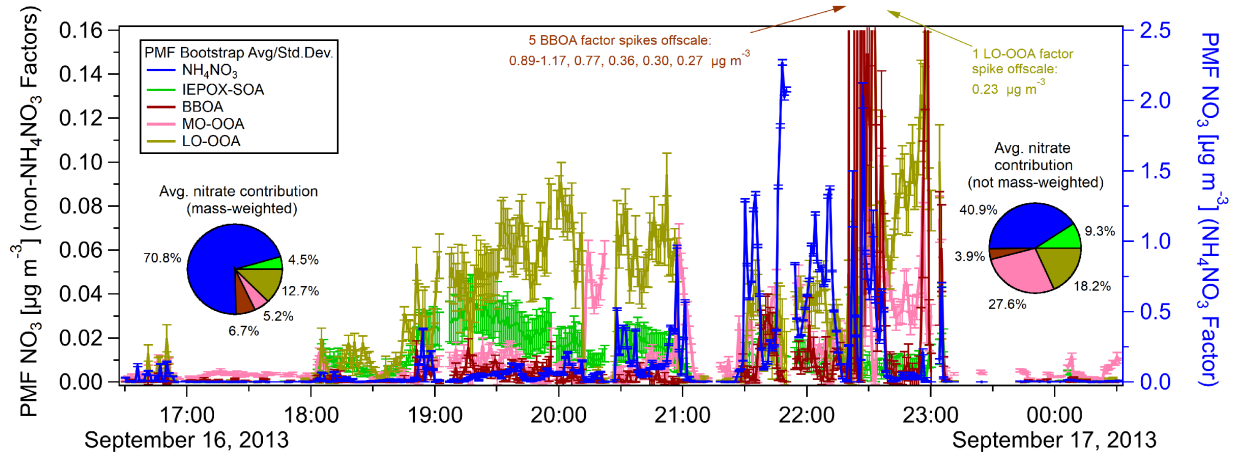


**Figure S27.** Time series of nitrate component of PMF factor for SEAC[4]RS RF18 (FPEAK = -0.1). Averages and standard deviations for each point in the time series as well as the all-flight averages (shown as pies) were computed from 100 bootstrapping runs. For aircraft sampling altitude see Fig. S26.

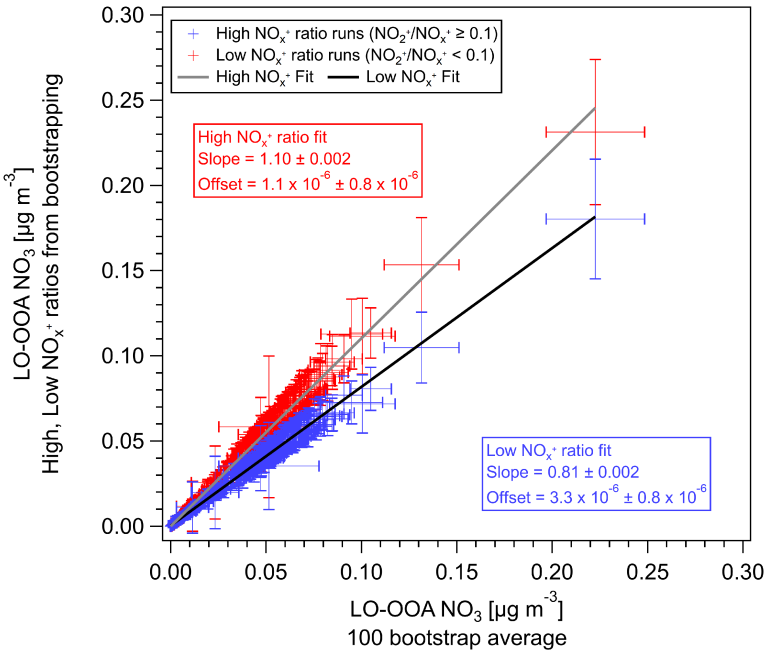


**Figure S28.** Nitrate concentrations apportioned to the PMF LO-OOA factor for different ranges of $NO_x^+$ ratios (in the factor spectra) vs the average of all runs for 100 bootstrapping runs (SEAC[4]RS RF18). The averages and standard deviations for the different subsets are shown for each time point.

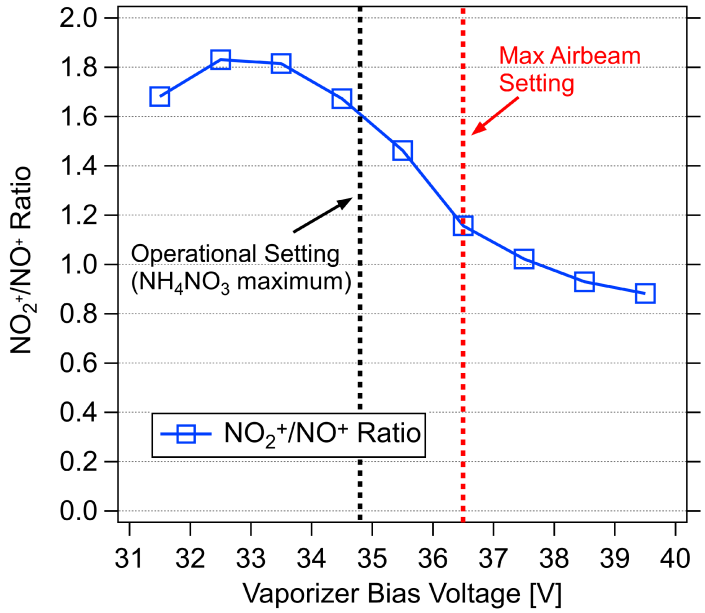


**Figure S29**. $NO_x^+$ ratio vs vaporizer bias voltage while sampling pure $NH_4NO_3$ particles. In this example the particle signal and airbeam signal ($N_2^+$) are not coincident; however, this is not always the case. In other cases, we have observed $NO_x^+$ ratio minima near the particle signal maxima and increasing with higher and lower vaporizer bias. Similar trends and magnitude of the $NO_x^+$ ratio (i.e., *m/z* 30 / *m/z* 46) changes vs vaporizer bias has been observed for the ACSMs (Jayne et al., 2015; slide 21).

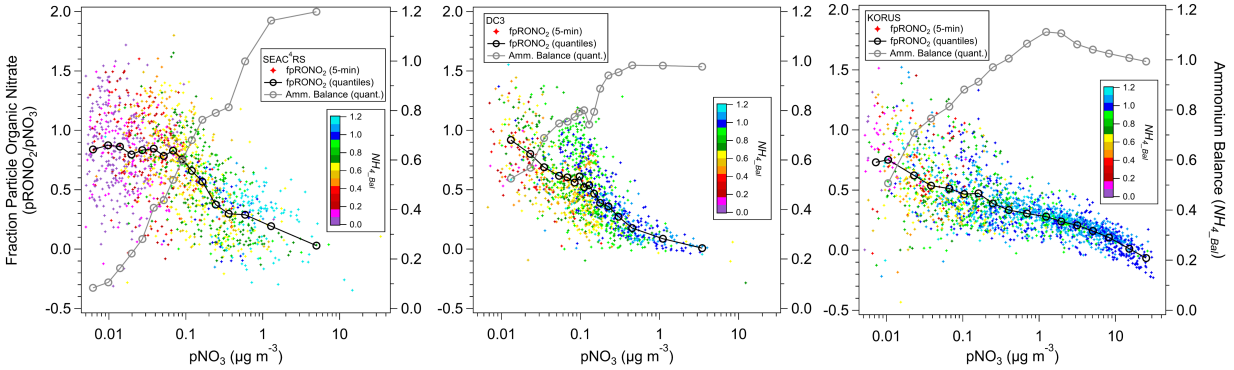


**Figure S30.** $f_{pRONO2}$ vs. $pNO_3$ for aircraft campaigns (5-min, quantile averages). 5-min $f_{pRONO2}$ is colored by ammonium balance ($NH_{4\_Bal}$, molar ion charge ratio of $NH_4^+$ to $NO_3^-$ + $SO_4^{2-}$) and quantile averages of $NH_{4\_Bal}$ are also shown. At lower $pNO_3$, $NH_{4\_Bal}$ was much lower for SEAC[4]RS compared to the other campaigns, while DC3 was slightly lower than for KORUS.

## References


Aiken, A. C., Decarlo, P. F., Kroll, J. H., Worsnop, D. R., Huffman, J. A., Docherty, K. S., Ulbrich, I. M., Mohr, C., Kimmel, J. R., Sueper, D., Sun, Y., Zhang, Q., Trimborn, A., Northway, M., Ziemann, P. J., Canagaratna, M. R., Onasch, T. B., Alfarra, M. R., Prevot, A. S. H., Dommen, J., Duplissy, J., Metzger, A., Baltensperger, U. and Jimenez, J. L.: O/C and OM/OC Ratios of Primary, Secondary, and Ambient Organic Aerosols with High-Resolution Time-of-Flight Aerosol Mass Spectrometry, Environ. Sci. Technol., 42(12), 4478–4485, 2008.

Aiken, A. C., Salcedo, D., Cubison, M. J., Huffman, J. A., DeCarlo, P. F., Ulbrich, I. M., Docherty, K. S., Sueper, D., Kimmel, J. R., Worsnop, D. R., Trimborn, A., Northway, M., Stone, E. A., Schauer, J. J., Volkamer, R. M., Fortner, E., de Foy, B., Wang, J., Laskin, A., Shutthanandan, V., Zheng, J., Zhang, R., Gaffney, J., Marley, N. A., Paredes-Miranda, G., Arnott, W. P., Molina, L. T., Sosa, G. and Jimenez, J. L.: Mexico City aerosol analysis during MILAGRO using high resolution aerosol mass spectrometry at the urban supersite (T0) – Part 1: Fine particle composition and organic source apportionment, Atmos. Chem. Phys., 9(17), 6633–6653, 2009.

Aiken, A. C., De Foy, B., Wiedinmyer, C., Decarlo, P. F., Ulbrich, I. M., Wehrli, M. N., Szidat, S., Prevot, A. S. H., Noda, J., Wacker, L., Volkamer, R., Fortner, E., Wang, J., Laskin, A., Shutthanandan, V., Zheng, J., Zhang, R., Paredes-Miranda, G., Arnott, W. P., Molina, L. T., Sosa, G., Querol, X., Jimenez, J. L., Prévôt, a. S. H., Noda, J., Wacker, L., Volkamer, R., Fortner, E., Wang, J., Laskin, A., Shutthanandan, V., Zheng, J., Zhang, R., Paredes-Miranda, G., Arnott, W. P., Molina, L. T., Sosa, G., Querol, X. and Jimenez, J. L.: Mexico city aerosol analysis during MILAGRO using high resolution aerosol mass spectrometry at the urban supersite (T0)-Part 2: Analysis of the biomass burning contribution and the non-fossil carbon fraction, Atmos. Chem. Phys., 10(12), 5315–5341, 2010.

Alfarra, M. R.: Insights into atmospheric organic aerosols using an aerosol mass spectrometer, PhD Thesis, University of Manchester Institute of Science and Technology., 2004.

Alfarra, M. R., Paulsen, D., Gysel, M., Garforth, A. a., Dommen, J., Prévôt, a. S. H., Worsnop, D. R., Baltensperger, U. and Coe, H.: A mass spectrometric study of secondary organic aerosols formed from the photooxidation of anthropogenic and biogenic precursors in a reaction chamber, Atmos. Chem. Phys., 6, 5279–5293, 2006.

Ayres, B. R., Allen, H. M., Draper, D. C., Brown, S. S., Wild, R. J., Jimenez, J. L., Day, D. A., Campuzano-Jost, P., Hu, W., de Gouw, J., Koss, A., Cohen, R. C., Duffey, K. C., Romer, P., Baumann, K., Edgerton, E., Takahama, S., Thornton, J. A., Lee, B. H. H., Lopez-Hilfiker, F. D., Mohr, C., Wennberg, P. O., Nguyen, T. B., Teng, A., Goldstein, A. H., Olson, K. and Fry, J. L.: Organic nitrate aerosol formation via $NO_3$ + biogenic volatile organic compounds in the southeastern United States, Atmos. Chem. Phys., 15(23), 13377–13392, 2015.

Bahreini, R., Ervens, B., Middlebrook, A. M., Warneke, C., De Gouw, J. A., DeCarlo, P. F., Jimenez, J. L., Brock, C. A., Neuman, J. A., Ryerson, T. B., Stark, H., Atlas, E., Brioude, J., Fried, A., Holloway, J. S., Peischl, J., Richter, D., Walega, J., Weibring, P., Wollny, a. G., Fehsenfeid, F. C. and Fehsenfeld, F. C.: Organic aerosol formation in urban and industrial plumes near Houston and Dallas, Texas, J. Geophys. Res., 114(16), D00F16–D00F16, 2009.

Barth, M. C., Cantrell, C. A., Brune, W. H., Rutledge, S. A., Crawford, J. H., Huntrieser, H., Carey, L. D.,

MacGorman, D., Weisman, M., Pickering, K. E., Bruning, E., Anderson, B., Apel, E., Biggerstaff, M., Campos, T., Campuzano-Jost, P., Cohen, R., Crounse, J., Day, D. A., Diskin, G., Flocke, F., Fried, A., Garland, C., Heikes, B., Honomichl, S., Hornbrook, R., Huey, L. G., Jimenez, J. L., Lang, T., Lichtenstern, M., Mikoviny, T., Nault, B., O'Sullivan, D., Pan, L. L., Peischl, J., Pollack, I., Richter, D., Riemer, D., Ryerson, T., Schlager, H., Clair, J. S., Walega, J., Weibring, P., Weinheimer, A., Wennberg, P., Wisthaler, A., Wooldridge, P. J. and Ziegler, C.: The deep convective clouds and chemistry (DC3) field campaign, Bull. Am. Meteorol. Soc., 96(August), 1281–1309, 2015.

Boyd, C. M., Sanchez, J., Xu, L., Eugene, a. J., Nah, T., Tuet, W. Y., Guzman, M. I. and Ng, N. L.: Secondary organic aerosol formation from the β-pinene+$NO_3$ system: effect of humidity and peroxy radical fate, Atmos. Chem. Phys., 15(13), 7497–7522, 2015.

Bruns, E. A., Perraud, V., Zelenyuk, A., Ezell, M. J., Johnson, S. N., Yu, Y., Imre, D., Finlayson-Pitts, B. J., Alexander, M. L., Bruns, A. E., Perraud, V., Zelenyuk, A., Ezell, M. J., Johnson, S. N., Yu, Y., Imre, D., Finlayson-Pitts, B. J. and Alexander, M. L.: Comparison of FTIR and particle mass spectrometry for the measurement of particulate organic nitrates, Environ. Sci. Technol., 44(3), 1056–1061, 2010.

Canagaratna, M. R., Jimenez, J. L., Kroll, J. H., Chen, Q., Kessler, S. H., Massoli, P., Hildebrandt Ruiz, L., Fortner, E., Williams, L. R., Wilson, K. R., Surratt, J. D., Donahue, N. M., Jayne, J. T., Worsnop, D. R., Ruiz, L. H., Hildebrandt Ruiz, L., Fortner, E., Williams, L. R., Wilson, K. R., Surratt, J. D., Donahue, N. M., Jayne, J. T., Worsnop, D. R., Attribution, C. C., Canagaratna, M. R., Canagaratna, M. R., Jimenez, J. L., Kroll, J. H., Chen, Q., Kessler, S. H., Massoli, P., Hildebrandt Ruiz, L., Fortner, E., Williams, L. R., Wilson, K. R., Surratt, J. D., Donahue, N. M., Jayne, J. T. and Worsnop, D. R.: Elemental ratio measurements of organic compounds using aerosol mass spectrometry: characterization, improved calibration, and implications, Atmos. Chem. Phys., 15(1), 253–272, 2015.

Canonaco, F., Crippa, M., Slowik, J. G., Baltensperger, U. and Prévôt, A. S. H.: Atmos. Meas. Tech.SoFi, an IGOR-based interface for the efficient use of the generalized multilinear engine (ME-2) for the source apportionment: ME-2 application to aerosol mass spectrometer data, Atmos. Meas. Tech., 6(12), 3649–3661, 2013.

Carlton, A. G., de Gouw, J., Jimenez, J. L., Ambrose, J. L., Attwood, A. R., Brown, S., Baker, K. R., Brock, C., Cohen, R. C., Edgerton, S., Farkas, C. M., Farmer, D., Goldstein, A. H., Gratz, L., Guenther, A., Hunt, S., Jaeglé, L., Jaffe, D. A., Mak, J., McClure, C., Nenes, A., Nguyen, T. K., Pierce, J. R., de Sa, S., Selin, N. E., Shah, V., Shaw, S., Shepson, P. B., Song, S., Stutz, J., Surratt, J. D., Turpin, B. J., Warneke, C., Washenfelder, R. A., Wennberg, P. O. and Zhou, X.: Synthesis of the Southeast Atmosphere Studies: Investigating Fundamental Atmospheric Chemistry Questions, Bull. Am. Meteorol. Soc., 99(3), 547–567, 2018.

Chen, Y., Takeuchi, M., Nah, T., Xu, L., Canagaratna, M. R., Stark, H., Baumann, K., Canonaco, F., Prévôt, A. S. H., Gregory Huey, L., Weber, R. J. and Ng, N. L.: Chemical characterization of secondary organic aerosol at a rural site in the southeastern US: insights from simultaneous high-resolution time-of-flight aerosol mass spectrometer (HR-ToF-AMS) and FIGAERO chemical ionization mass spectrometer (CIMS) measurements, Atmospheric Chemistry and Physics, 20(14), 8421–8440, doi:10.5194/acp-20-8421-2020, 2020.

Cubison, M. J. and Jimenez, J. L.: Statistical precision of the intensities retrieved from constrained fitting

of overlapping peaks in high-resolution mass spectra, Atmos. Meas. Tech., 8(6), 2333–2345, 2015.

DeCarlo, P. F., Kimmel, J. R., Trimborn, A., Northway, M. J., Jayne, J. T., Aiken, A. C., Gonin, M., Fuhrer, K., Horvath, T., Docherty, K. S., Worsnop, D. R. and Jimenez, J. L.: Field-Deployable, High-Resolution, Time-of-Flight Aerosol Mass Spectrometer, Anal. Chem., 78(24), 8281–8289, 2006.

Docherty, K. S., Aiken, A. C., Huffman, J. A., Ulbrich, I. M., DeCarlo, P. F., Sueper, D., Worsnop, D. R., Snyder, D. C., Peltier, R. E., Weber, R. J., Grover, B. D., Eatough, D. J., Williams, B. J., Goldstein, A. H., Ziemann, P. J. and Jimenez, J. L.: The 2005 Study of Organic Aerosols at Riverside (SOAR-1): instrumental intercomparisons and fine particle composition, Atmos. Chem. Phys., 11(23), 12387–12420, 2011.

Drewnick, F., Diesch, J.-M., Faber, P. and Borrmann, S.: Aerosol mass spectrometry: particle–vaporizer interactions and their consequences for the measurements, Atmos. Meas. Tech., 8(9), 3811–3830, 2015.

Eris, G., Takeuchi, M., Wood, E. C., Tanner, D. J., Huey, L. G. and Ng, N. L.: Characterization of Thermal Dissociation Cavity Attenuated Phase Shift Spectroscopy (TD-CAPS) for Total Gas-Phase and Particle-Phase Alkyl Nitrates and Peroxy Nitrates Measurements, p. Conference abstract 11IM.6–Conference abstract 11IM.6., 2018.

Farmer, D. K., Matsunaga, A., Docherty, K. S., Surratt, J. D., Seinfeld, J. H., Ziemann, P. J. and Jimenez, J. L.: Response of an aerosol mass spectrometer to organonitrates and organosulfates and implications for atmospheric chemistry, Proceedings of the National Academy of Sciences, 107(15), 6670–6675, 2010.

Fisher, J. A., Jacob, D. J., Travis, K. R., Kim, P. S., Marais, E. A., Chan Miller, C., Yu, K., Zhu, L., Yantosca, R. M., Sulprizio, M. P., Mao, J., Wennberg, P. O., Crounse, J. D., Teng, A. P., Nguyen, T. B., St. Clair, J. M., Cohen, R. C., Romer, P., Nault, B. A., Wooldridge, P. J., Jimenez, J. L., Campuzano-Jost, P., Day, D. A., Hu, W., Shepson, P. B., Xiong, F., Blake, D. R., Goldstein, A. H., Misztal, P. K., Hanisco, T. F., Wolfe, G. M., Ryerson, T. B., Wisthaler, A. and Mikoviny, T.: Organic nitrate chemistry and its implications for nitrogen budgets in an isoprene- and monoterpene-rich atmosphere: constraints from aircraft (SEAC$^4$RS) and ground-based (SOAS) observations in the Southeast US, Atmos. Chem. Phys., 16(9), 5969–5991, 2016.

Fry, J. L., Kiendler-Scharr, A., Rollins, A. W., Wooldridge, P. J., Brown, S. S., Fuchs, H., Dubé, W., Mensah, A., dal Maso, M., Tillmann, R., Dorn, H.-P., Brauers, T. and Cohen, R. C.: Organic nitrate and secondary organic aerosol yield from $NO_3$ oxidation of β-pinene evaluated using a gas-phase kinetics/aerosol partitioning model, Atmos. Chem. Phys., 9(4), 1431–1449, 2009.

Fry, J. L., Kiendler-Scharr, A., Rollins, A. W., Brauers, T., Brown, S. S., Dorn, H.-P., Dubé, W. P., Fuchs, H., Mensah, A., Rohrer, F., Tillmann, R., Wahner, A., Wooldridge, P. J., Cohen, R. C. and Dube, W.: SOA from limonene: role of $NO_3$ in its generation and degradation, Atmos. Chem. Phys., 11(8), 3879–3894, 2011.

Fry, J. L., Draper, D. C., Zarzana, K. J., Campuzano-Jost, P., Day, D. A., Jimenez, J. L., Brown, S. S., Cohen, R. C., Kaser, L., Hansel, A., Cappellin, L., Karl, T., Hodzic Roux, A., Turnipseed, A., Cantrell, C., Lefer, B. L. and Grossberg, N.: Observations of gas- and aerosol-phase organic nitrates at BEACHON-RoMBAS 2011, Atmos. Chem. Phys., 13(17), 8585–8605, 2013.

Hao, L. Q., Kortelainen, A., Romakkaniemi, S., Portin, H., Jaatinen, A., Leskinen, A., Komppula, M., Miettinen, P., Sueper, D., Pajunoja, A., Smith, J. N., Lehtinen, K. E. J., Worsnop, D. R., Laaksonen, A. and Virtanen, A.: Atmospheric submicron aerosol composition and particulate organic nitrate formation in a boreal forestland–urban mixed region, Atmos. Chem. Phys., 14(24), 13483–13495, 2014.

Huang, W., Saathoff, H., Shen, X., Ramisetty, R., Leisner, T. and Mohr, C.: Chemical Characterization of Highly Functionalized Organonitrates Contributing to Night-time Organic Aerosol Mass Loadings and Particle Growth, Environ. Sci. Technol., 53(3), acs.est.8b05826–acs.est.8b05826, 2019.

Hu, W., Palm, B. B., Day, D. A., Campuzano-Jost, P., Krechmer, J. E., Peng, Z., de Sá, S. S., Martin, S. T., Alexander, M. L. L., Baumann, K., Hacker, L., Kiendler-Scharr, A., Koss, A. R., de Gouw, J. A., Goldstein, A. H., Seco, R., Sjostedt, S. J., Park, J.-H., Guenther, A. B., Kim, S., Canonaco, F., Prévôt, A. S. H., Brune, W. H. and Jimenez, J. L.: Volatility and lifetime against OH heterogeneous reaction of ambient isoprene-epoxydiols-derived secondary organic aerosol (IEPOX-SOA), Atmos. Chem. Phys., 16(18), 11563–11580, 2016.

Hu, W., Campuzano-Jost, P., Day, D. A., Croteau, P., Canagaratna, M. R., Jayne, J. T., Worsnop, D. R. and Jimenez, J. L.: Evaluation of the new capture vapourizer for aerosol mass spectrometers (AMS) through laboratory studies of inorganic species, Atmos. Meas. Tech., 10(6), 2897–2921, 2017.

Jayne, J. T., Croteau, P. L., Lambe, A. T., Xu, W., Onasch, T. B., Wolff, L. and Canagaratna, M. R.: Investigation of f44 variability in AMS and ACSM instruments, in 16th Aerosol Mass Spectrometer Users' Meeting, Milan, Italy. [online] Available from: http://cires1.colorado.edu/jimenez-group/UsrMtgs/UsersMtg16/Jayne_f44Intro.pdf (Accessed 11 August 2021), 2015.

Jimenez, J. L., Canagaratna, M. R., Drewnick, F., Allan, J. D., Alfarra, M. R., Middlebrook, A. M., Slowik, J. G., Zhang, Q., Coe, H., Jayne, J. T. and Worsnop, D. R.: Comment on "The effects of molecular weight and thermal decomposition on the sensitivity of a thermal desorption aerosol mass spectrometer," Aerosol Sci. Technol., 50(9), i–xv, 2016.

Joo, T., Rivera-Rios, J. C., Takeuchi, M., Alvarado, M. J. and Ng, N. L.: Secondary Organic Aerosol Formation from Reaction of 3-Methylfuran with Nitrate Radicals, ACS Earth and Space Chemistry, 3(6), acsearthspacechem.9b00068–acsearthspacechem.9b00068, 2019.

Kang, H., Day, D. A., Krechmer, J. E., Ayres, B. R., Keehan, N. I., Thompson, S., Hu, W., Campuzano-Jost, P., Schroder, J. C., Stark, H., Ranney, A., Ziemann, P. J., Zarzana, K. J., Wild, R. J., Dube, W. P., Brown, S. S., Fry, J. L. and Jimenez, J. L.: Secondary organic aerosol mass yields from the dark $NO_3$ oxidation of α-pinene and Δ-carene: effect of $RO_2$ radical fate, in American Geophysical Union Fall Meeting, San Francisco. [online] Available from: https://agu.confex.com/agu/fm16/meetingapp.cgi/Paper/135842 (Accessed 11 August, 2021), 2016.

Keehan, N. I., Brownwood, B., Marsavin, A., Day, D. A. and Fry, J. L.: A thermal-dissociation–cavity ring-down spectrometer (TD-CRDS) for the detection of organic nitrates in gas and particle phases, Atmos. Meas. Tech., 13(11), 6255–6269, 2020.

Kenagy, H. S., Romer, P. S., Wooldridge, P. J., Nault, B. A., Campuzano-Jost, P., Day, D. A., Jimenez, J. L., Zare, A., Pye, H. O. T., Yu, J., Song, C. H., Blake, D. R., Woo, J.-H., Kim, Y. and Cohen, R. C.:

Contribution of organic nitrates to organic aerosol over South Korea during KORUS-AQ, In Prep., 2021.

Kiendler-Scharr, A., Mensah, A. A., Friese, E., Topping, D., Nemitz, E., Prevot, A. S. H., Äijälä, M., Allan, J., Canonaco, F., Canagaratna, M., Carbone, S., Crippa, M., Dall Osto, M., Day, D. A., DeCarlo, P., Di Marco, C. F., Elbern, H., Eriksson, A., Freney, E., Hao, L., Herrmann, H., Hildebrandt, L., Hillamo, R., Jimenez, J. L., Laaksonen, A., McFiggans, G., Mohr, C., O'Dowd, C., Otjes, R., Ovadnevaite, J., Pandis, S. N., Poulain, L., Schlag, P., Sellegri, K., Swietlicki, E., Tiitta, P., Vermeulen, A., Wahner, A., Worsnop, D. and Wu, H.-C.: Organic nitrates from night-time chemistry are ubiquitous in the European submicron aerosol, Geophys. Res. Lett., 43(14), 7735–7744, 2016.

Kim, H., Zhang, Q. and Heo, J.: Influence of intense secondary aerosol formation and long-range transport on aerosol chemistry and properties in the Seoul Metropolitan Area during spring time: Results from KORUS-AQ, Atmos. Chem. Phys., 18(10), 7149–7168, 2018.

Kimmel, J. R., Farmer, D. K., Cubison, M. J., Sueper, D., Tanner, C., Nemitz, E., Worsnop, D. R., Gonin, M. and Jimenez, J. L.: Real-time aerosol mass spectrometry with millisecond resolution, Int. J. Mass Spectrom., 303(1), 15–26, 2011.

Kortelainen, A., Hao, L., Tiitta, P., Jaatinen, A., Miettinen, P., Kulmala, M., Smith, J. N., Laaksonen, A., Worsnop, D. R. and Virtanen, A.: Sources of particulate organic nitrates in the boreal forest in Finland, Boreal Environ. Res., 22, 13–26, 2017.

Kostenidou, E., Florou, K., Kaltsonoudis, C., Tsiflikiotou, M., Vratolis, S., Eleftheriadis, K. and Pandis, S. N.: Sources and chemical characterization of organic aerosol during the summer in the eastern Mediterranean, Atmos. Chem. Phys., 15(19), 11355–11371, 2015.

Krechmer, J. E., Day, D. A., Ziemann, P. J. and Jimenez, J. L.: Direct Measurements of Gas/Particle Partitioning and Mass Accommodation Coefficients in Environmental Chambers, Environ. Sci. Technol., 51(20), 11867–11875, 2017.

Lee, B. H., Mohr, C., Lopez-Hilfiker, F. D., Lutz, A., Hallquist, M., Lee, L., Romer, P., Cohen, R. C., Iyer, S., Kurtén, T., Hu, W., Day, D. A., Campuzano-Jost, P., Jimenez, J. L., Xu, L., Ng, N. L., Guo, H., Weber, R. J., Wild, R. J., Brown, S. S., Koss, A., de Gouw, J., Olson, K., Goldstein, A. H., Seco, R., Kim, S., McAvey, K., Shepson, P. B., Starn, T., Baumann, K., Edgerton, E. S., Liu, J., Shilling, J. E., Miller, D. O., Brune, W., Schobesberger, S., D'Ambro, E. L. and Thornton, J. A.: Highly functionalized organic nitrates in the southeast U.S.: Contribution to secondary organic aerosol and reactive nitrogen budgets, Proc. Natl. Acad. Sci., 113(6), 1516–1521, 2016.

Liu, S., Shilling, J. E., Song, C., Hiranuma, N., Zaveri, R. A. and Russell, L. M.: Hydrolysis of Organonitrate Functional Groups in Aerosol Particles, Aerosol Sci. Technol., 46(12), 1359–1369, 2012.

Liu, X., Day, D. A., Krechmer, J. E., Brown, W., Peng, Z., Ziemann, P. J. and Jimenez, J. L.: Direct measurements of semi-volatile organic compound dynamics show near-unity mass accommodation coefficients for diverse aerosols, Commun. Chem., 2(98), 1–9, 2019.

Martin, S. T., Artaxo, P., Machado, L. A. T., Manzi, A. O., Souza, R. A. F., Schumacher, C., Wang, J., Andreae, M. O., Barbosa, H. M. J., Fan, J., Fisch, G., Goldstein, A. H., Guenther, A., Jimenez, J. L., Pöschl, U., Silva Dias, M. A., Smith, J. N. and Wendisch, M.: Introduction: Observations and Modeling

of the Green Ocean Amazon (GoAmazon2014/5), Atmos. Chem. Phys., 16(8), 4785–4797, 2016.

Martin, S. T., Artaxo, P., Machado, L., Manzi, A. O., Souza, R. A. F., Schumacher, C., Wang, J., Biscaro, T., Brito, J., Calheiros, A., Jardine, K., Medeiros, A., Portela, B., de Sá, S. S., Adachi, K., Aiken, A. C., Albrecht, R., Alexander, L., Andreae, M. O., Barbosa, H. M. J., Buseck, P., Chand, D., Comstock, J. M., Day, D. A., Dubey, M., Fan, J., Fast, J., Fisch, G., Fortner, E., Giangrande, S., Gilles, M., Goldstein, A. H., Guenther, A., Hubbe, J., Jensen, M., Jimenez, J. L., Keutsch, F. N., Kim, S., Kuang, C., Laskin, A., McKinney, K., Mei, F., Miller, M., Nascimento, R., Pauliquevis, T., Pekour, M., Peres, J., Petäjä, T., Pöhlker, C., Pöschl, U., Rizzo, L., Schmid, B., Shilling, J. E., Silva Dias, M. A., Smith, J. N., Tomlinson, J. M., Tóta, J. and Wendisch, M.: The green ocean amazon experiment (GOAMAZON2014/5) observes pollution affecting gases, aerosols, clouds, and rainfall over the rain forest, Bull. Am. Meteorol. Soc., 98(5), 981–997, 2017.

Middlebrook, A. M., Bahreini, R., Jimenez, J. L. and Canagaratna, M. R.: Evaluation of Composition-Dependent Collection Efficiencies for the Aerodyne Aerosol Mass Spectrometer using Field Data, Aerosol Sci. Technol., 46(3), 258–271, 2012.

Minguillon´, M. C., Perron, N., Querol, X., Szidat, S., Fahrni, S. M., Alastuey, A., Jimenez, J. L., Mohr, C., Ortega, A. M., Day, D. A., Lanz, V. A., Wacker, L., Reche, C., Cusack, M., Amato, F., Kiss, G., Hoffer, A., Decesari, S., Moretti, F., Hillamo, R., Teinila, K., Seco, R., Penuelas, J., Metzger, A., Schallhart, S., Muller, M., Hansel, A., Burkhart, J. F., Baltensperger, U. and Prevot, A. S. H.: Fossil versus contemporary sources of fine elemental and organic carbonaceous particulate matter during the DAURE campaign in Northeast Spain, Atmos. Chem. Phys., 11(23), 12067–12084, 2011.

Molina, L. T., Madronich, S., Gaffney, J. S., Apel, E., de Foy, B., Fast, J., Ferrare, R., Herndon, S., Jimenez, J. L., Lamb, B., Osornio-Vargas, A. R., Russell, P., Schauer, J. J., Stevens, P. S., Volkamer, R. and Zavala, M.: An overview of the MILAGRO 2006 Campaign: Mexico City emissions and their transport and transformation, Atmos. Chem. Phys., 10(18), 8697–8760, 2010.

Nault, B. A., Garland, C., Wooldridge, P. J., Brune, W. H., Campuzano-Jost, P., Crounse, J. D., Day, D. A., Dibb, J., Hall, S. R., Huey, L. G., Jimenez, J. L., Liu, X., Mao, J., Mikoviny, T., Peischl, J., Pollack, I. B., Ren, X., Ryerson, T. B., Scheuer, E., Ullmann, K., Wennberg, P. O., Wisthaler, A., Zhang, L. and Cohen, R. C.: Observational Constraints on the Oxidation of $NO_x$ in the Upper Troposphere, J. Phys. Chem. A, 120(9), doi:10.1021/acs.jpca.5b07824, 2016.

Nault, B. A., Campuzano-Jost, P., Day, D. A., Schroder, J. C., Anderson, B., Beyersdorf, A. J., Blake, D. R., Brune, W. H., Choi, Y., Corr, C. A., de Gouw, J. A., Dibb, J., DiGangi, J. P., Diskin, G. S., Fried, A., Huey, L. G., Kim, M. J., Knote, C. J., Lamb, K. D., Lee, T., Park, T., Pusede, S. E., Scheuer, E., Thornhill, K. L., Woo, J.-H. and Jimenez, J. L.: Secondary organic aerosol production from local emissions dominates the organic aerosol budget over Seoul, South Korea, during KORUS-AQ, Atmos. Chem. Phys., 18(24), 17769–17800, 2018.

Ortega, J., Turnipseed, A., Guenther, A. B., Karl, T. G., Day, D. A., Gochis, D., Huffman, J. A., Prenni, A. J., Levin, E. J. T., Kreidenweis, S. M., DeMott, P. J., Tobo, Y., Patton, E. G., Hodzic, A., Cui, Y. Y., Harley, P. C., Hornbrook, R. S., Apel, E. C., Monson, R. K., Eller, A. S. D., Greenberg, J. P., Barth, M. C., Campuzano-Jost, P., Palm, B. B., Jimenez, J. L., Aiken, A. C., Dubey, M. K., Geron, C., Offenberg, J., Ryan, M. G., Fornwalt, P. J., Pryor, S. C., Keutsch, F. N., Digangi, J. P., Chan, A. W. H., Goldstein, A. H., Wolfe, G. M., Kim, S., Kaser, L., Schnitzhofer, R., Hansel, A., Cantrell, C. A., Mauldin, R. L. and Smith,

J. N.: Overview of the Manitou experimental forest observatory: Site description and selected science results from 2008 to 2013, Atmos. Chem. Phys., 14(12), 6345–6367, 2014.

Paatero, P.: The Multilinear Engine: A Table-Driven, Least Squares Program for Solving Multilinear Problems, including the n-Way Parallel Factor Analysis Model, J. Comput. Graph. Stat., 8(4), 854–854, 1999.

Pagonis, D., Campuzano-Jost, P., Guo, H., Day, D. A., Schueneman, M. K., Brown, W. L., Nault, B. A., Stark, H., Siemens, K., Laskin, A., Piel, F., Tomsche, L., Wisthaler, A., Coggon, M. M., Gkatzelis, G. I., Halliday, H. S., Krechmer, J. E., Moore, R. H., Thomson, D. S., Warneke, C., Wiggins, E. B. and Jimenez, J. L.: Airborne extractive electrospray mass spectrometry measurements of the chemical composition of organic aerosol, Atmos. Chem. Phys., 14(2), 1545–1559, 2021.

Palm, B. B., Campuzano-Jost, P., Day, D. A., Ortega, A. M., Fry, J. L., Brown, S. S., Zarzana, K. J., Dube, W., Wagner, N. L., Draper, D. C., Kaser, L., Jud, W., Karl, T., Hansel, A., Gutiérrez-Montes, C. and Jimenez, J. L.: Secondary organic aerosol formation from in situ OH, $O_3$, and $NO_3$ oxidation of ambient forest air in an oxidation flow reactor, Atmos. Chem. Phys., 17(8), 5331–5354, 2017.

Palm, B. B., de Sá, S. S., Day, D. A., Campuzano-Jost, P., Hu, W., Seco, R., Sjostedt, S. J., Park, J.-H., Guenther, A. B., Kim, S., Brito, J., Wurm, F., Artaxo, P., Thalman, R., Wang, J., Yee, L. D., Wernis, R., Isaacman-VanWertz, G., Goldstein, A. H., Liu, Y., Springston, S. R., Souza, R., Newburn, M. K., Alexander, M. L., Martin, S. T. and Jimenez, J. L.: Secondary organic aerosol formation from ambient air in an oxidation flow reactor in central Amazonia, Atmos. Chem. Phys., 18(1), 467–493, 2018.

Pandolfi, M., Querol, X., Alastuey, A., Jimenez, J. L., Jorba, O., Day, D. A., Ortega, A., Cubison, M. J., Comerón, A., Sicard, M., Mohr, C., Prévôt, A. S. H., Minguillón, M. C., Pey, J., Baldasano, J. M., Burkhart, J. F., Seco, R., Peñuelas, J., Van Drooge, B. L., Artiñano, B., Di Marco, C., Nemitz, E., Schallhart, S., Metzger, A., Hansel, A., Llorente, J., Ng, S., Jayne, J. and Szidat, S.: Effects of sources and meteorology on particulate matter in the Western Mediterranean Basin: An overview of the DAURE campaign, J. Geophys. Res. D: Atmos., 119(8), 4978–5010, 2014.

Paul, D., Furgeson, A. and Osthoff, H. D.: Measurements of total peroxy and alkyl nitrate abundances in laboratory-generated gas samples by thermal dissociation cavity ring-down spectroscopy, Rev. Sci. Instrum., 80(11), 114101–114101, 2009.

Reyes-Villegas, E., Priestley, M., Ting, Y.-C., Haslett, S., Bannan, T., Le Breton, M., Williams, P. I., Bacak, A., Flynn, M. J., Coe, H., Percival, C., Allan, J. D., Breton, M. L., Attribution, Creative Commons, Reyes-Villegas, E., Reyes-Villegas, E. and By, C. C.: Simultaneous aerosol mass spectrometry and chemical ionisation mass spectrometry measurements during a biomass burning event in the UK : insights into nitrate chemistry, Atmos. Chem. Phys., 18(6), 4093–4111, 2018.

Rollins, A. W., Kiendler-Scharr, A., Fry, J. L., Brauers, T., Brown, S. S., Dorn, H.-P., Dubé, W. P., Fuchs, H., Mensah, A., Mentel, T. F., Rohrer, F., Tilmann, R., Wegener, R., Wooldridge, P. J. and Cohen, R. C.: Isoprene oxidation by nitrate radical: alkyl nitrate and secondary organic aerosol yields, Atmos. Chem. Phys., 9, 6685–6703, 2009.

Rollins, A. W., Fry, J. L., Hunter, J. F., Kroll, J. H., Worsnop, D. R., Singaram, S. W. and Cohen, R. C.: Elemental analysis of aerosol organic nitrates with electron ionization high-resolution mass spectrometry,

Atmos. Meas. Tech., 3(1), 301–310, 2010a.

Rollins, A. W., Smith, J. D., Wilson, K. R. and Cohen, R. C.: Real time in situ detection of organic nitrates in atmospheric aerosols, Environ. Sci. Technol., 44(14), 5540–5545, 2010b.

Rollins, A. W., Pusede, S., Wooldridge, P., Min, K.-E., Gentner, D. R., Goldstein, A. H., Liu, S., Day, D. A., Russell, L. M., Rubitschun, C. L., Surratt, J. D. and Cohen, R. C.: Gas/particle partitioning of total alkyl nitrates observed with TD-LIF in Bakersfield, J. Geophys. Res. D: Atmos., 118(12), 6651–6662, 2013.

de Sá, S. S., Palm, B. B., Campuzano-Jost, P., Day, D. A., Hu, W., Isaacman-VanWertz, G., Yee, L. D., Brito, J., Carbone, S., Ribeiro, I. O., Cirino, G. G., Liu, Y. J., Thalman, R., Sedlacek, A., Funk, A., Schumacher, C., Shilling, J. E., Schneider, J., Artaxo, P., Goldstein, A. H., Souza, R. A. F., Wang, J., McKinney, K. A., Barbosa, H., Alexander, M. L., Jimenez, J. L. and Martin, S. T.: Urban influence on the concentration and composition of submicron particulate matter in central Amazonia, Atmos. Chem. Phys., 18(16), 12185–12206, 2018.

de Sá, S. S., Rizzo, L. V., Palm, B. B., Campuzano-Jost, P., Day, D. A., Yee, L. D., Wernis, R., Isaacman-VanWertz, G., Brito, J., Carbone, S., Liu, Y. J., Sedlacek, A., Springston, S., Goldstein, A. H., Barbosa, H. M. J., Alexander, M. L., Artaxo, P., Jimenez, J. L. and Martin, S. T.: Contributions of biomass-burning, urban, and biogenic emissions to the concentrations and light-absorbing properties of particulate matter in central Amazonia during the dry season, Atmos. Chem. Phys., 19, 7973–8001, 2019.

Sato, K., Takami, A., Isozaki, T., Hikida, T., Shimono, A. and Imamura, T.: Mass spectrometric study of secondary organic aerosol formed from the photo-oxidation of aromatic hydrocarbons, Atmos. Environ., 44(8), 1080–1087, 2010.

Sato, K., Takami, A., Kato, Y., Seta, T., Fujitani, Y., Hikida, T., Shimono, A. and Imamura, T.: AMS and LC/MS analyses of SOA from the photooxidation of benzene and 1,3,5-trimethylbenzene in the presence of $NO_x$: effects of chemical structure on SOA aging, Atmos. Chem. Phys., 12(10), 4667–4682, 2012.

Schroder, J. C., Campuzano-Jost, P., Day, D. A., Shah, V., Larson, K., Sommers, J. M., Sullivan, A. P., Campos, T., Reeves, J. M., Hills, A., Hornbrook, R. S., Blake, N. J., Scheuer, E., Guo, H., Fibiger, D. L., McDuffie, E. E., Hayes, P. L., Weber, R. J., Dibb, J. E., Apel, E. C., Jaeglé, L., Brown, S. S., Thornton, J. A. and Jimenez, J. L.: Sources and Secondary Production of Organic Aerosols in the Northeastern United States during WINTER, J. Geophys. Res. D: Atmos., 123(14), 7771–7796, 2018.

Schwantes, R. H., Charan, S. M., Bates, K. H., Huang, Y., Nguyen, T. B., Mai, H., Kong, W., Flagan, R. C. and Seinfeld, J. H.: Low-volatility compounds contribute significantly to isoprene secondary organic aerosol (SOA) under high-$NO_x$ conditions, Atmos. Chem. Phys., 19(11), 7255–7278, 2019.

Shingler, T., Crosbie, E., Ortega, A., Shiraiwa, M., Zuend, A., Beyersdorf, A., Ziemba, L., Anderson, B., Thornhill, L., Perring, A. E., Schwarz, J. P., Campazano-Jost, P., Day, D. A., Jimenez, J. L., Hair, J. W., Mikoviny, T., Wisthaler, A. and Sorooshian, A.: Airborne Characterization of Sub-saturated Aerosol Hygroscopicity and Dry Refractive Index from the Surface to 6.5 km during the SEAC4RS Campaign, J. Geophys. Res. D: Atmos., 121(8), 4188–4210, 2016.

Sueper, D.: ToF-AMS Data Analysis Software Webpage, [online] Available from:

http://cires1.colorado.edu/jimenez-group/wiki/index.php/ToF-AMS_Analysis_Software (Accessed 11 August 2021), 2021.

Sun, Y. L., Zhang, Q., Schwab, J. J., Yang, T., Ng, N. L. and Demerjian, K. L.: Factor analysis of combined organic and inorganic aerosol mass spectra from high resolution aerosol mass spectrometer measurements, Atmos. Chem. Phys., 12(18), 8537–8551, 2012.

Takeuchi, M. and Ng, N. L.: Chemical composition and hydrolysis of organic nitrate aerosol formed from hydroxyl and nitrate radical oxidation of α-pinene and β-pinene, Atmos. Chem. Phys., 19(19), 12749–12766, 2019.

Thieser, J., Schuster, G., Schuladen, J., Phillips, G. J., Reiffs, A., Parchatka, U., Pöhler, D., Lelieveld, J. and Crowley, J. N.: A two-channel thermal dissociation cavity ring-down spectrometer for the detection of ambient $NO_2$, $RO_2NO_2$ and $RONO_2$, Atmos. Meas. Tech., 9(2), 553–576, 2016.

Tiitta, P., Leskinen, A., Hao, L., Yli-Pirilä, P., Kortelainen, M., Grigonyte, J., Tissari, J., Lamberg, H., Hartikainen, A., Kuuspalo, K., Kortelainen, A.-M. M., Virtanen, A., Lehtinen, K. E. J., Komppula, M., Pieber, S., Prévôt, A. S. H., Onasch, T. B., Worsnop, D. R., Czech, H., Zimmermann, R., Jokiniemi, J. and Sippula, O.: Transformation of logwood combustion emissions in a smog chamber: formation of secondary organic aerosol and changes in the primary organic aerosol upon daytime and nighttime aging, Atmos. Chem. Phys., 16(20), 13251–13269, 2016.

Toon, O. B., Maring, H., Dibb, J., Ferrare, R., Jacob, D. J., Jensen, E. J., Luo, Z. J., Mace, G. G., Pan, L. L., Pfister, L., Rosenlof, K. H., Redemann, J., Reid, J. S., Singh, H. B., Thompson, A. M., Yokelson, R., Minnis, P., Chen, G., Jucks, K. W. and Pszenny, A.: Planning, implementation, and scientific goals of the Studies of Emissions and Atmospheric Composition, Clouds and Climate Coupling by Regional Surveys (SEAC 4 RS) field mission, J. Geophys. Res. D: Atmos., 121(9), 4967–5009, 2016.

Ulbrich, I. M., Canagaratna, M. R., Zhang, Q., Worsnop, D. R. and Jimenez, J. L.: Interpretation of organic components from Positive Matrix Factorization of aerosol mass spectrometric data, Atmos. Chem. Phys., 9(9), 2891–2918, 2009.

Xu, L., Suresh, S., Guo, H., Weber, R. J. and Ng, N. L.: Aerosol characterization over the southeastern United States using high-resolution aerosol mass spectrometry: spatial and seasonal variation of aerosol composition and sources with a focus on organic nitrates, Atmos. Chem. Phys., 15(13), 7307–7336, 2015a.

Xu, L., Guo, H., Boyd, C. M., Klein, M., Bougiatioti, A., Cerully, K. M., Hite, J. R., Isaacman-VanWertz, G., Kreisberg, N. M., Knote, C., Olson, K., Koss, A., Goldstein, A. H., Hering, S. V., de Gouw, J., Baumann, K., Lee, S.-H., Nenes, A., Weber, R. J. and Ng, N. L.: Effects of anthropogenic emissions on aerosol formation from isoprene and monoterpenes in the southeastern United States, Proceedings of the National Academy of Sciences, 112(1), 37–42, 2015b.

Xu, W., Lambe, A., Silva, P., Hu, W., Onasch, T., Williams, L., Croteau, P., Zhang, X., Renbaum-Wolff, L., Fortner, E., Jimenez, J. L., Jayne, J., Worsnop, D. and Canagaratna, M.: Laboratory evaluation of species-dependent relative ionization efficiencies in the Aerodyne Aerosol Mass Spectrometer, Aerosol Sci. Technol., 52(6), 626–641, 2018.

Xu, W., Takeuchi, M., Chen, C., Qiu, Y., Xie, C., Xu, W., Ma, N., Worsnop, D. R., Ng, N. L. and Sun, Y.: Estimation of particulate organic nitrates from thermodenuder–aerosol mass spectrometer measurements in the North China Plain, Atmospheric Measurement Techniques, 14(5), 3693–3705, doi:10.5194/amt-14-3693-2021, 2021.

Yu, K., Zhu, Q., Du, K. and Huang, X.-F.: Characterization of nighttime formation of particulate organic nitrates based on high-resolution aerosol mass spectrometry in an urban atmosphere in China, Atmos. Chem. Phys., 19(7), 5235–5249, 2019.

Zare, A., Fahey, K. M., Sarwar, G., Cohen, R. C. and Pye, H. O. T.: Vapor-Pressure Pathways Initiate but Hydrolysis Products Dominate the Aerosol Estimated from Organic Nitrates, ACS Earth and Space Chemistry, 3(8), 1426–1437, 2019.

Zhang, J. K., Cheng, M. T., Ji, D. S., Liu, Z. R., Hu, B., Sun, Y. and Wang, Y. S.: Characterization of submicron particles during biomass burning and coal combustion periods in Beijing, China, Sci. Total Environ., 562, 812–821, 2016.

Zhu, Q., Cao, L.-M., Tang, M.-X., Huang, X.-F., Saikawa, E. and He, L.-Y.: Characterization of Organic Aerosol at a Rural Site in the North China Plain Region: Sources, Volatility and Organonitrates, Adv. Atmos. Sci., 38(7), 1115–1127, 2021.